



MINISTÉRIO DA CIÊNCIA, TECNOLOGIA, INOVAÇÕES E COMUNICAÇÕES  
**INSTITUTO NACIONAL DE PESQUISAS ESPACIAIS**

Referência / REFERENCE	Classificação do Documento / DOCUMENT CLASSIFICATION
CPRIME-GER-RTE-01/2018_v01	Restrito / RESTRICT
Tipo / TYPE	Número de Páginas / NUMBER OF PAGES
Mission Study Report	101

Título / TITLE

# Galileo Solar Space Telescope

## Mission Study Report

Publicado Por / PUBLISHED BY



**Centro de Projeto Integrado de Missões Espaciais – CPRIME**  
Divisão de Sistemas Espaciais – DIDSE  
Coordenação-Geral de Engenharia e Tecnologia Espacial – CGETE  
Instituto Nacional de Pesquisas Espaciais – INPE  
Av. do Astronautas 1758, Jd. da Granja  
São José dos Campos, SP, 12227-010, Brasil

## Autores / AUTHORS

## Divisão / DIVISION

Ana Paula de Sá Santos Rabello	Risk Analysis	SESEQ/CGETE/INPE
Antonio Lopes Filho	Optical Payloads Electronics	DIDEA/CGETE/INPE
Arcélio Costa Louro	Power	DIDSE/CGETE/INPE
Bráulio Fonseca C. de Albuquerque	Optical Payloads	DIDEA/CGETE/INPE
Douglas Felipe da Silva	Thermal Analysis	DIDSE/CGETE/INPE
Fabiano Luis de Sousa	Systems	DIDSE/CGETE/INPE
Gino Genaro	Thermal Analysis	DIDSE/CGETE/INPE
João Paulo Estevam de Sousa	Programmatics	SESEQ/CGETE/INPE
Jognes Panasiewicz Jr	Communications	DIDEA/CGETE/INPE
Lucas Lopes Costa	Risk Analysis	SESEQ/CGETE/INPE
Luis Eduardo Antunes Vieira	GSST Mission Principal Investigator	DIDGE/CGCEA/INPE
Maria de Fátima Mattiello Francisco	Operations / Ground Systems	COCRE/INPE
Mario Eugênio Saturno	On-board Computer and Data Handling	DIDSE/CGETE/INPE
Mateus Carlos Ferraz de Aguiar	Communications	DIDSE/CGETE/INPE
Miguel Adrian Carretero	Ground Systems	DIDSS/CGETE/INPE
Renato Henrique Ferreira Branco	Cost Analysis	CGETE/INPE
Ronan Arraes Jardim Chagas	Orbit Analysis / AOCS / Simulation	DIDSE/CGETE/INPE
Sebastião Eduardo Corsatto Varotto	Mechanisms / Launchers	DIDSE/CGETE/INPE
Sérgio Luís de Andrade e Silva	Communications	DIDSE/CGETE/INPE
Willer Gomes dos Santos	Propulsion / Orbit Analysis / AOCS	PCI/DIDSE/CGETE/INPE
Valentino Lau	Layout / Structures	SESMF/CGETE/INPE

## Comitê de Consultoria Científica / SCIENCE ADVISORY BOARD

Alisson Dal Lago	Solar Physics / Magnetospheric Physics	DIDGE/INPE
Cláudia Medeiros	Magnetospheric Physics	GES/DIDGE/INPE
Flávia Reis Cardoso	Magnetospheric Physics/Solar Irradiance	EEL-USP
Franciele Carlesso	Material Science/Solar Irradiance	PCI/CNPq
Graziela Savonov	Material Science/Solar Irradiance	CTE/INPE
Jenny Rodriguez	Solar Physics	PCI/CNPq
Joaquim E.R. Costa	Solar Physics	DIDAS/INPE
José R. Cecatto	Solar Physics	DIDAS/INPE
Judith Palacios	Solar Physics	Universidad de Alcalá
Ligia Alves da Silva	Magnetospheric Physics	Pos-Doc/CNPq
Livia Ribeiro Alves	Magnetospheric Physics	DIDGE/INPE
Luis Eduardo Antunes Vieira	Solar Physics/Magnetospheric Physics	DIDGE/INPE
Luiz Berni	Material Science/Solar Irradiance	LABAS/INPE
Marlos Rockenbach	Solar Physics/Magnetospheric Physics	DIDGE/INPE
Odim Mendes Jr.	Solar Physics/Magnetospheric Physics	DIDGE/INPE
Renato S. Dallaqua	Plasma Physics	LABAP/INPE
Tardelli Stekel	Solar Physics	IF/GES/DIDGE/INPE
Vitor Moura	Magnetospheric Physics	Pos-Doc/FAPESP
Waldeir Amaral Vilela	Solar Irradiance	LABAS/INPE

## Histórico de Revisões / REVISION HISTORY

---

Versão VERSION	Data DATE	Modificações MODIFICATIONS
01	25/05/2018	First version.

## Folha de Aprovação / APPROVAL SHEET

---

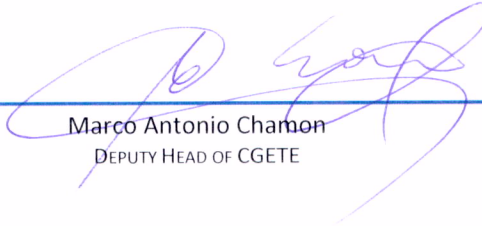
Esta versão do documento foi aprovada por:

THIS VERSION OF THE DOCUMENT WAS APPROVED BY:



---

Fabiano Luis de Sousa  
DEPUTY HEAD OF DIDSE



---

Marco Antonio Chamon  
DEPUTY HEAD OF CGETE

**Este documento é de propriedade do Instituto Nacional de Pesquisas Espaciais - INPE, não podendo ser reproduzido sem prévia autorização.**

**THIS DOCUMENT IS PROPERTY OF INSTITUTO NACIONAL DE PESQUISAS ESPACIAIS - INPE AND CANNOT BE REPRODUCED WITHOUT AUTHORIZATION.**

Direitos autorais © 2018 Instituto Nacional de Pesquisas Espaciais - INPE  
COPYRIGHT © 2018 BY INSTITUTO NACIONAL DE PESQUISAS ESPACIAIS - INPE

## Índice / TABLE OF CONTENTS

<b>LISTA DE FIGURAS / LIST OF FIGURES .....</b>	<b>8</b>
<b>LISTA DE TABELAS / LIST OF TABLES .....</b>	<b>10</b>
<b>LISTA DE SIGLAS E ABREVIATURAS / LIST OF ACRONYMS AND ABBREVIATIONS .....</b>	<b>11</b>
<b>1 INTRODUCTION .....</b>	<b>13</b>
1.1 BACKGROUND .....	13
1.2 DOCUMENT STRUCTURE .....	13
1.3 SUMMARY OF GSST MISSION OBJECTIVES, REQUIREMENTS, AND STUDY SCOPE .....	13
1.4 SYSTEM DRIVERS AND CRITICAL REQUIREMENTS IDENTIFICATION, TRADE-OFF DESIGN TREE AND DEFINITION OF BASELINE SYSTEM CONCEPTS TO BE CONSTRUCTED .....	16
1.5 SUMMARY OF BASELINE SYSTEM CONCEPTS .....	20
<b>2 PAYLOADS CONCEPTION AND DESCRIPTION .....</b>	<b>22</b>
2.1 APPROACH FOR THE IMAGING PAYLOADS .....	22
2.2 APPROACH FOR THE NON-IMAGING PAYLOADS .....	27
<b>3 CONCEPT OF OPERATIONS ANALYSIS .....</b>	<b>28</b>
<b>4 CANDIDATE SYSTEM CONCEPT SOLUTIONS FOR THE MISSION .....</b>	<b>30</b>
4.1 OPC3-1 .....	30
4.1.1 <i>OPC3-1: Orbit Analysis</i> .....	30
4.1.1.1 Eclipse Time .....	31
4.1.1.2 $\Delta V$ budget .....	32
4.1.1.3 General considerations .....	32
4.1.2 <i>OPC3-1: Orbit and attitude control analysis</i> .....	33
4.1.2.1 Actuators design .....	33
4.1.2.2 Sensors design .....	34
4.1.2.3 AOCS design validation .....	35
4.1.2.4 Antenna gimbals pointing .....	36
4.1.2.5 General considerations .....	37
4.1.3 <i>OPC3-1: Propulsion analysis</i> .....	37
4.1.4 <i>OPC3-1: Communications analysis</i> .....	41
4.1.5 <i>OPC3-1: On-board computer analysis</i> .....	47
4.1.6 <i>OPC3-1: Power analysis</i> .....	47
4.1.7 <i>OPC3-1: Thermal analysis</i> .....	48
4.1.8 <i>OPC3-1: Mechanisms</i> .....	52
4.1.9 <i>OPC3-1: Layout and structure concept</i> .....	54
4.1.10 <i>OPC3-1: Launcher options</i> .....	63
4.1.11 <i>OPC3-1: Ground system concept</i> .....	63
4.1.12 <i>OPC3-1: Satellite disposal analysis</i> .....	64
4.1.13 <i>OPC3-1: Satellite mass and power budget</i> .....	65
4.2 OPC3-2 .....	67
4.2.1 <i>OPC3-2: Orbit Analysis</i> .....	67
4.2.1.1 Eclipse Time .....	67
4.2.1.2 $\Delta V$ budget .....	68
4.2.2 <i>OPC3-2: Orbit and attitude control subsystem analysis</i> .....	69
4.2.2.1 Actuators design .....	69
4.2.2.2 Sensors design .....	71
4.2.2.3 AOCS design validation .....	72
4.2.2.4 Antenna gimbals pointing .....	73
4.2.2.5 General considerations .....	73
4.2.3 <i>OPC3-2: Propulsion analysis</i> .....	74
4.2.4 <i>OPC3-2: Communications analysis</i> .....	76
4.2.5 <i>OPC3-2: On-board computer analysis</i> .....	80

4.2.6	<i>OPC3-2: Power analysis.....</i>	<i>80</i>
4.2.7	<i>OPC3-2: Thermal analysis .....</i>	<i>80</i>
4.2.8	<i>OPC3-2: Mechanisms .....</i>	<i>84</i>
4.2.9	<i>OPC3-2: Layout and structures analysis.....</i>	<i>84</i>
4.2.10	<i>OPC3-2: Launcher options.....</i>	<i>92</i>
4.2.11	<i>OPC3-2: Ground systems concept .....</i>	<i>93</i>
4.2.12	<i>OPC3-2: Satellite disposal analysis.....</i>	<i>94</i>
4.2.13	<i>OPC3-2: Satellite mass and power budget.....</i>	<i>96</i>
<b>5</b>	<b>PROGRAMMATICS, MISSION RISK AND COST ANALYSIS .....</b>	<b>97</b>
5.1	PROGRAMMATICS ANALYSIS .....	97
5.2	RISK ANALYSIS.....	99
<b>6</b>	<b>FINAL REMARKS.....</b>	<b>100</b>
	<b>REFERENCES.....</b>	<b>101</b>

## Lista de Figuras / LIST OF FIGURES

Figure 1 - Preliminary trade tree for the system drivers. ....	16
Figure 2 - Optical payload architecture.....	17
Figure 3 - Tradeoff of number and position of ground stations versus data transmission rate between them and the satellite at LEO, considering an onboard data storage of 4 Gbits. ....	18
Figure 4 - Updated system drivers trade tree showing defined option for further analysis. The options marked with a red X were not considered viable or worth for further analysis on the scope of the present study. ....	19
Figure 5 - Updated system drivers trade tree. OPC3-1 and OPC3-2 are the options chosen for further analysis on the scope of the present study. ....	20
Figure 6 - Summary of orbit parameters for OPC3-1 and OPC3-2. ....	21
Figure 7 - GSST satellite layout concepts for OPC3-1 and OPC3-2. ....	21
Figure 8 - Ground segment conceptual architectures for OPC3-1 and OPC3-2. ....	22
Figure 9 - Optical design layout of the HR payload.....	24
Figure 10 - Conceptual mechanical design for the HR payload. Dimensions in mm. ....	25
Figure 11 - Optical design layout for the FD cameras.....	26
Figure 12 - Mechanical conceptual layout for the FD cameras. Dimensions in mm. ....	27
Figure 13 - Flow of science and service data between the GSST satellite and the mission's ground segment.....	29
Figure 14 - Screenshot of FOrPlan concept of operations simulation, showing the status of power and data balance, as well as the GSST satellite's states of functioning along the orbit, for the OPC3-2 option. ....	30
Figure 15 - Eclipse time for OPC3-1 considering an orbit inclination of 5°.....	31
Figure 16 - Eclipse time for OPC3-1 considering an orbit inclination of 28.5°.....	32
Figure 17 - Absolute pointing error (left) and angular velocity norm (right) for OPC3-1 (GEO) obtained from a simplified simulation using the star trackers. ....	36
Figure 18 - Relative pointing error (left) and angular velocity norm (right) for OPC3-1 (GEO) obtained from a simplified simulation using the tracking camera. ....	36
Figure 19 - Antenna pointing error caused by the position estimation error. ....	37
Figure 20 - Total mass and required power for different propulsion subsystems. ....	38
Figure 21 - Bipropellant propulsion subsystem concept architecture (Based on SDO's propulsion subsystem, illustrated in Leyva, 2011). ....	38
Figure 22 - Configuration of the reaction control system with 12 thrusters. ....	40
Figure 23 - Sketch of the thruster nozzle (adapted from De Sousa and Muraoka, 2006). ....	41
Figure 24 - Schematic drawing of the GSST satellite in two positions of the GEO orbit with 28.5o inclination, as seen from the Sun.....	42
Figure 25 - Science data X-band communication link chain for OPC3-1.....	44
Figure 26 - Service data S-band communication link chain for OPC3-1. ....	46
Figure 27 -Power subsystem architecture for OPC3-1.....	48
Figure 28 - Representation of the GSST satellite in GEO orbit for thermal analysis. ....	51
Figure 29 - OPC3-1 satellite external layout. Views for orbit (X-band antennas, SAG and magnetometers booms deployed) and launch configurations. ....	54
Figure 30 - OPC3-1 external dimensions, for orbit and launch configurations (dimensions in mm). ...	55
Figure 31 - Dimensions of GSST satellite structure for OPC3-1 (dimensions in mm). ....	56
Figure 32 - Y+ side view of GSST satellite, showing equipment layout for OPC3-1.....	58
Figure 33 - Y- side view of GSST satellite, showing equipment layout for OPC3-1. ....	58
Figure 34 - Z+ side view of GSST satellite, showing equipment layout for OPC3-1.....	59
Figure 35 - Z- side view of GSST satellite, showing equipment layout for OPC3-1.....	59
Figure 36 - PM Top Panel & PM Lower Panel side views of GSST satellite, showing equipment layout for OPC3-1. ....	60



Figure 37 - SM1 Top Panel side view of GSST satellite, showing equipment layout for OPC3-1. ....	60
Figure 38 - SM1 Lower Panel side view of GSST satellite, showing equipment layout for OPC3-1.....	61
Figure 39 - GSST satellite mass properties for OPC3-1, in launch and orbit configurations. ....	61
Figure 40 - Ground segment concept for OPC3-1.....	64
Figure 41 - Eclipse time for OPC3-2. ....	68
Figure 42 - Absolute pointing error (left) and angular velocity norm (right) for OPC3-2 (LEO) obtained from a simplified simulation using the star trackers. ....	73
Figure 43 - Relative pointing error (left) and angular velocity norm (right) for OPC3-2 (LEO) obtained from a simplified simulation using the tracking camera. ....	73
Figure 44 - Monopropellant propulsion subsystem (Wert, 2011). ....	75
Figure 45 - Science data Ka-band communication link chain for OPC3-2.....	77
Figure 46 - Service data S-band communication link chain for OPC3-2. ....	79
Figure 47 - Beta angle variation in one year. ....	82
Figure 48 - Satellite orbit and attitude for the cold and hot cases, for OPC3-2. ....	82
Figure 49 - OPC3-2 satellite external layout. Views for orbit and launch configurations. ....	84
Figure 50 - OPC3-2 external dimensions, for orbit and launch configurations. ....	85
Figure 51 - Dimensions of GSST satellite structure for OPC3-2. ....	86
Figure 52 - Y+ side view of GSST satellite, showing equipment layout for OPC3-2.....	88
Figure 53 - Y- side view of GSST satellite, showing equipment layout for OPC3-2. ....	88
Figure 54 - Z+ side view of GSST satellite, showing equipment layout for OPC3-2.....	89
Figure 55 - Z- side view of GSST satellite, showing equipment layout for OPC3-2.....	89
Figure 56 - PM Top Panel & PM Lower Panel side views of GSST satellite, showing equipment layout for OPC3-2. ....	89
Figure 57 - SM Shear Panels side views of GSST satellite, showing equipment layout for OPC3-2. ....	90
Figure 58 - SM Lower Panel side view of GSST satellite, showing equipment layout for OPC3-2.....	90
Figure 59 - GSST satellite mass properties for OPC3-2, in launch and orbit configurations. ....	91
Figure 60 - Ground segment concept for OPC3-2.....	94
Figure 61 - GSST satellite decay results for OPC3-2. ....	95
Figure 62 - Estimated development schedule for the GSST mission, option OPC3-1 (GEO). ....	98
Figure 63 - Estimated development schedule for the GSST mission, option OPC3-2 (LEO). ....	99

## Lista de Tabelas / LIST OF TABLES

Table 1 - Scientific objectives to payload requirements relation. ....	14
Table 2 - Mission requirements and constraints. ....	15
Table 3 - Main characteristics of the HR camera. ....	25
Table 4 - Main characteristics of the FD cameras. ....	27
Table 5 - Main characteristics of the non-imaging payloads. ....	28
Table 6 - Orbit parameters summary for OPC3-1. ....	31
Table 7 - Parameters to compute the $\Delta V$ for OPC3-1. ....	32
Table 8 - Input parameters used to compute the disturbance torques for OPC3-1. ....	33
Table 9 - Disturbance torques computed for OPC3-1. ....	33
Table 10 - Design parameters of the AOCS actuators. ....	34
Table 11 - Input data for the design of the propulsion subsystem for OPC3-1. ....	37
Table 12 - Mass budget of the bipropellant subsystem for OPC3-1. ....	39
Table 13 - Specification of bipropellant subsystem's components. ....	39
Table 14 - Inventory of fuel and oxidizer propellants. ....	40
Table 15 - Characteristics of the power subsystem conceived for OPC3-1. ....	48
Table 16 - Structure panels allowed temperature intervals, and average minimum and maximum equipment thermal loads applied over them in one orbit, for OPC3-1. ....	49
Table 17 - OPC3-1 thermal optical coatings properties. ....	50
Table 18 - Estimated Radiator area and heater power at satellite structural panels, for OPC3-1. ....	51
Table 19 - Nominal mass estimate for OPC3-1 thermal control. ....	52
Table 20 - Nominal dimensional, mass and functional characteristics of X-band antennas mechanisms. ....	53
Table 21 - Equipment positioning at satellite panels, for OPC3-1. ....	57
Table 22 - Structure panels breakdown for OPC3-1. Mass in kg. ....	62
Table 23 - Candidate launchers for the GSST satellite in configuration OPC3-1. ....	63
Table 24 - Mass and power budget for OPC3-1. ....	66
Table 25 - Orbit parameters summary for OPC3-2. ....	67
Table 26 - Parameters to compute the $\Delta V$ for OPC3-2. ....	68
Table 27 - Input parameters used to compute the disturbance torques for OPC3-2. ....	69
Table 28 - Disturbance torques computed for OPC3-2. ....	69
Table 29 - Angular velocity that each actuator set must remove from the satellite body. ....	70
Table 30 - Design parameters of the AOCS actuators. ....	70
Table 31 - Input data for the design of the propulsion subsystem for Opc3-2. ....	74
Table 32 - Mass budget of the monopropellant subsystem for Opc3-2 solution. ....	75
Table 33 - Specification of monopropellant subsystem's components. ....	75
Table 34 - Inventory mass of hydrazine propellant. ....	76
Table 35 - Structure panels allowed temperature intervals, and average minimum and maximum equipment thermal loads applied over them in one orbit, for OPC3-2. ....	80
Table 36 - OPC3-2 thermal optical coatings properties. ....	81
Table 37 - Environment thermal parameters for OPC3-2. ....	81
Table 38 - Estimated Radiator area and heater power at satellite structural panels, for OPC3-2. ....	82
Table 39 - Nominal mass estimate for the components of the thermal control subsystem of OPC3-2. .....	83
Table 40 - Equipment positioning at satellite panels, for OPC3-2. ....	87
Table 41 - Structure mass breakdown for OPC3-2. ....	92
Table 42 - Candidate launchers for the GSST satellite in configuration OPC3-2. ....	93
Table 43 - Input parameters for the disposal analysis. ....	94
Table 44 - Mass and power budget for OPC3-2. ....	96

## Lista de Siglas e Abreviaturas / LIST OF ACRONYMS AND ABBREVIATIONS

<b>Acrônimo / ACRONYM</b>	<b>Significado / MEANING</b>
ACDH	Attitude Control and Data Handling
AOCS	Attitude and Orbit Control Subsystem
BOL	Begin-of-Life
CCS	Centro de Controle de Satélites
CCSDS	Consultative Committee for Space Data Systems
CCD	Charged Coupled Device
CCS	Centro de Controle de Satélites
CCSDS	Consultative Committee for Space Data Systems
CFRP	Carbon Fiber Reinforced Plastic
CG	Center of Gravity
CGCEA	Coordenação-Geral de Ciências Espaciais
CGETE	Coordenação-Geral de Engenharia e Tecnologia Espacial
ConOps	Concept-of-Operations
CPRIME	Centro de Projeto Integrado para Missões Espaciais
CRC	Centro de Rastreo e Controle de Satélites
DDR	Digital Data Recorder
DOD	Depth of Discharge
DIDAS	Divisão de Astrofísica
DIDEA	Divisão de Eletrônica Aeroespacial
DIDGE	Divisão de Geofísica Espacial
DIDSE	Divisão de Sistemas Espaciais
DIDSS	Divisão de Sistemas Solo
EEL-USP	Escola de Engenharia de Lorena
EM	Engineering Model
EMBRACE	Estudo e Monitoramento Brasileiro do Clima Espacial
EOL	End-of-Life
ERD	Estação de Recepção de Dados (Payload data reception station)
FD	Full Disk
FDIR	Failure Detection, Isolation and Recovery
FM	Flight Model
FOV	Field-of-View
GB	Gigabytes
Gbps	Gigabits per second
GEO	Geosynchronous Orbit
GES	Programa de Pós-graduação em Geofísica Espacial
GPS	Global Positioning System
GSST	Galileo Solar Space Telescope
GTO	Geostationary Transfer Orbit
HEP	High Energy Particle
HR	High Resolution
HGA	High Gain Antenna
INPE	Instituto Nacional de Pesquisas Espaciais
IADC	Inter-Agency Space Debris Coordination Committee
IFSP	Instituto Federal – São Paulo - Jacareí
IR	Infrared
LEO	Low Earth Orbit
LR	Low Resolution
Mbps	Megabits per Second
MLI	Multilayer Insulation Blanket

OBC	Onboard Computer
OSR	Optical Surface Reflector
PCDU	Power Control and Distribution Unit
PI	Principal Investigator
PM	Payload Module
PMM	Plataforma Multi-Missão
QM	Qualification Model
RAAN	Right Ascension of the Ascending Node
ROM	Rough Order of Magnitude
SAG	Solar Array Generator
SESEQ	Serviço de Engenharia de Qualidade
SESMF	Serviço de Manufatura
SGDC	Satélite Geoestacionário de Defesa e Comunicações
SM	Service Module
SSO	Sun-Synchronous Orbit
TC	Telecommand
TCA	Tracking Camera
TM	Telemetry
TT&C	Telemetry, Tracking, and Command
UV	Ultra-Violet
VCDU	Virtual Channel Data Unit
VIS	Visible

# 1 Introduction

---

## 1.1 Background

In 2014, the Space and Atmospheric Sciences General Coordination (CGCEA) of the Brazilian's National Institute for Space Research (INPE) formed a multidisciplinary working group to develop instruments for Solar Observations. The primary aim of this initiative is contributing complementary to the efforts of the solar-terrestrial physics community to address the central unanswered questions on how our nearby Star works. In this framework, INPE's Space and Atmospheric Sciences General Coordination (GCCEA, 2016) requested to the Engineering and Technology General Coordination (CGETE) to perform a feasibility study of a space mission for Solar Observations, the Galileo Solar Space Telescope (GSST) mission. The GSST mission concept study was carried out at INPE's Space Missions Integrated Design Center (CPRIME), from 09 August to 18 December 2017. In this document, we describe candidate system conceptual solutions, designed to meet the objectives of the GSST mission.

## 1.2 Document Structure

In this *Introduction* the overall GSST mission is described, requirements for the system to be conceptualized posed, and the study scope stated. Moreover, a trade-off analysis is performed to identify possible system architectures for the mission, and some of them choose to be further explored. The results of this exploration are briefly summarized at the end of the *Introduction*, while detailed technical information about the elements of those architectures can be found in chapter 4. In chapter 2 the payloads are described. In chapter 3 the concept of operation (ConOps) devised for the mission is presented. Preliminary programmatic, risk and cost analysis are presented in chapter 5, followed by the study conclusions in chapter 6. The results of the cost analysis are not presented in this document. They are reported in a separate technical note delivered to the study's customer.

## 1.3 Summary of GSST mission objectives, requirements, and study scope

The GSST mission is to perform from space, solar observations in high resolution to characterize the evolution of the magnetic structure of the photosphere, chromosphere, transition region and corona and its impact on the Geospace.

Specifically, the mission has three main objectives, with different degrees of priorities:

- 1) Primary: Understand the evolution of the magnetic structures of the outer layer of the Sun;
- 2) Secondary: Understand the Sun's influence on Earth's Climate and;
- 3) Tertiary: Understand the Sun's influence on the Geospace.

To fulfill these three objectives, different kinds of instruments are necessary: For the primary one, imaging cameras in visible and UV spectra; for the secondary, a radiometer; and for the tertiary, particle detectors and a magnetometer. In Table 1 the relation of the instruments to the mission's scientific objectives are identified, and their main performance requirements stated. The information contained in Table 1 was provided by the GSST mission scientific team, headed by Dr. Luis Eduardo Antunes Vieira. From the mission objectives and instruments desired performance, a set of mission requirements and constraints were defined, as shown in Table 2.

The main scope of the GSST study carried out at CPRIME was to *provide system conceptual solutions to the mission, comprising ground and space segments, as well as a first assessment of the development time, risk and ROM cost associated to the proposed solutions.*

Table 1 - Scientific objectives to payload requirements relation.

Scientific Objectives	Phenomena to be addressed	Observations	Payload	Payload performance requirements
<b>Understand the evolution of the magnetic structures of the outer layer of the Sun.</b>	Fundamental plasma processes: reconnection, waves, shocks, particle acceleration and turbulence.	High spatial and temporal resolution observations of the magnetic structure of the photosphere, chromosphere, transition region and corona through the solar cycle.	High resolution UV/VIS imager.	Angular resolution of 0.25 arcsec; Field-of-View: 400x400 arcsec. Wavelength spectropolarimetry on Lyman-alpha (121.567 nm - 1215.67 Angstroms) and Fe 630.25 nm.
	Heating of the outer layers (chromosphere to corona). Solar Dynamo (Global and local).	Wide view observations of the Sun, the magnetic structure of the photosphere, chromosphere, transition region and corona through the solar cycle.	Low resolution, full Solar disk UV/VIS imager.	Field-of-View: 45x45 arcmin. Wavelength spectropolarimetry on Lyman alpha (125 Angstroms). Wavelength spectro polarimetry on Lyman-alpha (125 Angstroms) and and Fe 630.25 nm.
<b>Understand the Sun's influence on Earth's Climate</b>	Effects of the magnetic structure of the outer layers of the Sun on the evolution of the solar eletromagnetic emission and its impact on Earth's atmosphere.	Observation of the variability of the total solar irradiance.	Radiometer.	Spectra-integrated observations.
<b>Understand the Sun's influence on the geospace</b>	Effects observed in the Earth's inner magnetosphere due to interplanetary structures.	Relativistic electron flux dynamics in outer radiation belt.	Electron and proton detector	Distinguish particle species. Distinguish particles energy in two channels Pitch-angle resolution in at least 4 different degrees. Data acquisition in MHz sampling rate.
		Relativistic proton flux dynamics in the inner radiation belt. Energy spectra of the particles.		
		Ambient magnetic field vector variations.	Magnetometer	Tri-axial measurement with sensibility of unities of nT.

Table 2 - Mission requirements and constraints.

Requirement	Description
<b>Functional Requirements</b>	
<b>Performance</b>	Instruments, platform and ground systems must collect and transmit solar and <i>in situ</i> observations to the scientific operations center with sufficient quality to meet the objective goals of the GSST Mission.
<b>Orbit</b>	Solar Visibility (full disk): Imaging in 90% of total mission time; Suggestion: Sun-synchronous orbit - dawn/dusk orbit. Used for solar observing missions such as Yohkoh, TRACE, Hinode and PROBA2. Altitude range: 600–800 km.
<b>Orbit determination</b>	It is necessary to know with 0,1 m/s precision the satellite velocity
<b>Is there any requirement for orbit maintenance</b>	There is no specific requirement for orbit maintenance, other than assure a mission lifetime of at least five years.
<b>Quantization resolution of optical telescope images (bits)</b>	12
<b>Best angular resolution</b>	0.25 arcsec
<b>Satellite absolute pointing knowledge</b>	10 arcsec
<b>Satellite pointing accuracy relative to a reference in the Sun</b>	10 arcsec
<b>Satellite pointing stability</b>	0.833 arcs/s (0.25/3 arcsec - 1/3 of pixel size in 0,1 s)
<b>Pointing determination</b>	0.1 arc-second knowledge after post-processing.
<b>Operational Requirements</b>	
<b>Payloads duty cycle</b>	All payloads should operate continuously around each satellite orbit.
<b>Payloads pointing targets</b>	The optical payloads shall point towards the Sun; The radiometer shall point towards the sun.
<b>Mission control</b>	Use INPE's CRC.
<b>Data availability to users</b>	Data acquired in orbit, shall be delivered to EMBRACE. From there it will be delivered to other end-users.
<b>Design mission lifetime</b>	5 years.
<b>Satellite disposal</b>	The satellite shall be disposed from orbit within 25 years after its operational phase.
<b>Ground infrastructure</b>	Use preferentially INPE's ground infrastructure.
<b>Constraints</b>	
<b>For payloads</b>	Particle detector payload field of view shall not be pointed towards the Earth or Sun at any time.

## 1.4 System drivers and critical requirements identification, trade-off design tree and definition of baseline system concepts to be constructed

From the analysis of possible trade-off options for the mission architecture's elements, it was first identified that six of them could be traded. Three of them would have a big impact on the system performance, cost, risk or development schedule, depending on the solution chosen for the design. These elements, namely, the optical payload architecture, the satellite orbit and the available ground stations to received scientific data from the satellite, were then chosen as the drivers for the system. They were also related to the critical requirements identified for the system: satellite pointing accuracy, payload pointing stability and high rate of scientific data acquisition.

The identified system drivers were then used to build a preliminary trade tree, shown in Figure 1, with possible design options comprising each one of the drivers.

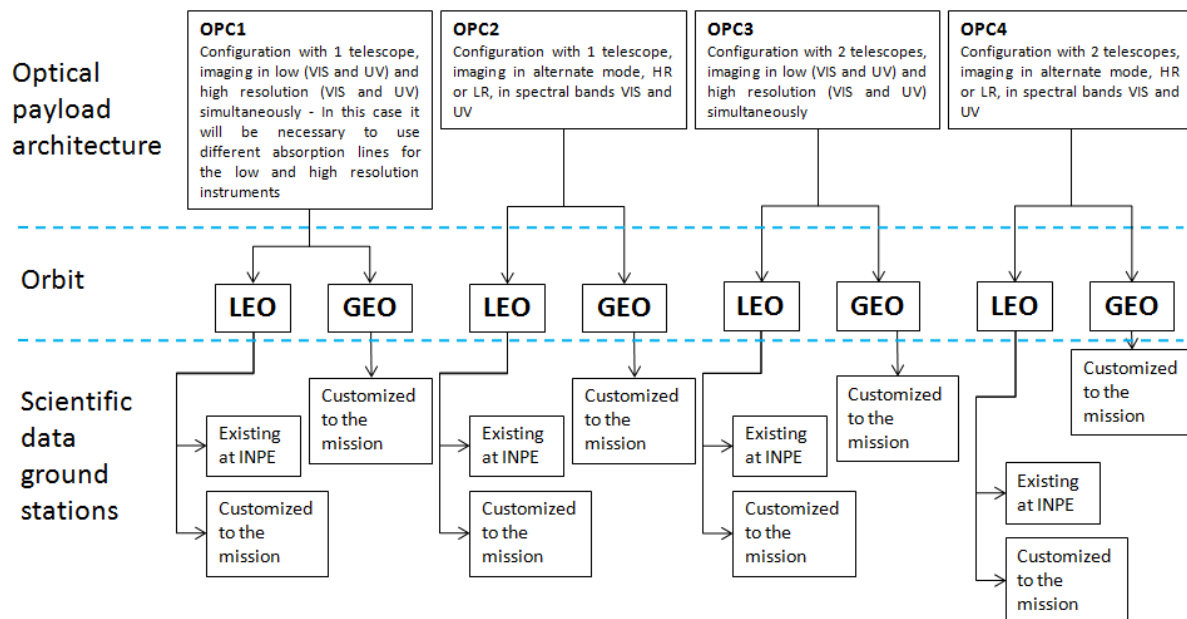


Figure 1 - Preliminary trade tree for the system drivers.

Although it has been first envisioned that the optical payload would consist of one or two telescopes, it was later defined that a solution that better fulfills the mission requirements of imaging the Sun in high definition and also allow the imaging of the Solar the full disk, simultaneously in VIS and UV spectra, would be a solution with three telescopes: One for the high-resolution imaging, and two for the full disk imaging. The sunlight gathered in the high-resolution telescope is split into two light beams that are sent to CCD detectors, one is VIS and the other in UV bands. For the Sun's full disk imaging is used a telescope for VIS and another for UV, as depicted schematically in Figure 2. The optical payload is described in Section 2.1 of this report.



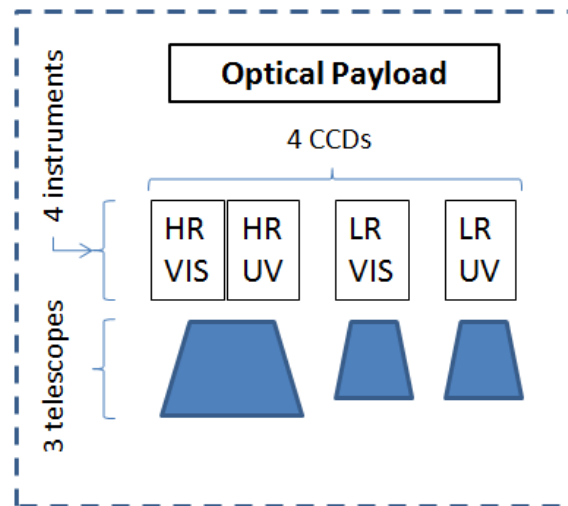


Figure 2 - Optical payload architecture.

For each instrument, it was considered a CCD sensor with 16.8 Mpixels, each of them being quantized with 12 bits resolution, from the functional requirements. With this detector images can be produced at rates of 0,5 or 1,333 images/second, both rates being acceptable from the scientific point of view. In order to reduce the total amount of data to be generated, and hence the need for high onboard data storage and/or capacity of transmission to Earth ground stations, it was decided to use the lower data rate. Moreover, was considered that the data acquired could be compressed two times on board, which also would not compromise its quality from the scientific point of view. Hence, the total raw data rate generated by the optical payload is  $(0.5 \text{ frames/s} \times 4 \text{ CCDs} \times 16.8 \cdot 10^6 \text{ pixels} \times 12 \text{ bits/pixel}) = 403.2 \text{ Mbps}$  or 201.6 Mbps when compressed two times. The data rate generated by the optical payload is by far greater than the ones generated by the other payloads (see Section 2.2 of this report). In fact, it would imply in a huge amount of data to be downloaded to ground stations, when is considered that the mission requires that the Sun would be imaged almost all the time. Considering all payloads and adding margins to take into account auxiliary information sent together with scientific data, and also possible signal degradation during transmission from the satellite to ground stations due, for example, to atmospheric interference, for all subsequent results shown in this report, was considered that the total generation of data from all payloads is 250 Mbps.

From the preliminary trade tree shown in Figure 1, the convenience of using a LEO satellite in terms of cost, risk and development time, and also considering the operational requirement of using preferentially INPE's ground infrastructure, it was first performed an analysis in order to verify possible combinations of onboard data storage, availability of ground stations and data transmission from the satellite that would satisfy the mission, if the LEO orbit was chosen. It was found that by using a polar station, an architectural communication configuration using only two ground stations is feasible, as shown in Figure 3.

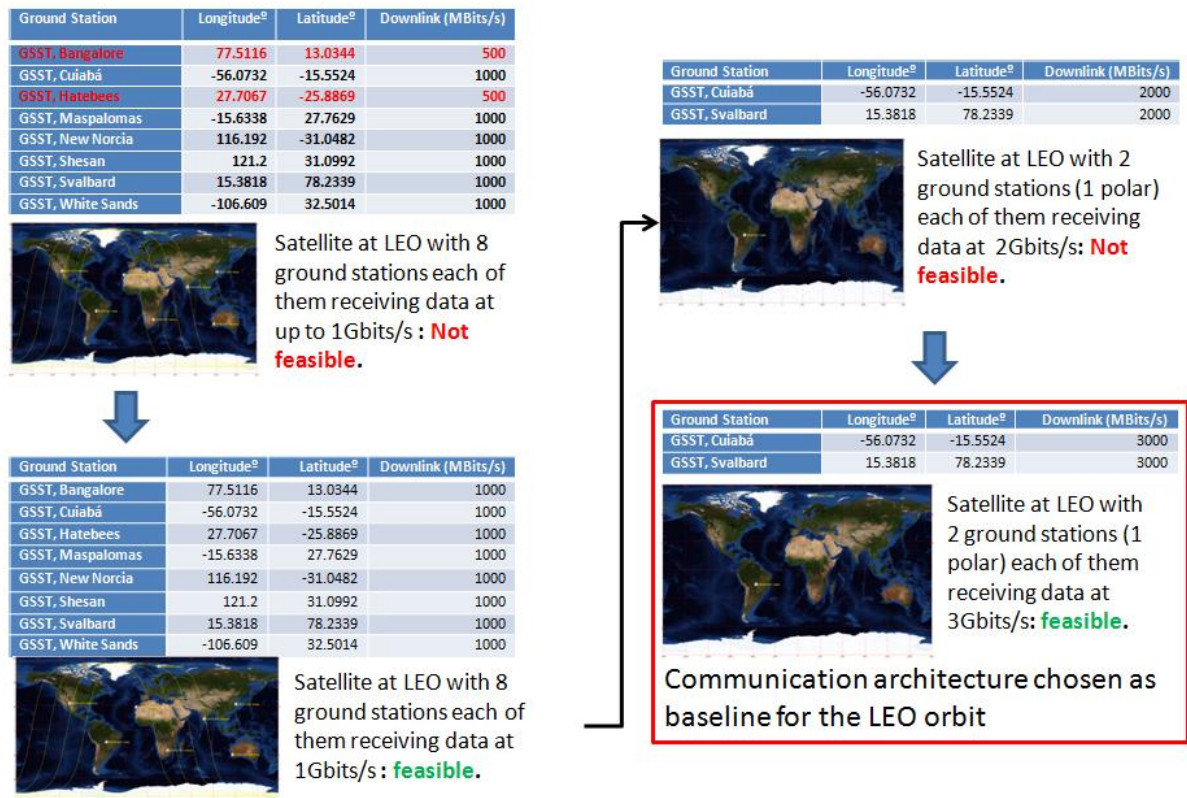


Figure 3 - Tradeoff of number and position of ground stations versus data transmission rate between them and the satellite at LEO, considering an onboard data storage of 4 Gbits.

The communication architecture using two ground stations for scientific data download was then considered as the baseline for the GSST mission using a satellite in LEO. It is important to note that the "two-ground station" solution is only valid if one of them is located in a polar region. For the purposes of the present study, the Norwegian Svalbard polar ground station was used as a reference, but others could be used if available. Other implication of using a satellite in LEO is that the existing INPE's ground infrastructure is not sufficient to meet the mission needs. The trade tree presented in Figure 1 must then be updated to reflect the consolidation of the optical payload architecture described in Figure 2 and the conclusion that a dedicated ground infrastructure for the mission with a satellite in LEO is needed. The refined trade tree is shown in Figure 4. Note that OPC3 now refers to the consolidated optical payload configuration.

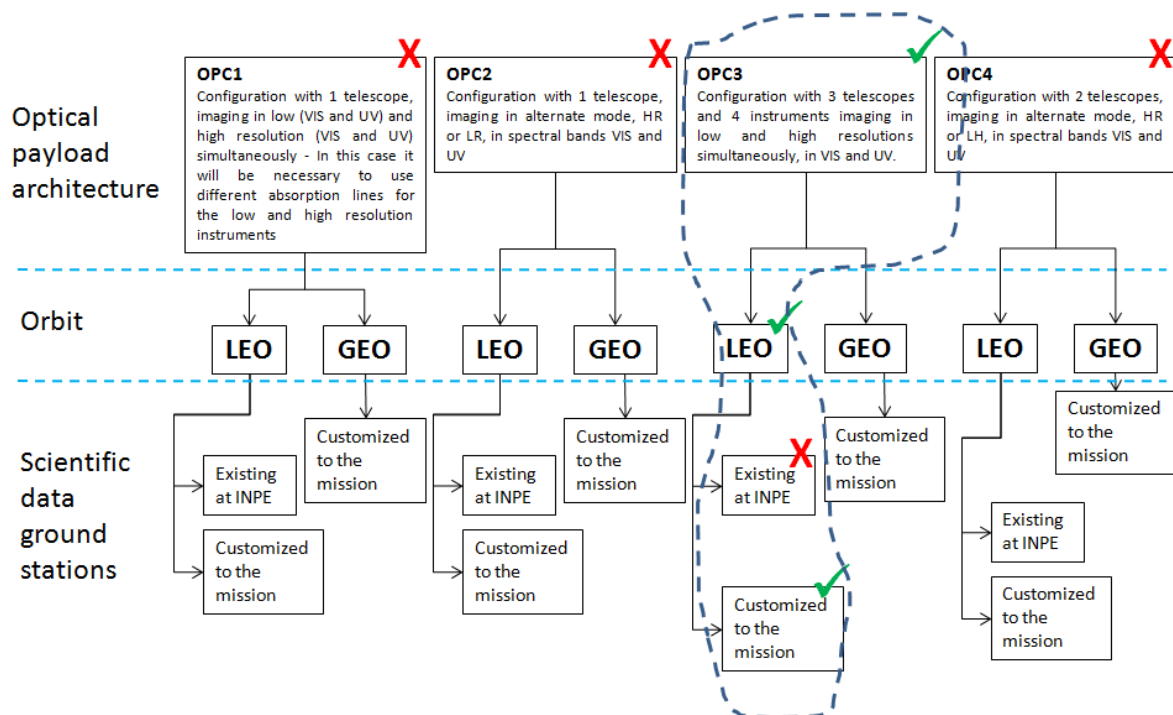


Figure 4 - Updated system drivers trade tree showing defined option for further analysis. The options marked with a red X were not considered viable or worth for further analysis on the scope of the present study.

As presented in Figure 4, an alternative option for the satellite orbit would be to put it in GEO. This would allow a permanent communication link between the satellite and the ground station which, in principle, could be the INPE's one existing in Cuiabá. This solution would also require a much lesser capacity for onboard data storage than the one needed for the LEO option. On the other hand, a GEO satellite would be much more complex and costlier to build than a LEO one. An intermediate option for the communication architecture would be to use a LEO satellite that could relay the scientific data to a GEO satellite which then send the data to the ground station.

A preliminary investigation of this "relay option" for the communication architecture, considered two hypothetical possibilities: 1) a scenario where the GSST satellite uses a microwave link to communicate with a GEO satellite in an orbital position similar to the SGDC satellite and; 2) a scenario where the GSST satellite uses Alphasat (Inmarsat-XL) as the relay satellite, through an optical communication link.

The first scenario can be feasible if a communication link between the GSST and the relay GEO satellite can be established at 600 Mbps, in 35 GHz, assuming a perfect pointing of the antennas used for the communication between the satellites. The necessary transmission power would be 200 W. Due to the orbital characteristics of the satellites, the link is established in a time window lesser than 45 min, and that's why a higher transmission data rate between the satellites, than the rate of scientific data acquisition, is required. Moreover, onboard data storage for the LEO satellite is needed, which is estimated in at least 1.5 Tbits. If there is no capacity for onboard data storage in the GEO satellite, the transmission rate between it and the ground station must be at least 600 Mbps, which can be in X or Ka bands. If X band is used, the existing INPE's X-band antenna at Cuiabá could be used for reception of the scientific data, provided an upgrade is performed on its associated communication equipment.

In the second scenario, the relay can be done via an optical communication link between the GSST in LEO and a GEO satellite such as Alphasat or, in the case of an eventual international cooperation with ESA, satellites of the European Data Relay System (EDRS). Due to the high rate of the optical link, in the case of Alphasat 1.8 Gbps, the need for onboard data storage in the LEO satellite would be lesser than the one needed if a microwave link were used. Moreover, the optical technology allows a lesser power consumption for the communication equipment and transmission signal. On the

other hand, the use of a solution that uses Alphasat or the EDRS would depend on the availability of such assets to the GSST mission. Even in this case, it must also be pointed out that the scientific data sent through the GEO satellite would be, in principle, first downloaded to a ground station not belonging to INPE, which would imply in a more complex communication architecture and possible increase of the mission's operational cost. In fact, the "relay option" for the GSST requires a deeper analysis of the availability of relay satellites for the mission, either using a microwave or optical links, which are very uncertainty as of today. Hence, for the purposes of the present study, no further analysis was performed for the "relay option".

In Figure 5 is shown an updated version of the trade tree that considers now only the branch related to the OPC3 payload.

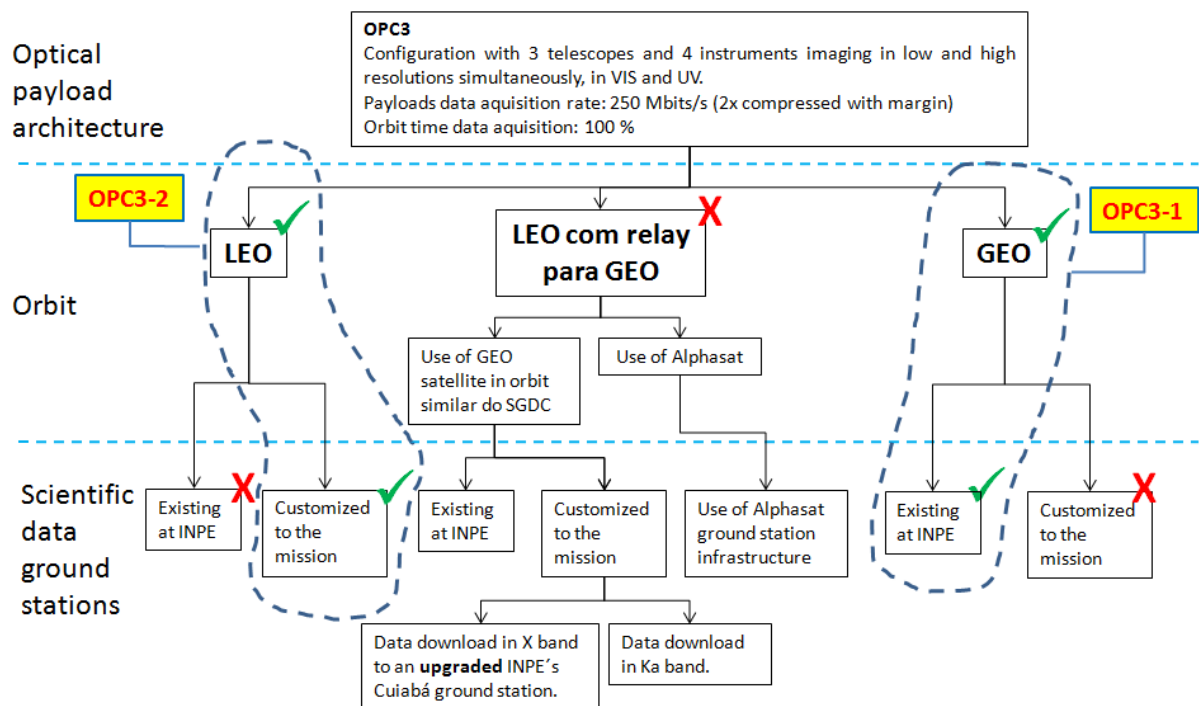


Figure 5 - Updated system drivers trade tree. OPC3-1 and OPC3-2 are the options chosen for further analysis on the scope of the present study.

From Figure 5 it can be seen that, after a tradeoff analysis over different combinations of the system drivers, two options were chosen for the construction of complete system conceptual solutions. They were named as OPC3-1 and OPC3-2. Both consider the same optical payload architecture, OPC3 (see Figure 2), but different options for the orbit and ground station for receiving scientific data. In Section 1.3 a summary of the system solutions conceived are presented. A detailed description of these solutions is shown in Sections 2 through 4.

## 1.5 Summary of baseline system concepts

As described in Section 1.2, derived from the system drivers, a tradeoff tree of possible system configurations was built, and two candidate baseline solutions were chosen to be constructed. They represent very different system concept solutions for the mission. This is the result of the possible orbits envisioned for the GSST satellite, LEO or GEO. In Figures 6 to 8, summarized information on the system solutions derived from the adoption of an LEO or GEO orbit are shown for some elements of the mission architecture. They highlight the main differences between the conceived system candidate solutions for the mission.

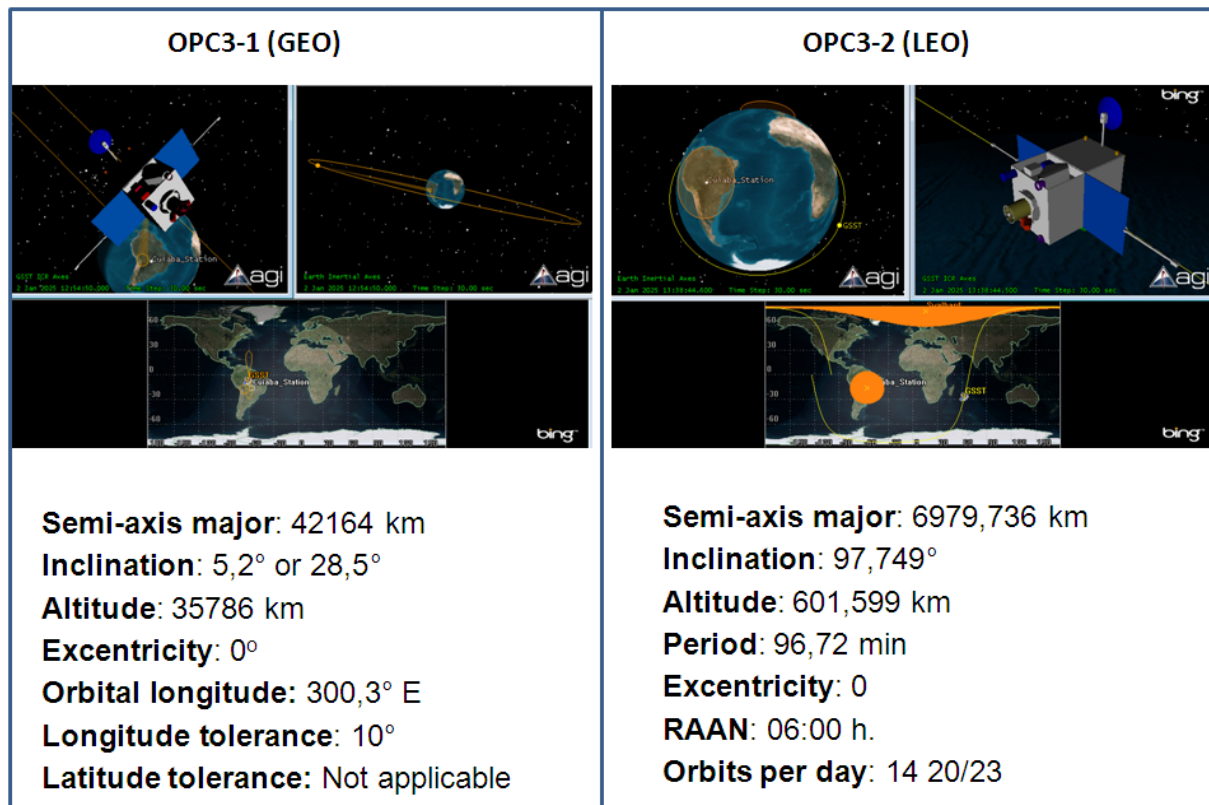


Figure 6 - Summary of orbit parameters for OPC3-1 and OPC3-2.

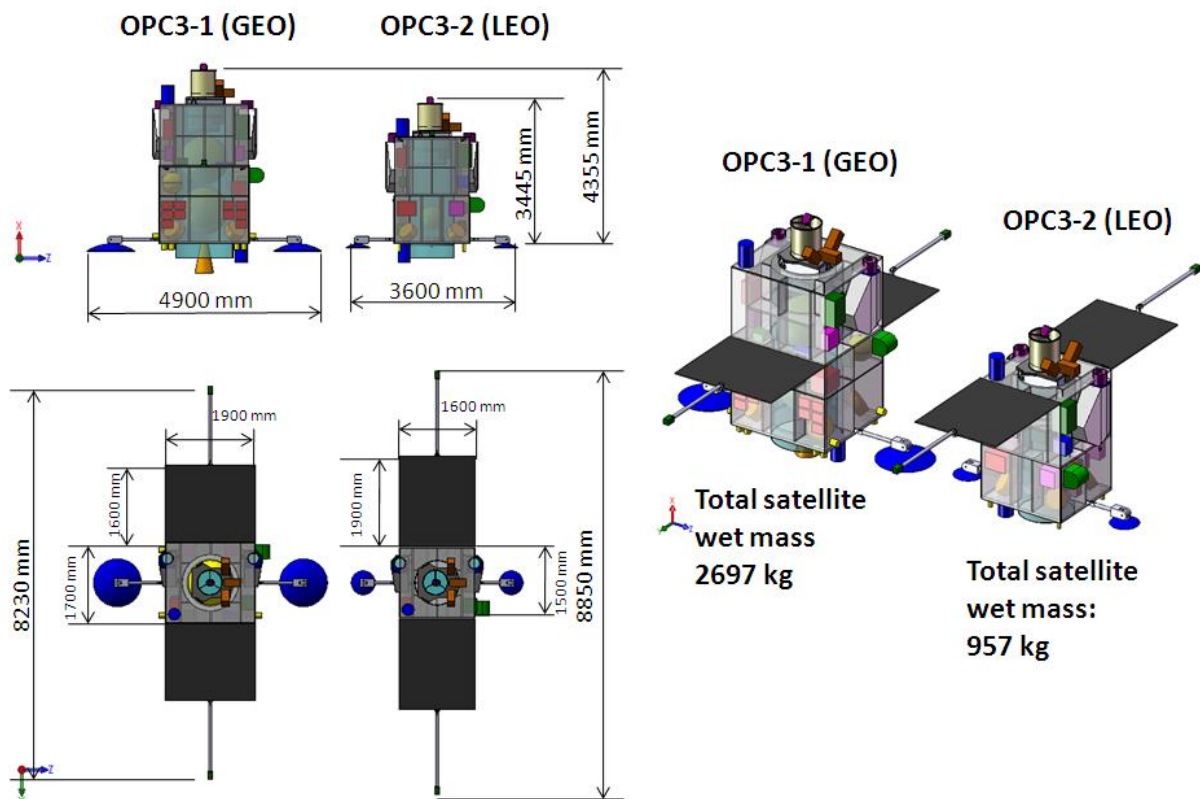


Figure 7 - GSST satellite layout concepts for OPC3-1 and OPC3-2.



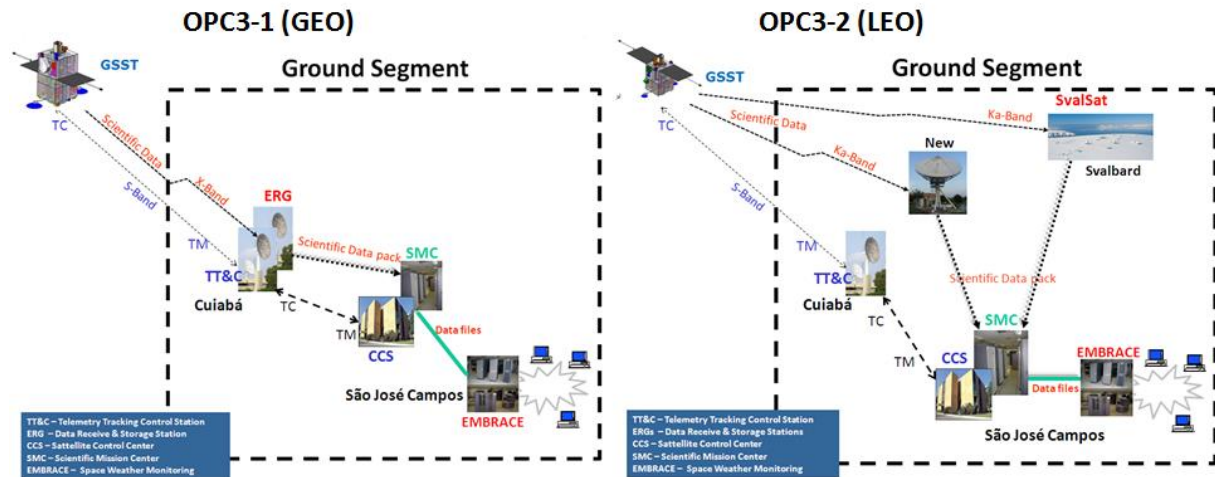


Figure 8 - Ground segment conceptual architectures for OPC3-1 and OPC3-2.

## 2 Payloads conception and description

The payloads of the GSST satellite are composed of six instruments. They can be grouped in imaging and non-imaging payloads. The concept of the equipment for the non-imaging payloads was not on the scope of the present study. Hence, for the purposes of the satellite layout conceptual design, they were considered as “boxes” with a given mass and size dimensional envelop, plus a given power consumption. Requirements for pointing and positioning associated to some of them were also considered for the setting of the layout. In Sections 2.1 and 2.2 the conceptual design of the imaging payloads and a brief description of the non-imaging payloads are shown, respectively.

### 2.1 Approach for the Imaging payloads

The imaging payloads, also referred as optical payload in this document, were designed to provide remote sensing estimates of the magnetic field structure of the solar surface and outer layers of the solar atmosphere based on observations of the polarization of the light at different wavelengths (spectropolarimetry) of the electromagnetic lines sensitive to Hanle and Zeeman effects.

The main requirement for the imaging payloads is the capability of capturing high resolution and full disk spectropolarimetric images in two regions of the solar spectrum that trace the magnetic field structure from the photosphere to the upper chromosphere. Here we proposed as candidates to estimate the magnetic field vector in the photosphere the Fe I 630.15 nm and 603.25 nm absorption lines, while the Mg-II 279.553 nm emission line was proposed to trace the magnetic and thermal structure in the region that spans from the photosphere to the upper chromosphere. Other spectral lines can be employed taking into account among several constraints the balance of the flux density and the efficiency of the optical components.

To better comply with these basic requirements, it was decided to design two different sets of cameras, one to meet the high-resolution requirement (HR Camera), and other to meet the full disk one (FD Camera).

The spectroscopy analyzes near the selected spectral lines is proposed to be done employing tunable Fabry-Perot interferometers.

The Stokes parameters, which comprise a four-component vector that completely characterizes the polarization of the light beam, is proposed to be estimated for each camera employing a polarization analyzer package. The analyzer packages are based on variable retarders and linear polarizers to untangle the circular and linear polarization states of the light beam needed to estimate the Stokes parameters.

### 2.1.1 HR Camera

For the high resolution (HR) images, it was conceived a single 500mm aperture telescope as the input optics, in which is attached two spectropolarimeters for the two different spectral regions. With the aperture fixed, the telescope focal length was defined in order to have the maximum F/# that can give a reasonable contrast in the Nyquist frequency for a red spectral band. Considering this, the HR instruments ended up with an effective focal length of 10 m and F/20. This gives a spatial resolution of 0.25 arcsec per pixel.

On the HR telescope it is also attached an auxiliary instrument, a “tracking camera” (TC), that will be used as a sensor for the satellite attitude control in the imaging mode, and also as the sensor for the imaging stabilizer mechanism used in each HR instrument, to ensure the acquisitions of sharp images.

The two HR instruments and the TC are all-reflective designs. The complete optical path for each HR instrument and the TC are composed of five mirrors with optical power. These mirrors are all sections of conic surfaces. The two instruments and the tracking camera share the primary mirror, with 500mm diameter, and the secondary mirror. The three other dedicated mirrors with optical power are equal in the three different optical paths in the HR Payload. To make the system compact, was used other three flat folding mirrors in each instrument optical path and four in the TC patch. The last folding mirror on each spectropolarimeter is considered to be a tip/tilt mirror driven by piezoelectric actuators intended for the imaging stabilization.

The primary mirror is considered to be made of Zerodur glass ceramic material and to have a dielectric broadband mirror coating. The secondary one is considered to be made of Fused Silica and have a dielectric mirror that only reflects a small portion of the spectrum, with a spectral bandwidth of around 50nm centered on the two bands of interest. The radiation that is not reflected by the secondary mirror, is transmitted through it and the largest amount of energy, not absorbed by the glass, is reflected out from the telescope by the heat rejection unit, positioned in 90 degrees with the optical axis. The Primary and secondary mirrors are arranged in a Cassegrain like configuration, which forms an intermediate aberrated image. The beam splitters are placed before the intermediate image is formed. The polarization package for each spectropolarimeter is placed close to this intermediate image. The polarization package for the UV band is composed of two mechanical rotary retarders and one fixed linear polarizer. Two tunable liquid crystal retarders and a linear polarizer form the red band polarization package.

The other mirrors in the system are all considered to be made of Zerodur with dielectric coating optimized for the maximum reflectance for the band of interest in its own specific optical path. All the plate beam splitters used in the system, as well as all the plane parallel plates used to compensate astigmatism introduced by the beam splitters, are considered to be made of Fused Silica with the appropriate coating to split the bands or provide the maximum transmittance (anti-reflex coating).

The third mirror with optical power, in each optical path, is responsible for collimating the light from the intermediate image, formed by the first two mirrors. This third mirror also provides a real pupil image. Tunable vacuum-gap Etalons (Fabry-Pérot interferometers) together with an ultra-narrow band filter, are placed in these collimated light beams in both polarimeters paths, with the Etalon gap centered in the pupil image. The pupil image has a diameter of around 33mm. In this way, the first three mirrors form an afocal system with 15x demagnification.

The collimated light is then reimaged in the CCD by the two remaining mirrors with optical power. The image formed is very well corrected, close to the diffraction limit for the whole field of view for all the optical paths.

The HR payload mechanical concept considered a lightweight mirror substrate for the primary and a structure made of carbon fiber reinforced with plastic (CFRP). The payload main structure

supports the primary mirror in one side and the instruments in the opposite side. We call this main structure the optical bench.

One of the highest resolution area detectors ever flown in a space mission was considered to be used for the HR payload spectro-polarimeters. Each CCD detector array has  $4096 \times 4096$  pixels with a  $12\mu\text{m}$  pitch. For the tracking camera, on the other hand, we considered a much smaller detector, with  $50 \times 50$  pixels, but with a high-frequency image rate, in the order of 500 Hz.

A dedicated electronic box for each CCD is considered. This electronic box drives the CCD, capture and digitizes the images. The digital image captured is sent by a space wire to the Payload Central Unit Box, which is responsible to receive the images from all the CCDs (from the HR and FD payloads), compress and pack the data to send it either to the Digital Data recorder (DDR) or to the data transmitter that download the images to the ground.

Apart from the CCD boxes, the HR payload also has an electronic box to control the etalons and the retarders of each spectropolarimeter.

In Figure 9 and Figure 10 are shown respectively the optical design and the conceptual mechanical design for the HR payload, with some parts identified.

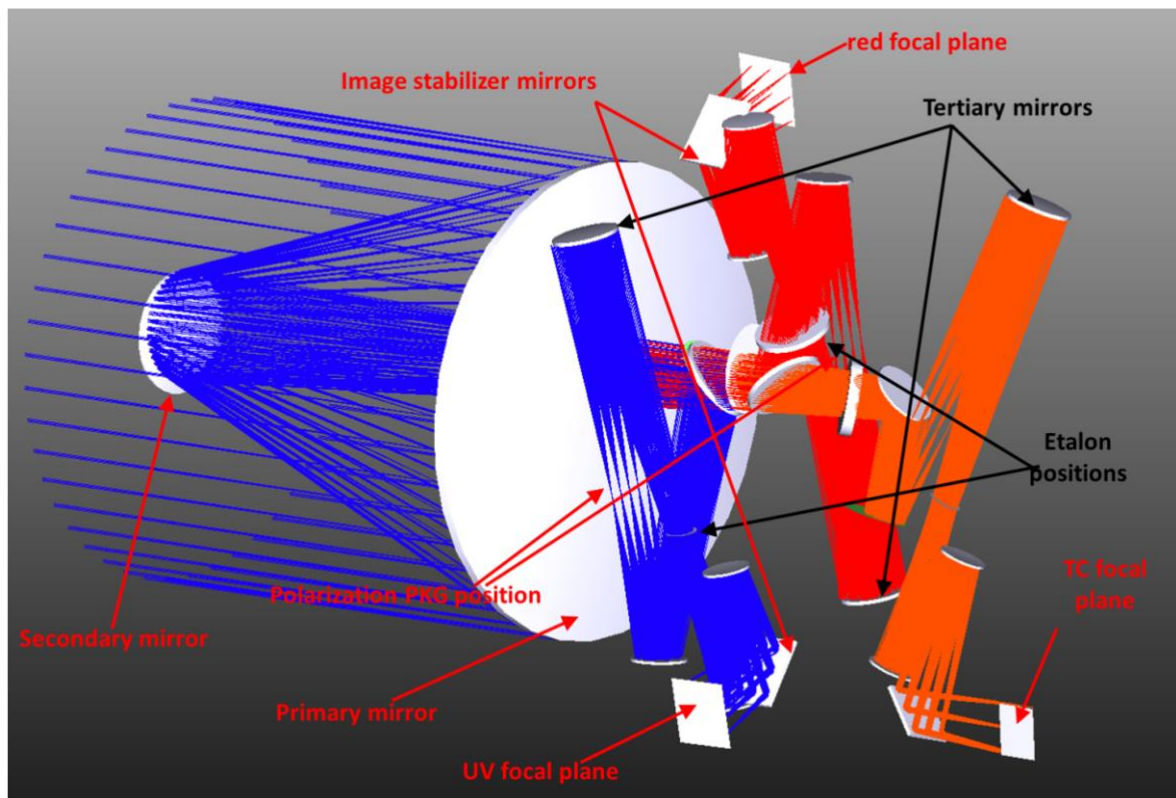


Figure 9 - Optical design layout of the HR payload.



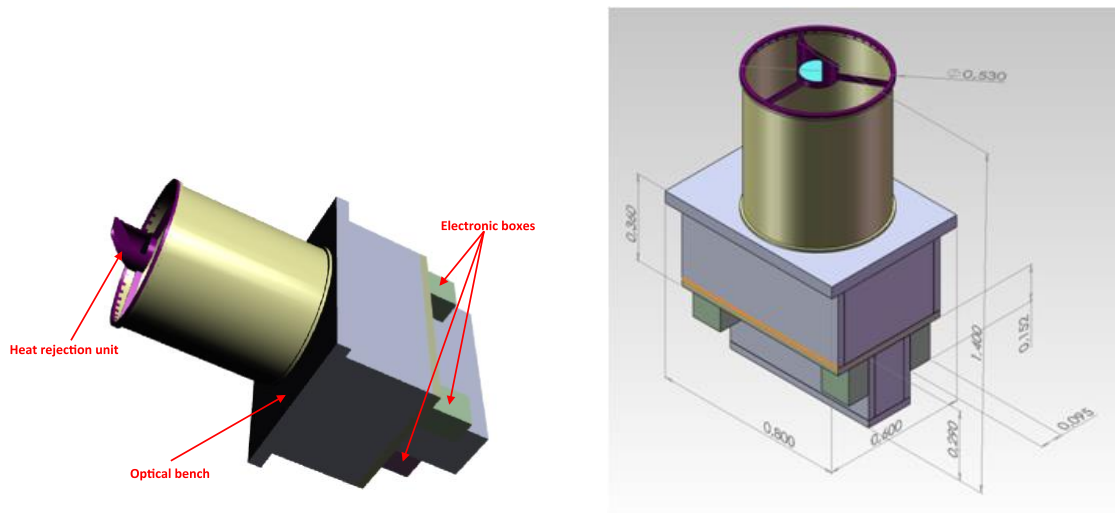


Figure 10 - Conceptual mechanical design for the HR payload. Dimensions in mm.

The main characteristics of the HR camera are summarized in Table 3.

Table 3 - Main characteristics of the HR camera.

Optical system	All-reflective off-axis system. After the secondary mirror, two beam splitters divide the light in three optical paths, one for each instrument.
Primary mirror	50 cm aperture diameter, ultralow TCE light weight glass ceramic.
Scientific Instruments	1) UV spectro-polarimeter (SP); 2) Red spectro-polarimeter;
Pointing instrument	Tracking camera (TC).
Spectral bands.	UV SP: 279.553nm (Mg-II) (279.4nm-280.4nm) Red SP: 630.25nm (Fe-I) (630.22nm-630.26); TC: 633nm-643nm.
FOV	UV and Red SP: 1024x1024 arc-sec; Tracking camera: 12.5 x 12.5 arc-sec.
Effective f ratio	20
Polarization Packages	UV SP: two rotary retarders and one linear polarizer; Red SP: two liquid crystal retarders and one linear polarizer.
Wavelength scanning method.	UV and Red SP: vacuum gap tunable Fabry-Perot interferometer.
Angular resolution	0.25 arc-sec per pixel for all instruments.
Frame rate	UV and Red SP: 0.5Hz; TC: > 500Hz.
Temporal resolution	2.5 minutes
SP Data rate Not compressed	UV: 96Mb/s; Red: 96Mb/s.
Power	55 W
Mass	88,6 kg

### 2.1.2 Full Disk LR Cameras

The same CCD detectors considered for the HR spectropolarimeters were also considered for the full disk payload (FD) instruments. The requirement for the field of view of these instruments is 1.4 times the solar disk size, what gives +/- 0.378 deg. With the considered detector size and this FOV, the

instrument effective focal length is 3.725m. The aperture needed for a system with the same F/# used for the HR payload (F/20) is approximately 186.25mm.

With this much smaller aperture, was decided that a better option would be to have two completely independent FD cameras, one for the UV and the other for the red, in exactly the same central wavelength used in the HR camera spectropolarimeter instruments. The optical design architecture for these FD cameras is very similar to the HR payload. The optical design of the UV and the Red instruments are identical, they only differ in the polarization package, narrow band filters, and coatings used in the mirrors. The UV considers mechanical rotary retarders and the red uses crystal liquid retarders. The optical design is composed of five mirrors with optical power; all of them are sections of conic surfaces and two folding mirrors. The two first mirrors form an intermediate aberrated image; the third mirror collimates the beam with a real pupil image with a diameter of 18.22mm. Finally, the last two mirrors with optical power form a diffraction-limited image on the CCD detector.

In order to always keep the Sun-centered in the FD cameras FOV during the satellite-imaging mode, independent of its pointing direction, a pair of rotating optical wedges was considered in the entrance for each camera as a pointing mechanism. These fused silica wedges also have a second function, to reject the energy out of the spectral band used in each instrument. For that, dielectric coatings are considered in the first and second surfaces of the first wedges. The IR energy is rejected by the first surface, while the second surface lets only a bandwidth of 50nm, or so, enters into the system.

Each FD camera has two electronic boxes, one for driving the CCD, identical to the ones used in the HR payloads and another to control the etalon, the retarders, and the optical wedges.

The FD cameras mechanical concept considers mechanical supports for each optical element, which are all connected to each other through a CFRP structure. An optical bench also made of CFRP, serves as the support for this truss structure and for the electronic boxes, as well as the interface between the instrument and the spacecraft.

In Figure 11 and Figure 12 are shown respectively the optical design and the conceptual mechanical design for the FD payload cameras.

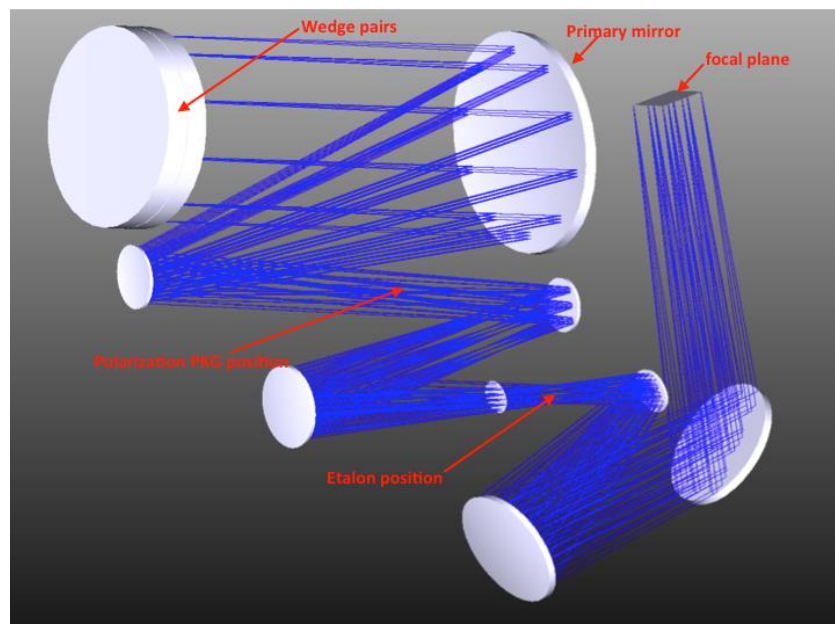


Figure 11 - Optical design layout for the FD cameras.

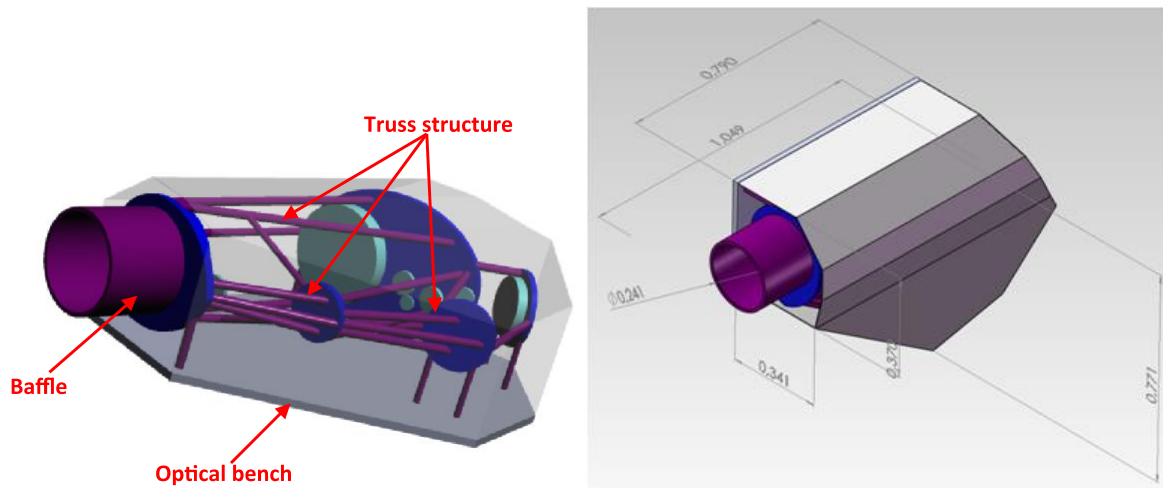


Figure 12 - Mechanical conceptual layout for the FD cameras. Dimensions in mm.

The main characteristics of the FD cameras are summarized in Table 4.

Table 4 - Main characteristics of the FD cameras.

Optical system	Two independent SP for each spectral region. All-reflective off-axis system with a wedge pair in the entrance for pointing.
Entrance Pupil Diameter	186.25mm.
Instruments	1) UV spectro-polarimeter; 2) Red spectro-polarimeter;
Spectral bands.	UV SP: 279.553nm (MgII) (279.4nm-280.4nm) Red SP: 630.25nm (Fe-I) (630.22nm-630.26);
FOV	UV and Red SP: 2721.6 x 2721.6 arc-sec.
Effective f ratio	20
Polarization Packages	UV SP: two rotary retarders and one linear polarizer; Red SP: two liquid crystal retarders and one linear polarizer.
Wavelength scanning method.	UV and Red SP: vacuum gap tunable Fabry-Perot interferometer.
Angular resolution	0.664 arc-sec per pixel.
Frame rate	0.5Hz;
Temporal resolution	2.5 min
SP Data rate	UV: 96Mb/s;
Not compressed	Red: 96Mb/s.
Power	25 W
Mass	46,7 kg

## 2.2 Approach for the non-imaging payloads

The non-imaging payloads are composed of three equipment: a radiometer, a particle detector, and a magnetometer. They are now in different phases of development and in the scope of the present study, they are considered as “boxes” with a defined nominal mass, volume and power consumption. These data, together with pointing requirements for some of them, were used to define the concept design of the power subsystem and mechanical layout of the GSST satellite. The main characteristics of the non-imaging payloads are described in Table 5.

Table 5 - Main characteristics of the non-imaging payloads.

Parameter	Payload		
	Radiometer	High energy particle detector	Magnetometer
Mass (kg)	3.5	10.0	Electronics: 3.0 Booms (each): 10.0 Sensors (each): 1.0
Power consumption (W)	10	10.0	3.0
Volume envelope (Length x Width x Height) in mm	500x300x300	300x300x300	Electronics: 200x200x150 Booms length: 3000 Sensors: 150x100x100
Layout requirement	Radiometer FOV must be always pointed towards the Sun.	Detector FOV must not point to Earth or Sun at any time.	Magnetometer sensors must be at least 3 m far from the satellite's body.

### 3 Concept of operations analysis

Assuming the same optical payload architecture (Figure 2) is carried on board either the candidate solution OPC3-1 (GEO) or OPC3-2 (LEO), they are considered similar in terms of satellite service control and scientific data flow needs, from operations analysis purposes, once the optical payload is required powered ON in SUNLIGHT for all orbits and the total raw data rate generated is  $(0.5 \text{ frames/s} \times 4 \text{ CCDs} \times 16.8 \cdot 10^6 \text{ pixels} \times 12 \text{ bits/pixel}) = 403.2 \text{ Mbps}$  or 201.6 Mbps when compressed two times. A huge amount of data to be downloaded to ground stations is because the mission requires that the Sun would be imaged almost all the time.

The diagram presented in Figure 13 comprises the two main branches to be addressed in the concept of operation analysis.

The satellite service represented in the left branch highlights the mission elements involved in tasks of sending telecommand (TC) to satellite and receiving satellite Telemetry (TM). This chain, at upload direction, counts on the Ground Stations available for TT&C activities that support the Satellite Control Center on the execution of the flight plan, which contains the TC to be sent to the satellite. The flight plan is prepared in the Mission Center context. At download direction, the TM service data packages from the satellite are received at Ground Stations and transferred by the Satellite Control Center to the mission engineering team for satellite health analysis purposes. Also, it makes some satellite information (TM) available to Mission Center for scientific analysis purpose.

The scientific data chain is represented in the right branch in Figure 13. It highlights the ground elements involved for receiving raw scientific data acquired by the satellite payload. Whenever the satellite passes over a reception ground station, the raw scientific data packages are transmitted to ground and transferred to the Mission Center for data pre-processing, which adds supplementary satellite information (TM) necessary to the scientific end users. Such information will be delivered to the EMBRACE data center<sup>1</sup>, which is an existing INPE's ground infrastructure that supports data interaction with different mission PIs and data dissemination to the scientific community. In this chain, it is also important to highlight the PIs relationship with the Mission Center for the purpose of flight plan collaborative construction.

<sup>1</sup><http://www2.inpe.br/climaespacial/portal/en/>

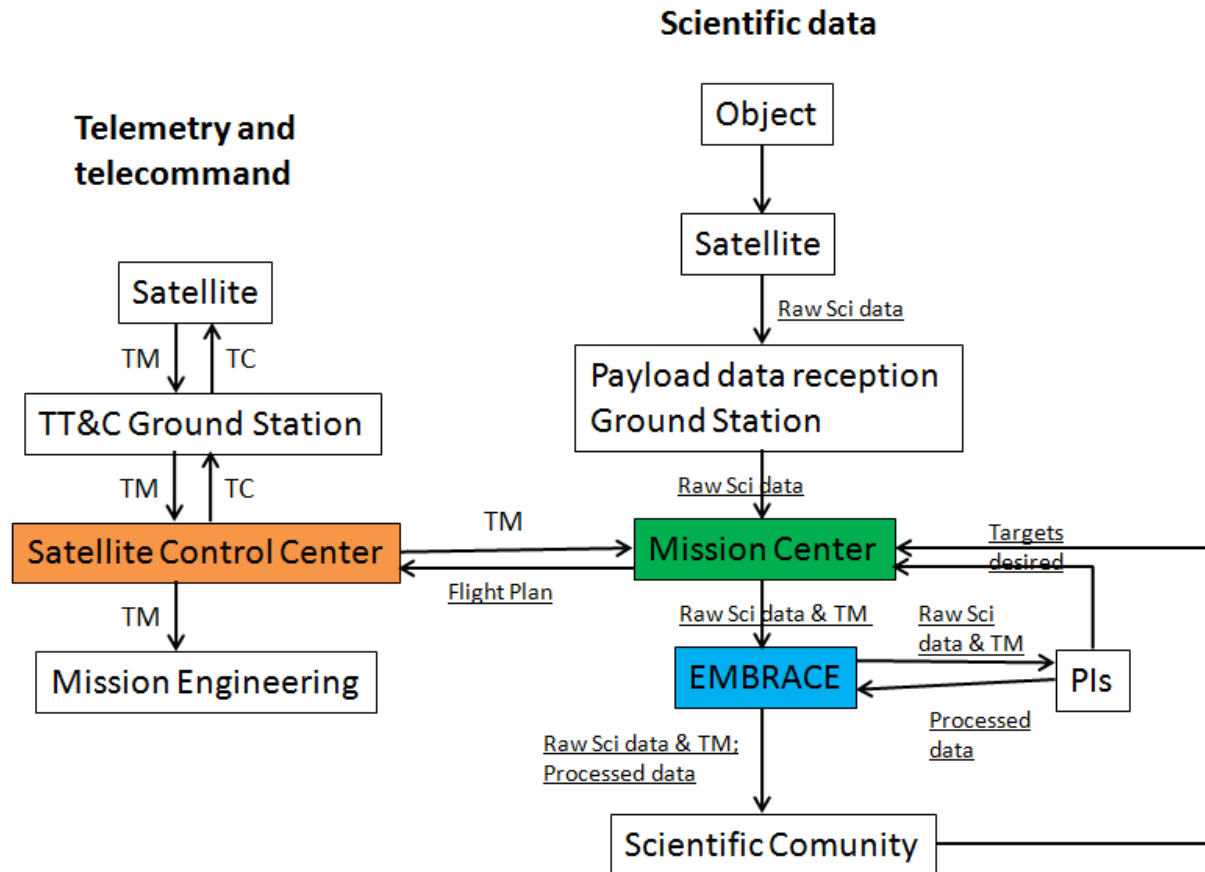


Figure 13 - Flow of science and service data between the GSST satellite and the mission's ground segment.

The use of existing INPE's ground infrastructure for the Telemetry and Telecommand chain is feasible to both candidate solutions OPC3-1 (GEO) and OPC3-2 (LEO). However, for the scientific data transmission, different solutions are needed as discussed in section 1.2.

Regarding OPC3-2 (LEO), two Ka-band Tx antennas onboard satellite were considered to operating in a supplementary way, depending on the pointing to the ground. Each antenna can download at 3Gbits/s and is powered ON 20 min for all orbits either in Eclipse or Sunlight station visibility in order to download payload acquired data, complying 201.6 Mbps data rate generated after compressing. As the baseline for the GSST mission using a satellite in LEO, two ground stations using Ka antenna are needed for scientific data download at 3Gbits/s, considering an onboard data storage of 4 Tbits. It is a valid solution only if one of them is located in the polar region. For the purposes of the present study, the Norwegian Svalbard polar ground station was used as a reference, but others could be used if available. Other implication of using a satellite in LEO is that the existing INPE's ground infrastructure is not sufficient to meet the mission needs. Thus, a Ka-band antenna infrastructure shall be added to the existing INPE's data reception ground stations for GSST scientific data with a satellite in LEO, in addition to the polar ground station.

Regarding OPC3-1 (GEO) in particular, two X band Tx antenna onboard satellite were considered operating in a supplementary way, depending on the pointing to the ground. Each antenna can download at 300Mbits/s and is powered ON all the time during its visibility to the ground station, Eclipse or Sunlight, in order to download the payload acquired data, complying 201.6 Mbps data rate generated after compressing. As the baseline for the GSST mission using a satellite in GEO, the X Band reception antennas existing at INPE's ground stations facilities, with appropriate upgrades, can be used for scientific data download at 300Mbits/s. Although such antennas will be probably shared with other INPE's missions, their use is feasible because there is a data storage of 4 Gbits available on board.

CPRIME's concept of operations simulator (FORPlan) was used to dynamically verify the proper balancing of power generation/consumption and science payload data download/onboard storage, as well as visualization of equipment modes of operation along the orbit. For OPC3-1 and 2, it was observed that the power and data balance closed for the concept of operations and communication architectures envisioned for both options. In Figure 14 is shown a screenshot of the FORPlan simulator for OPC3-2.

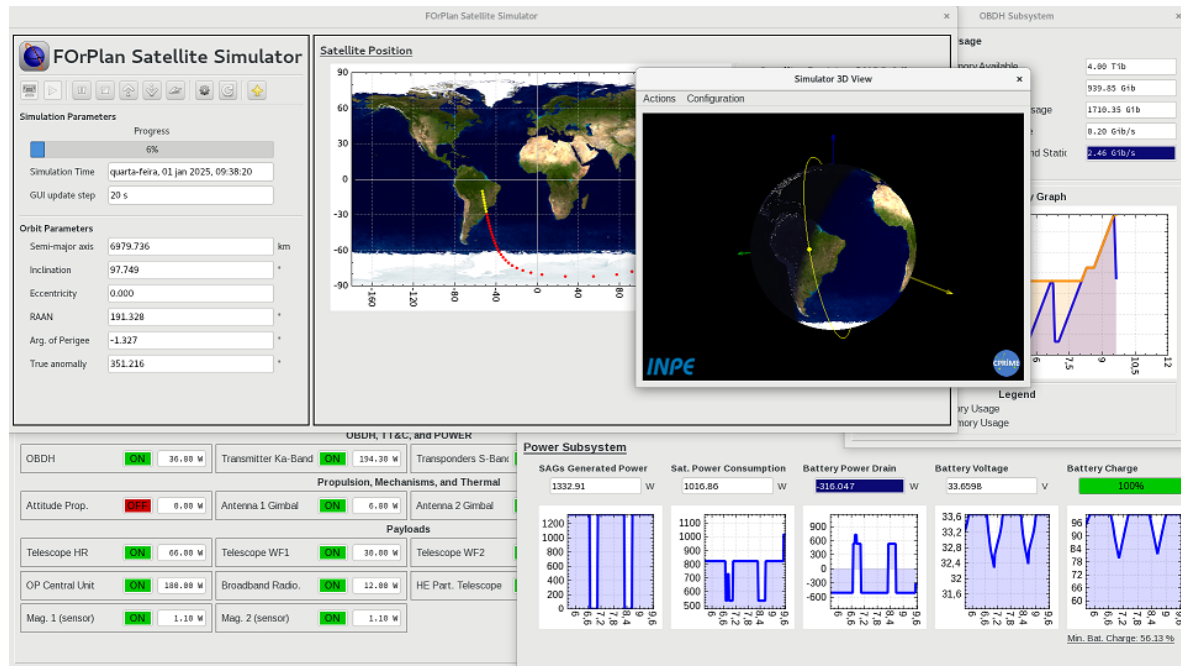


Figure 14 - Screenshot of FORPlan concept of operations simulation, showing the status of power and data balance, as well as the GSST satellite's states of functioning along the orbit, for the OPC3-2 option.

## 4 Candidate system concept solutions for the mission

In this Section candidate conceptual solutions for the elements of the GSST mission architecture, are presented for the two options selected from the design drivers tradeoff analysis presented in Section 1.2, OPC3-1 and OPC3-2.

### 4.1 OPC3-1

#### 4.1.1 OPC3-1: Orbit Analysis

The OPC3-1 is a Geostationary mission. Hence, only one type of orbit is possible. The semi-major axis shall be 42,164 km and the inclination shall be as closest as possible to 0°.

After a careful analysis of the available sites to launch a geostationary mission, it was verified that the orbit inclination after separation would be between 5° (if launched from Kourou) and 28.5° (if launched from Cape Canaveral). For this mission, it was decided not to do a maneuver to correct the orbit inclination, which will highly decrease the propulsion subsystem mass, yielding a more economical solution. Thus, each analysis shall consider the worst-case scenario in terms of the residual inclination between 5° and 28.5°.

The right ascension of the ascending node (RAAN) shall be selected to reduce the eclipse time. This is accomplished if it is placed at 6:00 AM.



The last variable is the position of the satellite in the orbit or the true anomaly. In this case, it will depend on the available geostationary slot. Since it is not possible to acquire in this phase any additional information about it, each discipline must also consider the worst-case scenario.

The orbit parameters summary for OPC3-1 can be seen in Table 6.

Table 6 - Orbit parameters summary for OPC3-1.

Parameter	Value
<b>Semi-major axis</b>	42,164 km
<b>Orbit period</b>	≈ 24h
<b>Eccentricity</b>	≈ 0.0
<b>Inclination</b>	Between 5° and 28.5°
<b>RAAN</b>	6:00 AM to reduce the eclipse time
<b>True anomaly</b>	Depends on the available slot.

#### 4.1.1.1 Eclipse Time

The eclipse time for the cases in which the orbit inclination is 5° and 28.5° can be seen, respectively, in Figure 15 and Figure 16. The analysis was performed for 1 year starting on January 1<sup>st</sup>, 2025. Notice that, in the worst day, the eclipse time is equivalent to 5% of the orbit, which is approximately 72 min, and eclipses only occur in two epochs of the year. This is in accordance with the requirement that the satellite must acquire Sun data more than 90% of the mission lifetime.

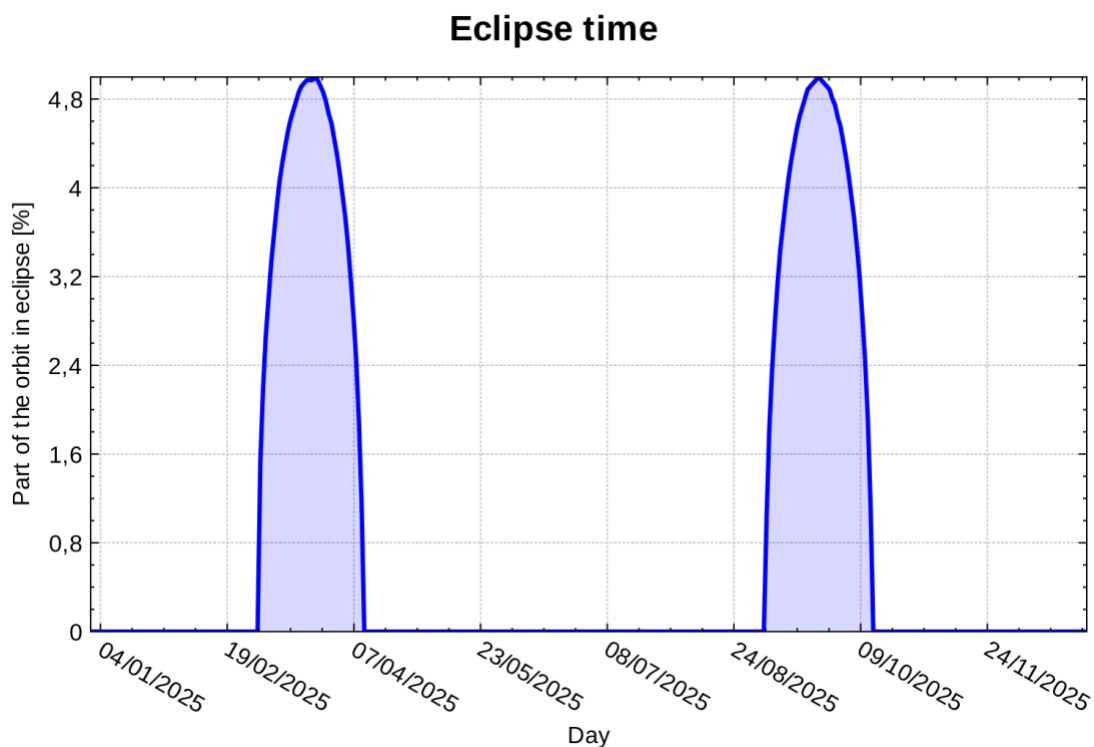


Figure 15 - Eclipse time for OPC3-1 considering an orbit inclination of 5°.

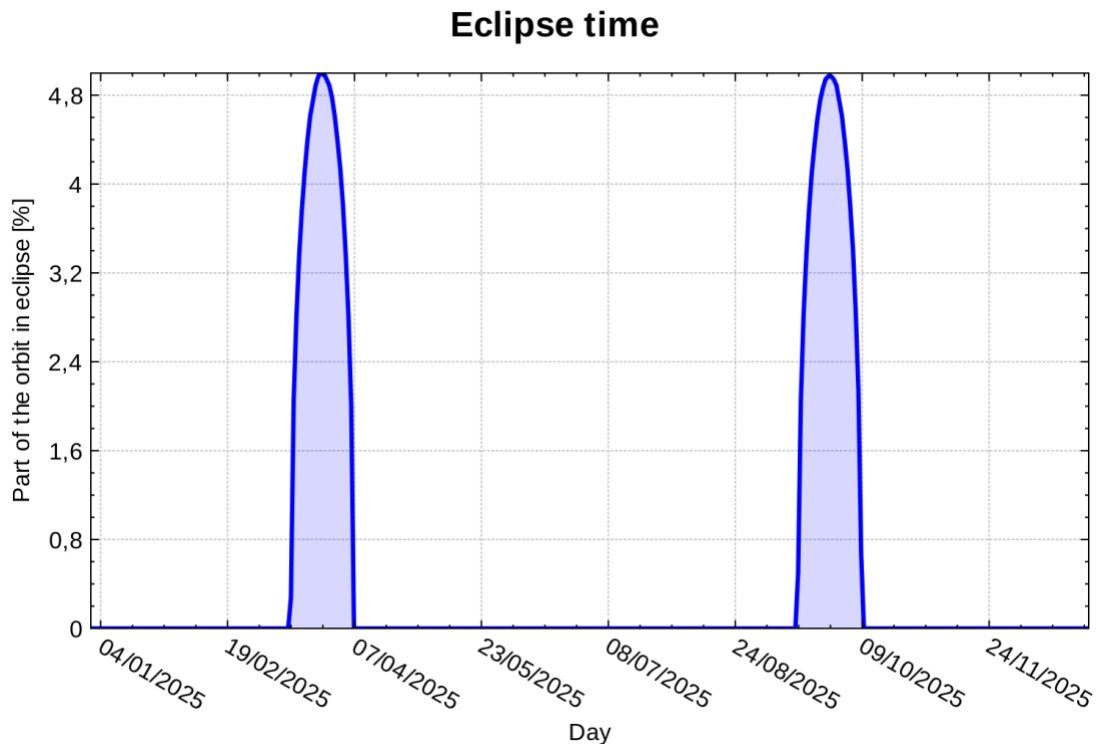


Figure 16 - Eclipse time for OPC3-1 considering an orbit inclination of  $28.5^\circ$ .

#### 4.1.1.2 $\Delta V$ budget

The  $\Delta V$  budget was computed using the parameters in Table 7. The mission will need 1407 m/s to acquire the nominal orbit after injection in the GTO, to maintain its orbit during the predicted lifetime, and to transfer the satellite to the disposal orbit, as shown in Section 4.1.2. Furthermore, only E-W station keeping maneuvers are required, N-S maneuvers will not be necessary during the mission lifetime.

It was verified that the expected time between maneuvers will be 31 days. At those instants, the spacecraft will not be able to acquire scientific data.

Table 7 - Parameters to compute the  $\Delta V$  for OPC3-1.

Parameter	Value
<b>Mission lifetime</b>	10 years
<b>Perigee of the GTO</b>	2500 km
<b>Orbital longitude</b>	$300.3^\circ$ , which yields the maximum $\Delta V$ budget
<b>Orbit inclination</b>	$28.5^\circ$ , which yields the maximum $\Delta V$ budget
<b>Longitude error limit</b>	$0.1^\circ$
<b>Inclination error limit</b>	N/A, inclination is not controlled
<b>Disposal orbit altitude</b>	276.6 km higher than GEO
<b>Margin</b>	10%

#### 4.1.1.3 General considerations

The orbit selection for OPC3-1 is straightforward. It is a usual Geostationary orbit without any major complications. The uncertainty lies in the available slot that is necessary to place the spacecraft, which availability is not guaranteed.



#### 4.1.2 OPC3-1: Orbit and attitude control analysis

##### 4.1.2.1 Actuators design

The actuators design of the attitude and orbit control subsystem (AOCS) depends on the system requirements, the environmental disturbances applied to the satellite and its mass properties. In Table 8 are shown the input parameters used for calculation of the disturbance torques over the GSST satellite for OPC3-1, considering a worst-case scenario (see Table 9).

Table 8 - Input parameters used to compute the disturbance torques for OPC3-1.

Parameter	Value
Orbit radius	42,164.200 km
Orbital period	86164 s
Sunlight period	86164 s
Spacecraft orbital velocity	3.074 km/s
Spacecraft inertia matrix	$\begin{bmatrix} 1511.0 & -53.0 & -11.2 \\ -53.0 & 2381.7 & -11.3 \\ -11.2 & -11.3 & 2520.2 \end{bmatrix} \text{ kg.m}^2$
Sunlit surface area	9.23 m <sup>2</sup>
Distance between the center of solar radiation pressure and the center of mass	0.01 m
Dimensionless reflectance factor	0.6
Spacecraft residual dipole moment	0.1
Ram area, which is the cross section in the ram direction that points towards the satellite motion <sup>2</sup>	16.5 m <sup>2</sup>
Drag coefficient	2.2
Distance between the center of aerodynamic pressure and the center of mass in the plane orthogonal to the velocity vector	0.1 m

Table 9 - Disturbance torques computed for OPC3-1.

Disturbance	Value (10 <sup>-5</sup> Nm)
Solar radiation pressure	0.0673
Atmospheric drag	0.0000
Magnetic field	0.0014
Gravity gradient <sup>3</sup>	0.1398
<b>Total disturbance torque</b>	<b>0.2086</b>

It is also necessary to define how the satellite will handle the tip-off angular velocity after separation from the launcher to acquire the initial Sun pointing. Since the magnetic field strength on the geostationary orbit is very low, it is not possible to use magneto-torquers to either desaturate the reaction wheels or remove the satellite momentum. Thus, thrusters will be needed to perform those actions and they will be used to remove the tip-off angular velocity.

<sup>2</sup>Since the satellite is inertially pointed, the velocity vector performs a full rotation per orbit as seen by the satellite body. Hence, the ram area was computed considering a mean value.

<sup>3</sup>Since the satellite is inertially pointed, the gravity gradient vector will ideally yield a periodic vector with possibly small secular component. However, the gravity gradient disturbance torque was computed as it was pointed to the Earth to obtain a worst-case scenario, because this geometry will indeed occur during the orbit correction maneuver. In this case, it was considered a misalignment between the body reference frame and the principal axes of 5° in pitch and roll.

Thus, the AOCS actuators will be a set of reaction wheels and thrusters. Notice that, since the design must be redundant, it was chosen as a solution a set of 4 reaction wheels in a pyramid configuration. The later was computed with a 100% of margin so that if a reaction wheel fails, the others can replace it with no impact for the system. The design parameters for the actuators can be seen in Table 10. Notice that the thruster design and specification can be seen in Section 4.1.3.

*Table 10 - Design parameters of the AOCS actuators.*

Design parameter	Value
<b>Reaction Wheels</b>	
<b>Maximum torque</b>	0.19600 Nm
<b>Momentum storage capacity</b>	95.3910 Nms

Finally, the set of the actuators selected for OPC3-1 are:

- **4 reaction wheels placed in a pyramid configuration responsible to control the satellite attitude.**
  - **Maximum torque capacity:** 0.2 Nm.
  - **Momentum storage capacity:** 100 Nms.
  - **Mass:** 12 kg.
  - **Peak power:** 195 W.
  - **Mean power during nominal operation:** 22 W.

Notice that this set of reaction wheels is capable to maneuver the satellite  $180^\circ$  in 540 s when one of them is failed.

#### 4.1.2.2 Sensors design

A set of 8 coarse solar sensors was selected to provide a rough Sun position estimate during the initial Sun point acquisition and in the emergency mode. Those sensors must be positioned on the corners of the satellite, similar to the solution chosen for the satellite Amazonia-1.

The orbit determination will be provided by an onboard SGP4 algorithm using the orbit information (TLE) sent by the ground station. In this configuration, the expected position accuracy is 1km.

The mission requires a very stringent pointing knowledge. The absolute accuracy must be better than 10 arcsec ( $3\sigma$ ). This can be provided by a set of two star-trackers. However, since the system must be redundant, a third one must be used, because with only one star-tracker the attitude estimation accuracy about the optical axis is degraded.

The pointing stability requirement ( $< 0.833$  arcsec/s) calls for a navigation-grade gyro. It was selected a gyro with four channels, for redundancy purposes, with bias stability of  $0.01^\circ/\text{h}$  ( $3\sigma$ ) and angular random walk of  $0.0016^\circ/\sqrt{\text{h}}$  ( $1\sigma$ ).

This set of sensors will not provide the pointing accuracy to a selected feature in the Sun that is required for the mission. Hence, the AOCS needs to receive data from the tracking camera, which can measure the position of a point in the Sun with respect to a reference with a precision better than 0.25 arcsec ( $3\sigma$ ). Notice that the pointing knowledge is not absolute, but relative to a reference point selected in the Sun. Thus, we can define two operation modes. The first one uses the star-tracker to provide an initial pointing of the satellite to the desired direction in the Sun. The second one discards the star trackers measurements and uses only the tracking camera data to keep the pointing error relative to a selected point in the Sun within the required interval.

Finally, the set of sensors selected for this mission is:

- **8 coarse solar sensors responsible to provide a rough Sun position estimation for initial pointing acquisition and in emergency mode.**
  - **Mass:** 0.02 kg.
  - **Power:** 0.01 W.
- **3 star trackers positioned on the edges of a cube to provide the absolute attitude determination.**
  - **Mass:** 3.7 kg.
  - **Power:** 10 W.
  - **Thermo-elastic error:** 0.055 arcsec/°C ( $1\sigma$ ).
  - **FOV spatial error:** 0.7 arcsec ( $3\sigma$ ).
  - **Pixel spatial error:** 3.4 arcsec ( $3\sigma$ ).
  - **Noise equivalent angle:** 0.8 arcsec/ $\sqrt{s}$  ( $3\sigma$ ).
- **1 inertial rotating unit with four sensing channels responsible to measure the satellite body velocity.**
  - **Mass of sensing head:** 2 kg.
  - **Mass of electronics:** 4.5 kg.
  - **Power:** 24 W.
  - **Bias stability:** 0.01°/h ( $3\sigma$ ).
  - **Angular random walk:** 0.0016 °/ $\sqrt{h}$  ( $1\sigma$ ).
- **1 tracking camera for fine attitude measurement with respect to a selected point in the Sun.**
  - For more information, see Section 2.

#### 4.1.2.3 AOCS design validation

Since this mission requires a very stringent pointing accuracy, it was decided to simulate the AOCS so that the design can be validated. The simulation was programmed using all the available information: actuators and sensors parameters, satellite perturbations, actuators saturation, DA/AD conversion resolution, etc. Notice, however, that many other parameters are not available in this mission phase, such as, for example, the reaction wheels unbalancing. This fact limits the fidelity of the results presented here that should be seen as a lower bound for the AOCS performance.

It is possible to see in Figure 17 the simulation results when the spacecraft is operating using the star trackers and the control subsystem was commanded to point the satellite to a fix location. This is the result of a Monte Carlo simulation with 100 realizations in which the initial pointing errors were sampled from a Gaussian distribution. On the left, it is possible to see the absolute pointing error statistics whereas, on the right, it is possible to see the angular velocity statistics. The black line is the mean value, the orange range encompasses all the results within  $1\sigma$  from the mean, and the blue range contains all the results within  $3\sigma$  from the mean. It is possible to verify that the selected gyro is capable to provide the angular stability required due to the camera design ( $< 0.833$  arcsec/s). However, the absolute pointing error considering only the star trackers is much larger than the requirement to observe a specific feature on the Sun. Thus, the measurements from the tracking camera are paramount to comply with the requirements.

It is possible to see in Figure 18 the simulation results when the spacecraft is operating using the tracking camera. In this case, the pointing error is not absolute, but relative to a point on the Sun that was chosen as reference. It is possible to see that all the requirements are met with margins. This is important because all non-modeled effects will increase the error as seen in those results, but the margin appears to be larger enough to encompass those error sources.

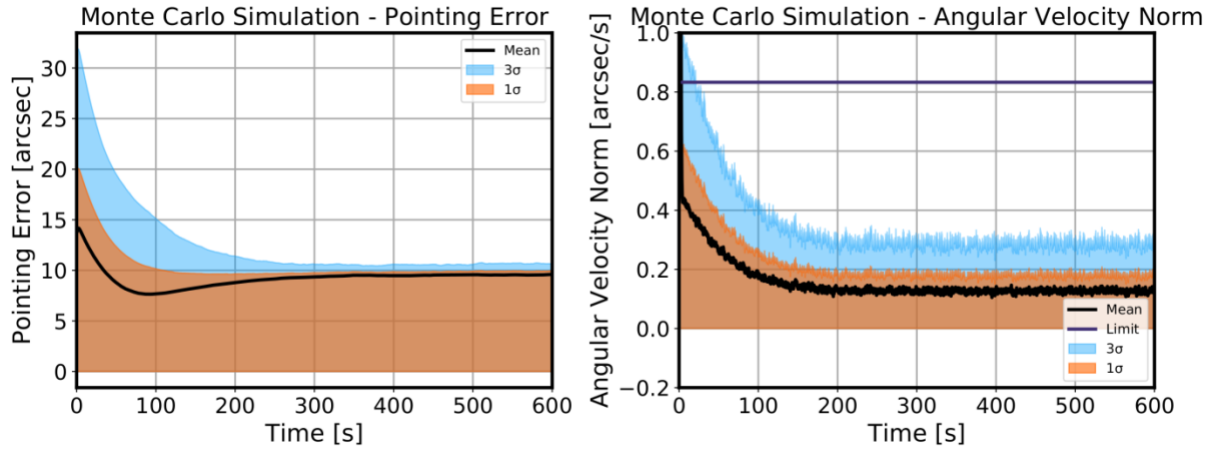


Figure 17 - Absolute pointing error (left) and angular velocity norm (right) for OPC3-1 (GEO) obtained from a simplified simulation using the star trackers.

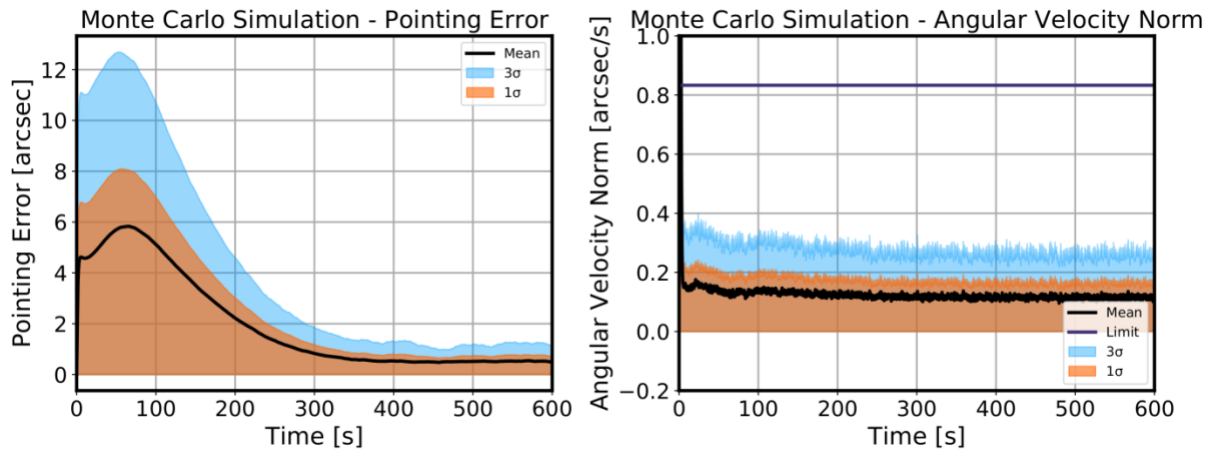


Figure 18 - Relative pointing error (left) and angular velocity norm (right) for OPC3-1 (GEO) obtained from a simplified simulation using the tracking camera.

#### 4.1.2.4 Antenna gimbals pointing

The AOCS will be responsible to point the antenna gimbals to the ground station so that the communication link for the scientific data can be acquired. Since the AOCS in this solution obtains the orbit position by an orbit propagator only, we must verify how accurate will be the antenna pointing. The problem can be geometrically posed as indicated in Figure 19, where  $\Delta p$  is the spacecraft position error and  $\Delta \alpha$  is the pointing error of the antenna gimbal. One can see that

$$\alpha \approx \frac{\Delta p}{d},$$

in which  $d$  is the distance between the satellite and the ground station. Using the smallest distance possible (altitude above the Equator) and a position error of 5km, which is a worst-case scenario for SGP4, then one gets

$$\alpha = 28 \text{ arcsec}.$$

However, this is the pointing error caused just by the position estimation uncertainty. Hence, it is also necessary to add the attitude determination error. Since this mission has star trackers, the attitude estimation error is expected to be better than 10 arcsec. Finally, in the worst-case scenario, the antenna pointing error to the ground will be 38 arcsec, which is much smaller than the antenna field of view. Finally, notice that this analysis considered an ideal gimbal. Thus, the pointing error caused by the gimbal itself must also be added to this result.

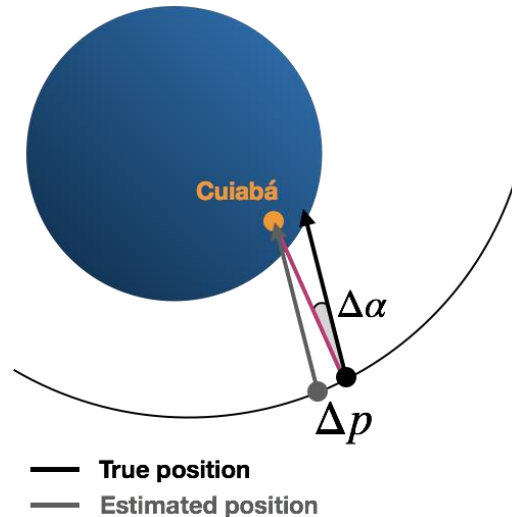


Figure 19 - Antenna pointing error caused by the position estimation error.

#### 4.1.2.5 General considerations

It is important to mention the following considerations about the AOCS design for this option:

- The fine pointing mode highly depends on the tracking camera. However, very little information was found about the operation and errors of this instrument. Furthermore, it is not a commercial product. Hence, it is not guaranteed that it will be available for purchase. This is the major risk of the AOCS design.
- The navigation-grade gyro necessary for the mission can be difficult to acquire.
- The attitude control software requires a more sophisticated approach than usual missions. The simulation results have shown that different PD gains must be used to maneuver the satellite in short times and to keep the attitude and angular velocity errors small during imaging mode. Hence, perhaps non-linear control techniques should be used, such as gain scheduling, for example.

#### 4.1.3 OPC3-1: Propulsion analysis

For the GEO orbit option, the propulsion subsystem should be able to carry out the following tasks: acquisition and circularization of Geosynchronous Earth Orbit (GEO), station keeping maneuvers, tip-off and slew maneuvers, reaction wheel unloading, and disposal maneuvers. In order to reduce the propellant mass, it is assumed that the launcher vehicle will leave the satellite on the Geosynchronous Transfer Orbit (GTO). The input data for the propulsion subsystem design is presented in Table 11.

Table 11 - Input data for the design of the propulsion subsystem for OPC3-1.

Parameter	Value	Unit
Dry mass	1560	kg
Total $\Delta V$	1407	m/s

Figure 20 shows results of the total mass and the required power for the following types of propulsion subsystems: cold-gas, monopropellant, bipropellant, and electrical system. As expected, due to the high  $\Delta V$  requirement, the cold gas and monopropellant systems presented a huge value of mass. An electrical system would be a good choice in terms of mass. However, the required electrical power to activate the thrusters turns out to be infeasible. Therefore, the **bipropellant propulsion subsystem** comes up as the best compromise solution. It was selected as the baseline design for the OPC3-1 solution.

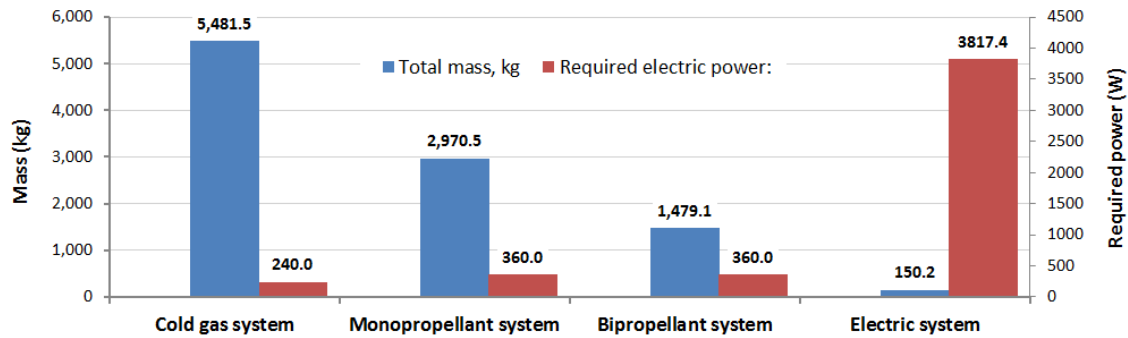


Figure 20 - Total mass and required power for different propulsion subsystems.

In a bipropellant system, a fuel and an oxidizer combust, either spontaneously, after they contact each other (hypergolic systems), or as a result of an ignition source. This type of system is much more complex than cold gas or monopropellant systems. On the other hand, it is a very versatile and high-performance system, providing a specific impulse of approximately 300s and a wide range of thrust capability, being the most used for high delta-V requirements (Wertz and Larson, 2011; Brown, 2002).

In Figure 21 is shown a schematic example of the regulated bipropellant propulsion subsystem conceived for OPC3-1. It includes a tank of fuel, tank of oxidizer, tanks of pressurant, thrusters, apogee kick motor, and components for feed system (valves, filters, lines and fittings, temperature and pressure transducers, heaters, etc). It is similar to the one used in the NASA's Solar Dynamic Observatory (SDO) mission, described in Leyva (2011).

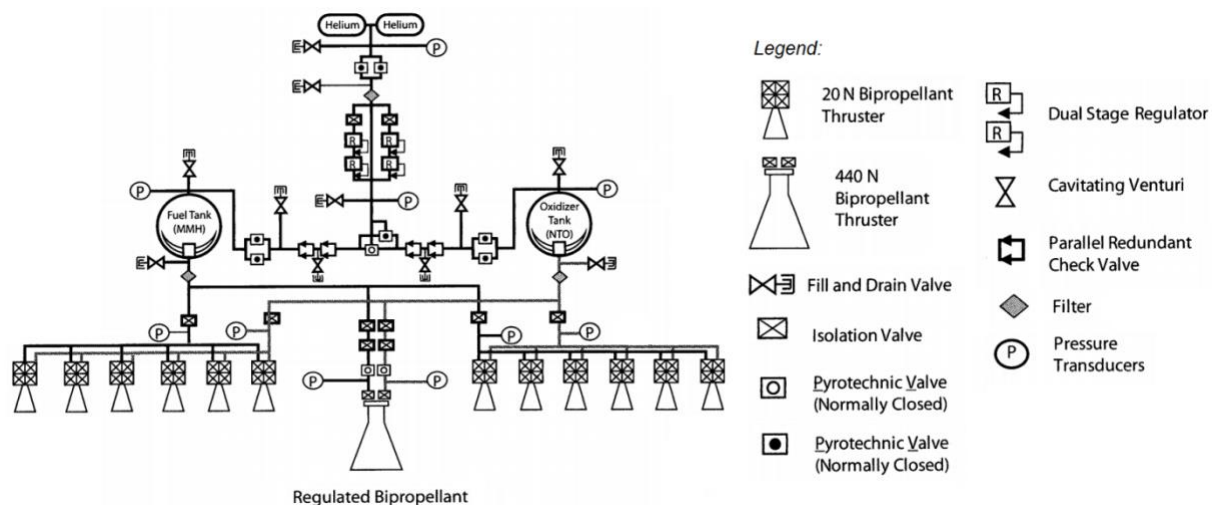


Figure 21 - Bipropellant propulsion subsystem concept architecture (Based on SDO's propulsion subsystem, illustrated in Leyva, 2011).

The mass budget of the propulsion subsystem for the OPC3-1 solution is presented in Table 12.

*Table 12 - Mass budget of the bipropellant subsystem for OPC3-1.*

Component	Unit mass, kg	Quantity	Total mass, kg
Propellant	1050.93	-	1050.93
Tank of fuel	17.10	1	17.10
Tank of oxidizer	17.10	1	17.10
Tank of pressurant	8.40	2	16.80
Thrusters	0.35	12	4.20
Apogee kick motor	4.31	1	4.31
Feed system <sup>§</sup>	368.71	-	368.71
<b>Total mass</b>			<b>1479.15</b>

<sup>§</sup> Valves, filters, lines and fittings, temperature and pressure transducers, heaters, etc.

In the design process, it was assumed an input working pressure of 19 bar and a mixture ratio of 1.6. Each thruster requires a power of 30W to operate (specific impulse of 291s) whereas 46W of power is required to activate the apogee kick motor (specific impulse of 311s). Based on a commercial database, it was selected models of tank and thruster that best meet the requirements of volume capacity and thrust levels, respectively. Some technical data, such as dimension and capacity, are described in Table 13.

*Table 13 - Specification of bipropellant subsystem's components.*

Component	Dimension (L x W x H), mm	Capacity
Tank of fuel	991 x 991 x 991	503.8 l
Tank of oxidizer	991 x 991 x 991	503.3 l
Tank of pressurant	442.2 x 420.1 x 420.1	30.8 l
Thruster	127 x 59 x 46	10 N
Apogee kick motor	737 x 381 x 381	490 N

The propulsion subsystem design considered the following propellants: monomethyl hydrazine (MMH) as the fuel, nitrogen tetroxide (N<sub>2</sub>O<sub>4</sub>) as the oxidizer, and helium as the pressurant. A design margin of 5% was considered in the design of the propellant mass, whose inventory is shown in Table 14. Concerning the pressurization regulated system, a value of 3.37 kg of helium pressurant mass is required to pressurize both fuel and oxidizer tanks. The required pressurant volume (59.2 l) is divided into two tanks with a capacity of 30.8 liters each.



Table 14 - Inventory of fuel and oxidizer propellants.

Propellant use	Fuel, kg	Oxidizer, kg	Total mass, kg
Usable propellant	367.95	588.72	956.67
Trapped propellant, 3%	11.04	17.66	28.7
Outage, 1%	3.68	5.89	9.57
Loading error, 0.5%	1.84	2.94	4.78
Propellant reserve, 5%	18.40	29.44	47.83
<b>Loaded propellant</b>	<b>402.91</b>	<b>644.65</b>	<b>1047.55</b>

As the propulsion subsystem has to be able to remove the residual angular velocity left by the launcher vehicle, as well as to unload the reaction wheels, and, eventually, to execute an attitude maneuver, then a reaction thruster control system was designed to meet those functions. A conceptual configuration with 12 thrusters is represented in Figure 22. Eight thrusters (since four is redundant) on the -X axis panel provide the satellite rotation capability on the Y and Z axes, in addition to translational motion, if necessary. Other four thrusters (two on -Z axis panels and two on +Z axis panel) provide rotational motion around the X axis. The apogee kick motor is located in the center of the -X axis panel. In addition, it worth mentioning that, according to our analysis, the reaction wheels are able to deal with the residual angular momentum imposed by the minimum impulse bit (MIB) of the thrusters.

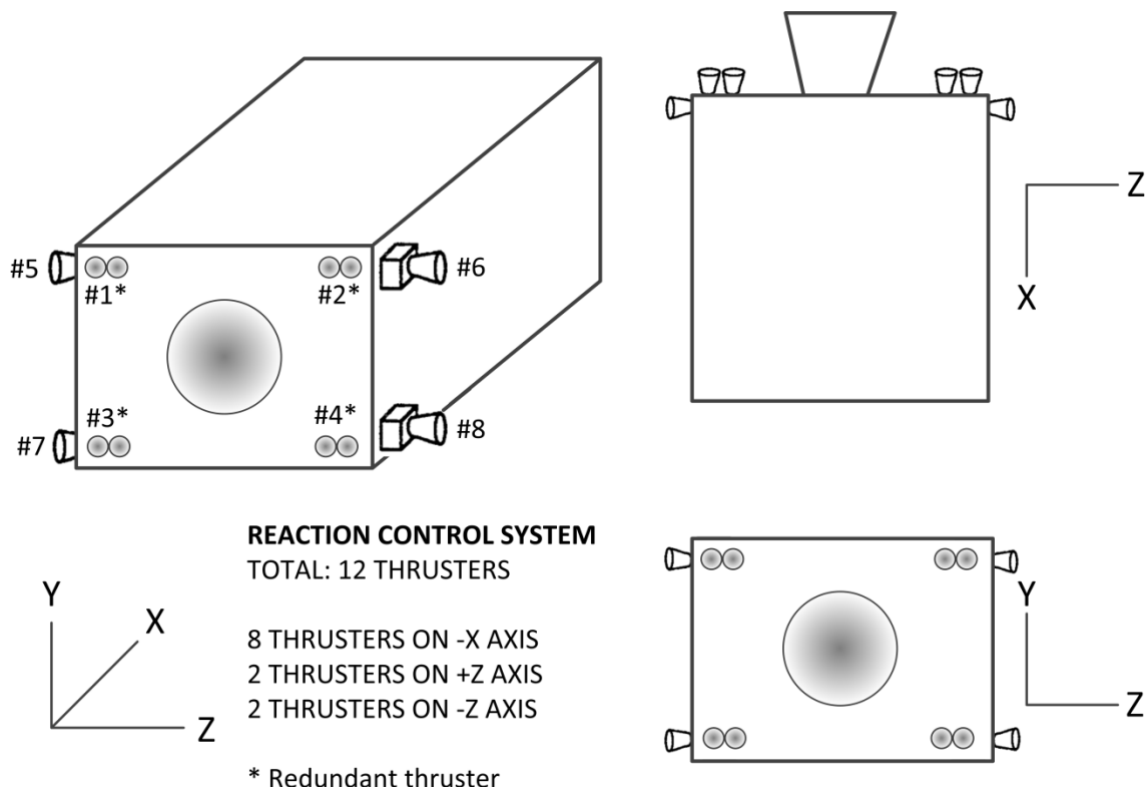


Figure 22 - Configuration of the reaction control system with 12 thrusters.

Concerns have risen on the possibility that the plume coming out of the thrusters #5, #6, #7 and #8 could strike on the structure, solar panel, or instruments. Due to the high velocity of the plume gases, its incidence over parts of the satellite could cause significant damage to the blankets, solar arrays, and optical devices or even cause interference on the attitude control. A simplified analysis,



based on the method used in (De Sousa and Muraoka, 2006), has been realized in order to identify critical points in this issue. The maximum plume envelope, that is, the cone covered by the plume as it exits the thruster's nozzle, can be calculated using the Prandtl-Meyer Function (Jr. Anderson, 1985) and the geometry of the nozzle exit. The basic geometry of the bipropellant thruster is shown in Figure 23.

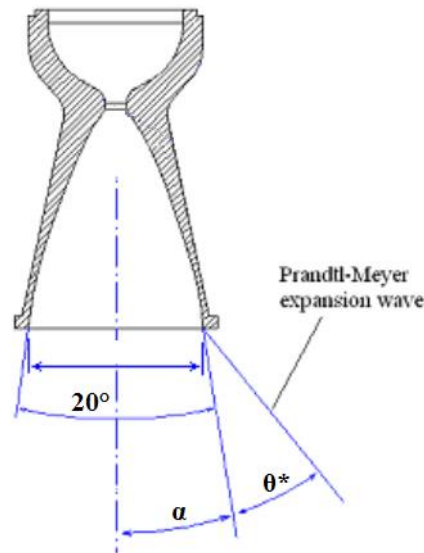


Figure 23 - Sketch of the thruster nozzle (adapted from De Sousa and Muraoka, 2006).

The angles  $\alpha$  and  $\theta^*$  define the boundaries of the plume of the gases exiting from the thrusters. Usually,  $\alpha$  is considered as 10 degrees (De Sousa and Muraoka, 2006). Using the mathematical expressions provided in (Jr. Anderson, 1985), a value of 60 degrees have been achieved for the  $\theta^*$  angle. Together with the structure specialists, it was verified, in computer-aided design (CAD) software, that the possibility of the strike coming from the plume gases is minimal. However, it is quite advisable to perform additional, and deeper, analysis on this issue in the next phases of the mission. A specific tool to evaluate thermodynamic gases effects should be used to reduce the risks of damage on the satellite.

#### 4.1.4 OPC3-1: Communications analysis

For the design of the communication subsystem, it was considered that the satellite is positioned in a GEO orbit with  $28.5^\circ$  of inclination, which gives a conservative solution, taking into account the possible range of GEO orbit inclinations considered in the present study (from  $5^\circ$  to  $28.5^\circ$ ).

The GSST satellite is in an inertial attitude along with its orbit, with its X+ axis always pointing towards the Sun. For the OPC3-1 option, it is considered that an X-band ground station positioned at Cuiabá will receive the scientific data coming from the satellite in a continuous mode.

Due to the satellite orbit inclination and attitude requirement, a communication solution using a pair of high gain antennas (HGAs) transmitting to the ground antenna in X-band was conceived. This is necessary in order to maintain a continuous scientific data link from the satellite to the ground station along the orbit, as shown schematically in Figure 24.

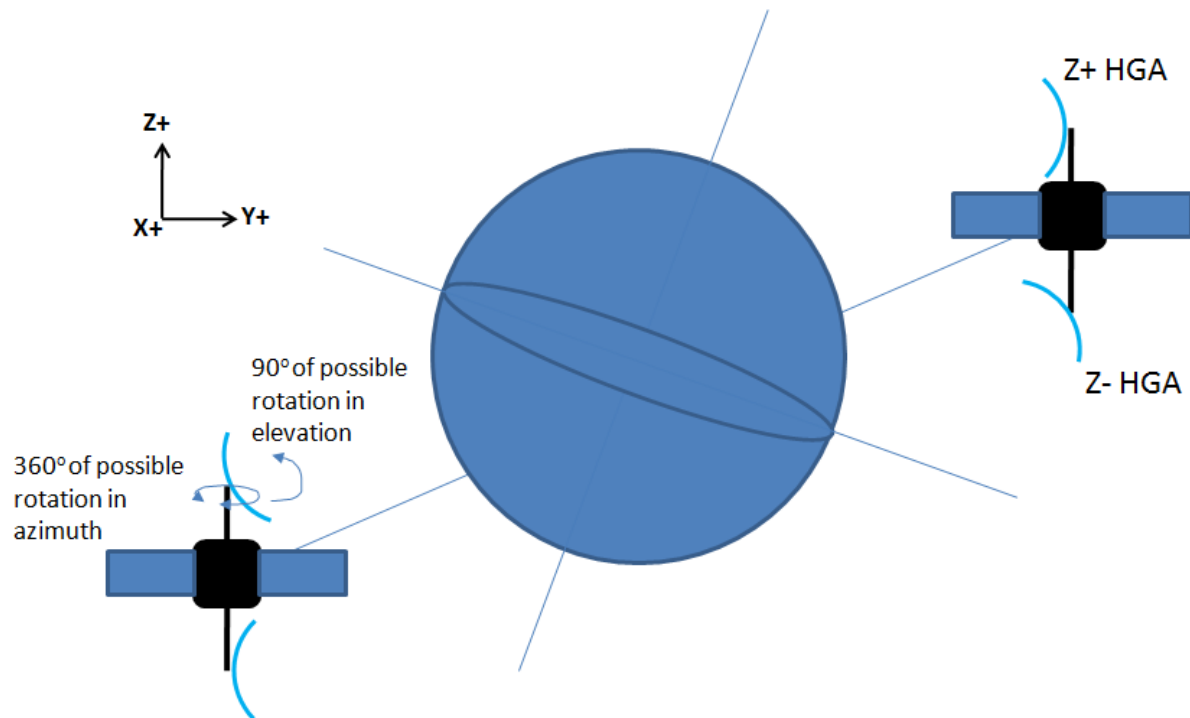


Figure 24 - Schematic drawing of the GSST satellite in two positions of the GEO orbit with 28.5° inclination, as seen from the Sun.

The GSST HGAs are located on opposite sides of the spacecraft (see Figure) and referred to as the +Z- and –Z-antennas. Each is pointed using a pair of gimbals. The azimuth gimbals rotate about the body Z-axis and can perform a full, unrestricted rotation. The elevation gimbals rotate about an axis perpendicular to the body Z-axis and parallel to the body Y-axis when the azimuth gimbal rotation is zero. These gimbals allow the HGAs to rotate from 0° to 90° in elevation. Each HGA can transmit 300 Mbps of data, and only one antenna is used at a time to download the scientific data to the Cuiabá ground station. Along the orbit, a downlink handover strategy between the antennas must be implemented, so that a continuous data link between the satellite and the ground station is assured.

The X-band system is designed for downlink operations only. During the mission, the science instruments will continuously generate raw sensor data.

The CCSDS Virtual Channel Data Units (VCDUs) transmits dedicated Virtual Channel data streams (several for each instrument) to the X-band RF system where they are downlinked through the High Gain Antenna (HGA) to the ground.

The X-band downlink is continuously acquired by the GSST ground segment. It receives, demodulates, decodes, frame synchronizes, quality checks, stores, and distributes the science data to the instrument.

The main characteristics of the communications science data subsystem conceived for OPC3-1 are presented below.

**Transmitter:** Carrier in 8.4 GHz, QPSK modulation, rate of 300 Mbps, RHCP polarization.  
Consumption (30W RF): 95W  
Dimensions: 200mm x 210mm x 200mm (W x H x D)  
Mass: 6 Kg

**Antenna:** Parabolic, 1m in diameter, 35 Watts of transmission, RHCP polarization.  
Dimensions: 1 m in diameter  
Mass: 6 kg (including mechanisms, auxiliary structures.)

**Subsystem**

Redundancy: Cold for data transmission.

**RF Consumption:** 95 W

Dimensions: 2 boxes of 300 mm x 170 mm x 300 mm (W x H x D)

Mass: 12 Kg

**Antennas:** two parabolic antennas, with respective pointing devices ("gimbals and booms").

Transmit Power: 35 W

Dimensions: 1 m in diameter

Mass: 12 kg (including mechanisms, auxiliary structures).

**Internal storage:** Minimum capacity of 100 Gbits

Writing/reading rate; 300 Mbps minimum

Consumption: 5 W

Dimensions: 150mm x 150mm x 150mm (W x H x D)

Mass: 3 kg

Total consumption: 100 W

Total Mass: 27 Kg (including antennas, mechanisms, auxiliary structures, internal storage).

In Figure 25 the satellite to ground station payload data communication link is summarized, for OPC3-1.

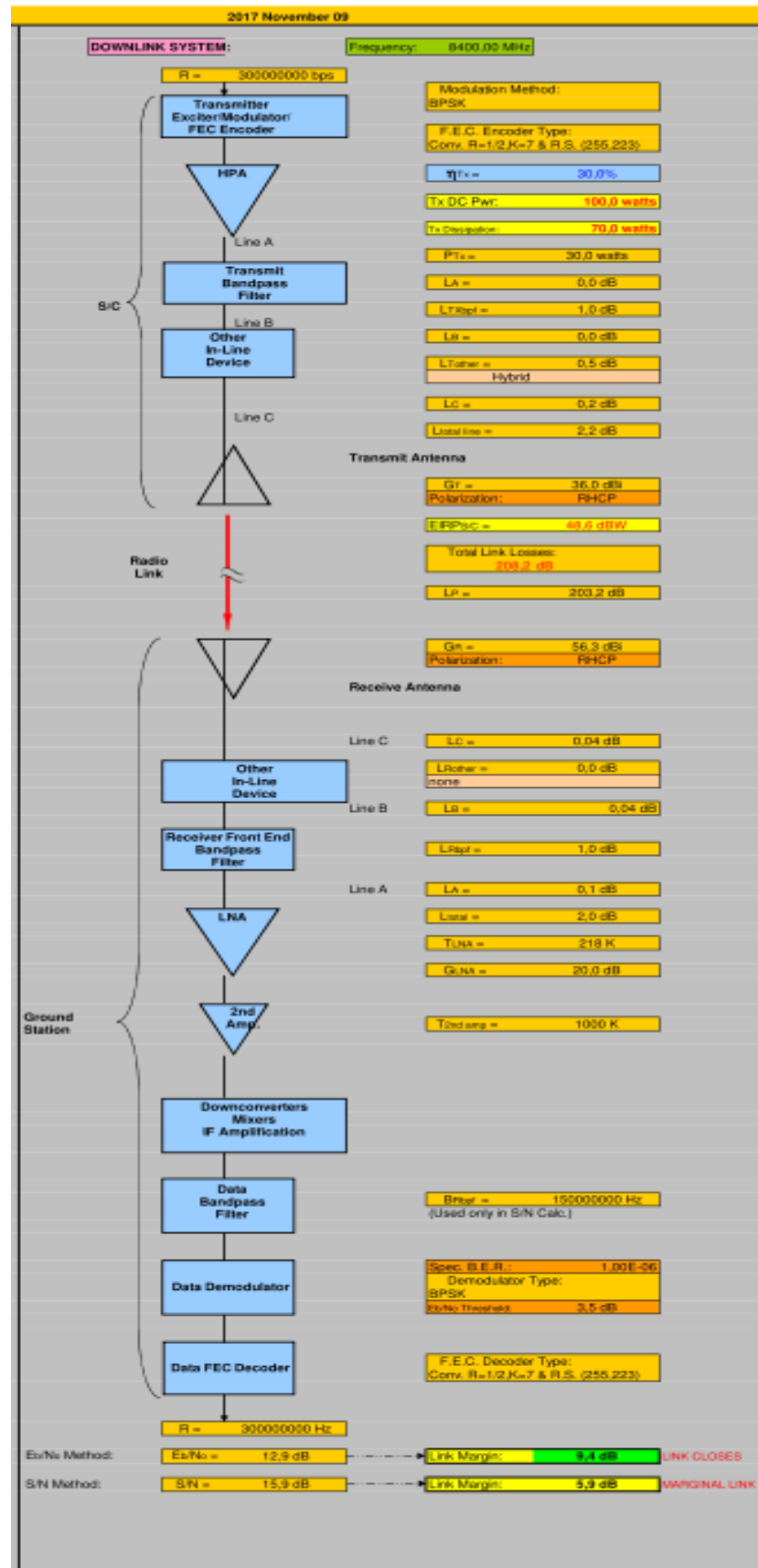


Figure 25 - Science data X-band communication link chain for OPC3-1.

For the service communication (telemetry and telecommand) of OPC3-1, was conceived a redundant subsystem with the following characteristics:

**Command Receiver (TC):** Carrier in 2208 MHz, BPSK modulation, rate of 9.6 Kbps.

**Telemetry Transmitter (TM):** Carrier in 2033.2 MHz, BPSK modulation, rate of 24 Kbps.

**Transponder:**

TC Receiver Consumption: 6 W

TM Transmitter Consumption (10 W RF): 40 W

Total Consumption: 46 W

Dimensions: 260 mm x 170 mm x 200 mm (W x H x D)

Mass: 5 kg

**TT&C subsystem:**

Redundancy:

- Cold for telemetry transmission.
- Warm up for remote commander reception.

**Transponders:**

Mass: 10 Kg

Dimensions: 2 boxes of 260 mm x 170 mm x 200 mm (W x H x D)

**Antennas:** Helicoidal (two Helix Quadrifilar antennas @ 4 dBi, for almost omnidirectional coverage).

Transmit Power: 15 W

Dimensions: 250mm x 400mm (W x D)

Mass: 2 kg (including auxiliary structures).

Total Consumption (1TX + 2RX): 52 W

Total mass: 12 kg (including auxiliary structures).

In Figure 26, the satellite from-to ground station service communication link is summarized, for OPC3-1.

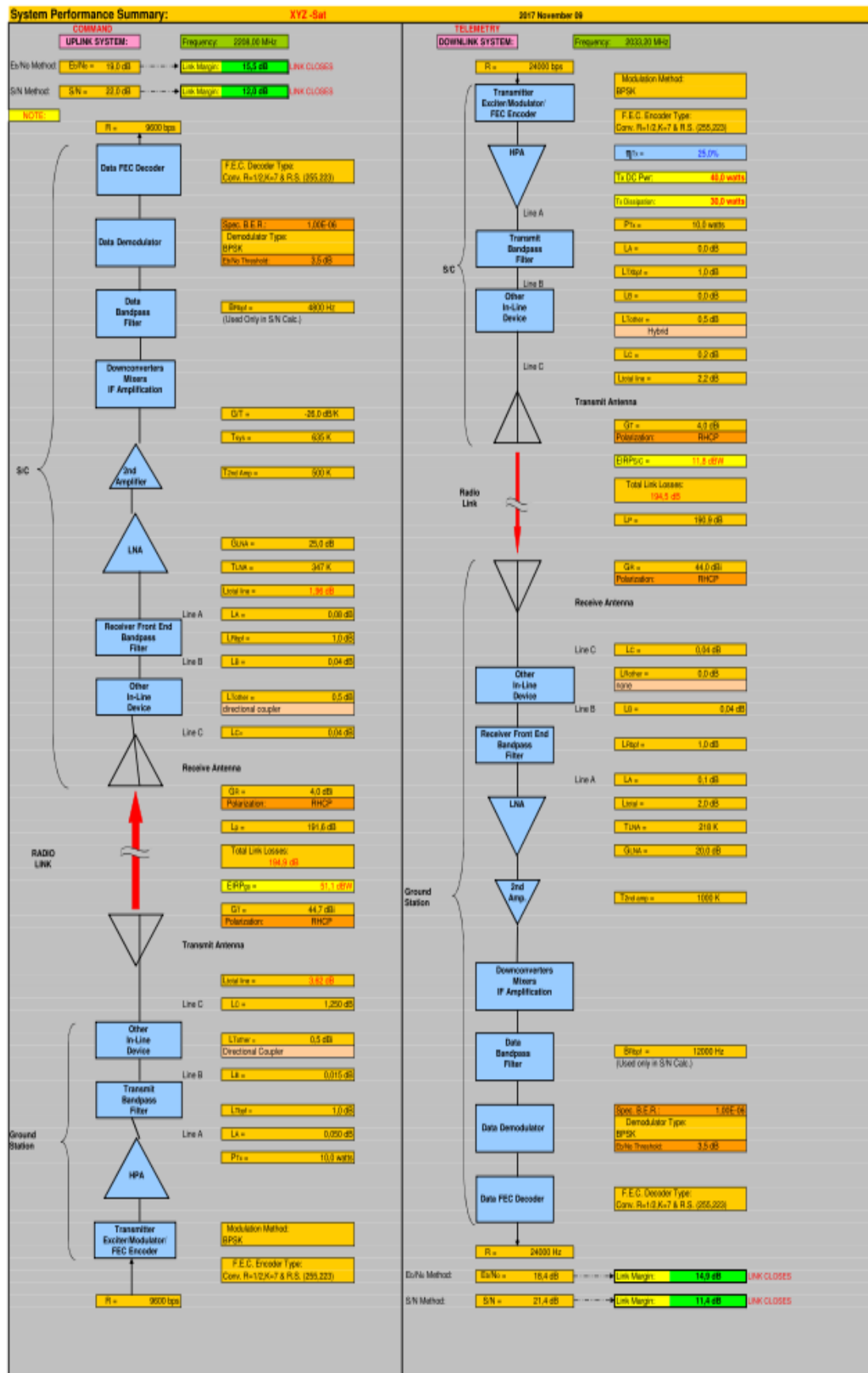


Figure 26 - Service data S-band communication link chain for OPC3-1.

#### 4.1.5 OPC3-1: On-board computer analysis

The data handling architecture (ACDH) for the GSST satellite was conceived based on a single central onboard computer (OBC) that performs all satellite housekeeping functions, plus the AOCS and Communications data processing. It should be redundant and implement Failure Detection, Isolation and Recovery (FDIR) functions.

The OBC should have the following interfaces:

- a) Analog telemetry acquisition, Bi-level e Temperatures;
- b) Direct ON-OFF commands or via computer;
- c) Propulsion;
- d) Reaction wheels;
- e) Magnetometer;
- f) Magnetotorquer;
- g) Solar sensor;
- h) Serial communication 1553 and assynchronous RS 422;
- i) Allow that other interfaces be added.

There are many possible options that could, in principle, be used as the GSST satellite OBC, including the COMAV, an onboard computer being developed at INPE. For the purposes of the present study, and only as a reference, a commercial computer with flight heritage was chosen as the GSST's OBC. Their dimensional, mass and power consumption characteristics, described in Table 24, were used in the estimation of the total satellite mass, power consumption and in the conceptual layout of the satellite.

#### 4.1.6 OPC3-1: Power analysis

The power subsystem concept design is built upon the following the steps:

- 1) Collect other subsystems information (number of equipment, power consumption, operation details, etc...);
- 2) Process other subsystem information resulting in satellite power consumption during all the orbit;
- 3) Design the subsystem equipment (Battery, solar panels, energy conditioning/distribution and other necessary equipment), considering the satellite's worst-case power consumption and generation conditions;
- 4) Simulation to verify the design of all the subsystem, including Solar panels and battery Depth of Discharge (DOD).

For simplicity, it was adopted a non-regulated bus for the subsystem, as can be seen in the diagram shown in Figure 27.



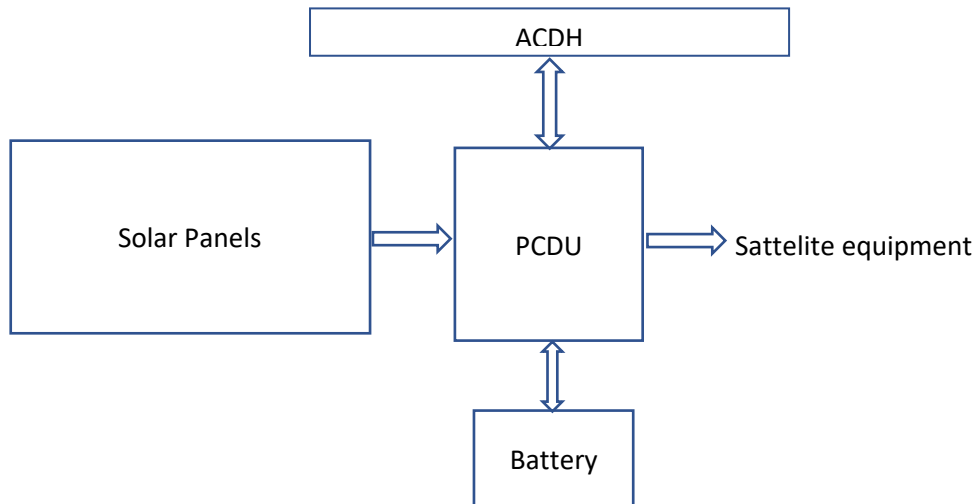


Figure 27 -Power subsystem architecture for OPC3-1.

In Table 15 is shown the characteristics of the power subsystem conceived for OPC3-1:

Table 15 - Characteristics of the power subsystem conceived for OPC3-1

EQUIPMENT	Capacity	Total QTY	Dimensões (CxLxA)	Mass (kg)	Contact area	Dissipation Eclipse (W)	Dissipation Sunlight (W)
PCDU	1500W	1	400x300x300	15,00	400x300	50	100
Battery (Lilon)	15Ah	10	230x170x95	4,30	230x170	6	6
Solar Panel (AsGa)	700	2	3m2	20,00			
Subsystem Total				98,00			

OBS: CxLxA is equivalent to Length x Width x Height.

The conceived power subsystem for OPC3-1 generates 1400 W and allows a satellite power consumption of approximately 1150 W.

#### 4.1.7 OPC3-1: Thermal analysis

The approach used for the conceptual thermal design of the GSST satellite was built upon the following premises:

- Each structural element (panel) is represented by only one thermal node;
- Steady state analysis;
- The equipment heat dissipation is applied directly to the panel each of them is positioned;
- Most of the satellite's external surfaces are thermally insulated from the outer environment using MLIs. OSRs are used to cover the satellite's thermal radiators;
- All internal surfaces of the structural panels, but the ones where are fixed the propulsion elements and batteries, are painted black, such that heat exchange is increased. The batteries and propulsion panels internal surfaces are covered with MLI, since their operational temperature range is different from the other satellite's panels;
- Conductive coupling with a value of 1 W/°C between adjacent panels, except for the battery and propellant tanks panels;

- PM Top, PM Vertical Z+, PM Vertical Z- and SM1 Lower Panels were considered not available for holding thermal radiators. For a description of all satellite panels and equipment allocation over them see Section 4.1.9;
- Autonomous thermal control for the HR camera, with interface temperature (PM Top) between -10 °C e 45 °C (HR telescope heat dissipation not included in the model).

The target temperature intervals allowed for each satellite structure panel is presented in Table 16. It is also shown the heat dissipation applied to them (correspondent to the heat dissipation of the equipment attached to them). It is noteworthy that the temperature intervals shown in Table 16 are shorter than the ones required for the panels, to accommodate a margin to the thermal design. Moreover, the heat dissipations consider the average equipment dissipation in one orbit.

*Table 16 - Structure panels allowed temperature intervals, and average minimum and maximum equipment thermal loads applied over them in one orbit, for OPC3-1.*

Panel	Temperatures (°C)		Heat dissipation (W)	
	Min.	Max.	Min.	Max.
SM1 Lower Panel	0	40	83.6	105.0
SM1 Lateral Z+	-5	40	0	3,2
SM1 Lateral Z-	-5	40	0	3,2
SM1 Lateral Y+	0	5	57.0	63.0
SM1 Lateral Y-	-5	40	0	0
SM1 Shear 1	0	30	0	0
SM1 Shear 2	-5	40	0	0
SM1 Shear 3	-5	40	0	0
SM1 Shear 4	-5	40	0	0
SM1 Shear 5	-5	40	0	0
SM1 Shear 6	0	40	22.8	25.2
SM1 Top Panel	0	30	128.3	141.8
SM2 Lateral Z+	0	30	8.0	12.0
SM2 Lateral Z-	-5	40	0	0
SM2 Lateral Y+	-5	40	0	0
SM2 Lateral Y-	-5	40	0	0
SM2 Shear 1	-5	40	0	0
SM2 Shear 2	-5	40	0	0
SM2 Shear 3	0	30	11.4	12.6
SM2 Shear 4	-5	40	0	0
SM2 Shear 5	-5	40	0	0
SM2 Shear 6	0	30	11.4	12.6
PM Lower Panel	0	30	64.2	71.9
PM Vertical Z+	0	30	116.9	147.0
PM Vertical Z-	0	30	133.0	210.0
PM Lateral Y+	-5	40	0	0
PM Lateral Y-	-5	40	0	0
PM Shear 1	-5	40	0	0
PM Shear 2	-5	40	0	0
PM Shear 3	-5	40	0	0

Panel	Temperatures (°C)		Heat dissipation (W)	
	Min.	Max.	Min.	Max.
PM Shear 4	-5	40	0	0
PM Shear 5	-5	40	0	0
PM Shear 6	-5	40	0	0
PM Central Panel	-5	40	0	0
PM Shear 7	-5	40	0	0
PM Shear 8	-5	40	0	0
PM Shear 9	-5	40	0	0
PM Shear 10	-5	40	0	0
PM Shear 11	-5	40	0	0
PM Shear 12	-5	40	0	0
PM Top Panel	0	30	0	0
Propellant Tank 1	5	30	0	0
Propellant Tank 2	5	30	0	0
Press Tank 1	15	30	0	0
Press Tank 2	15	30	0	0

Two analysis cases were considered for the GSST satellite conceptual thermal design: i) a cold case, where a combination of least internal and external heat loads is considered and; ii) a hot case, where a combination of maximum internal and external heat loads is considered. In the hot case, EOL degraded values for the radiators thermal coatings were assumed. In Table 17 the thermal coatings values used for the thermal coatings in the cold and hot cases are presented.

Table 17 - OPC3-1 thermal optical coatings properties.

Coating	Absorptivity		Emissivity
	BOL	**EOL	
*Kapton Al. 3 mil.	0.41	0.76	0.8
OSR	0.07	0.25	0.8
Black paint	0.95	0.95	0.88

\*The Kapton Al. is the outer layer of the MLI blankets. The effective thermal emissivity of the MLIs was considered to be 0.02. \*\*EOL values represent considered a mission lifetime of five years.

Due to the high altitude of the GEO orbit, the influence of the Earth's albedo and IR thermal radiation on the satellite's temperature was considered negligible. Hence, only the solar radiation was considered: 1326 W/m<sup>2</sup> for the cold case and 1418 W/m<sup>2</sup> for the hot case.

Two possible orbit inclinations were considered for the thermal analysis: 5°, and 28.5°. Note that the satellite keeps its X+ face always pointing to the Sun. In Figure 28 is shown a representation of the GSST in the GEO orbit.

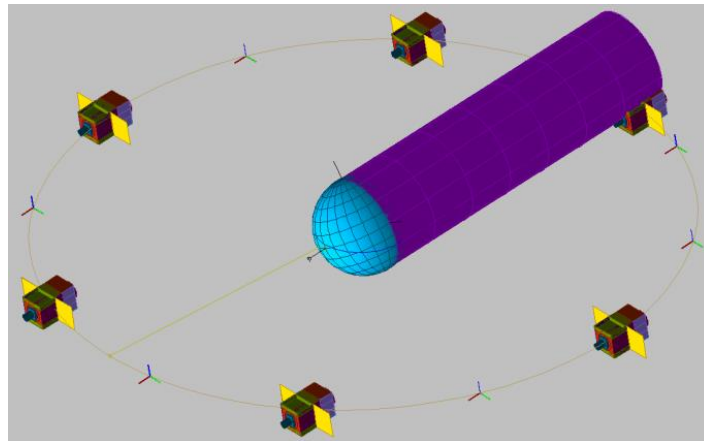


Figure 28 - Representation of the GSST satellite in GEO orbit for thermal analysis.

Simulations were performed for the satellite at cold and hot conditions, for both orbit inclinations, in order to find a combination of radiator areas and heater dissipation, and a proper position on the satellite for these devices, such that the temperature of their components are kept within the required operational ranges presented in Table 16. In Table 18 are presented the radiator areas and heater power found, for each structural panel considered.

Table 18 - Estimated Radiator area and heater power at satellite structural panels, for OPC3-1.

Element	Radiator area (m <sup>2</sup> )	Heater power (W)
SM1 Lower Panel	0	0
SM1 Lateral Z+	0.498	5.0
SM1 Lateral Z-	0.457	5.0
SM1 Lateral Y+	0.289	11.0
SM1 Lateral Y-	0.246	0
SM1 Shear 1	0	0
SM1 Shear 2	0	0
SM1 Shear 3	0	0
SM1 Shear 4	0	0
SM1 Shear 5	0	0
SM1 Shear 6	0	0
SM1 Top Panel	0	0
SM2 Lateral Z+	0.434	65.0
SM2 Lateral Z-	0.471	0
SM2 Lateral Y+	0.501	0
SM2 Lateral Y-	0.147	0
SM2 Shear 1	0	0
SM2 Shear 2	0	0
SM2 Shear 3	0	0
SM2 Shear 4	0	0
SM2 Shear 5	0	0
SM2 Shear 6	0	0
PM Lower Panel	0	38.0
PM Vertical Z+	0	0
PM Vertical Z-	0	0

Element	Radiator area (m <sup>2</sup> )	Heater power (W)
PM Lateral Y+	0.483	0
PM Lateral Y-	0.483	0
PM Shear 1	0	0
PM Shear 2	0	0
PM Shear 3	0	0
PM Shear 4	0	0
PM Shear 5	0	0
PM Shear 6	0	0
PM Central Panel	0	0
PM Shear 7	0	0
PM Shear 8	0	0
PM Shear 9	0	0
PM Shear 10	0	0
PM Shear 11	0	0
PM Shear 12	0	0
PM Top Panel	0	26.0
Propellant Tank 1	0	1.5
Propellant Tank 2	0	1.5
Press Tank 1	0	1.0
Press Tank 2	0	1.0
<b>Total</b>	<b>4.0</b>	<b>155.0</b>

From Table 18 it can be seen that the total estimated power required for the thermal control of the GSST satellite for OPC3-1 is 155 W, which increases to 186 W if a design margin of 20 % is assumed.

In Table 19 is presented the nominal estimated mass for of the various elements considered to be used in the GSST satellite thermal control.

*Table 19 - Nominal mass estimate for OPC3-1 thermal control.*

Component	Area(m <sup>2</sup> )	Density(kg/m <sup>2</sup> )	Mass(kg)
MLI blankets	41.5	0.50	20.8
Radiators (OSR)	4.0	0.50	2.0
Panels internal surface painting (black)	52.8	0.13	6.9
Others (doublers, interfiller, heaters, termistors, propulsion lines MLIs, etc)	-	-	15.0
<b>Total</b>			<b>44.7</b>

As for the heater's power, a 20 % design margin must be added for the mass of the thermal control elements, which projects an estimated total mass for the subsystem of 53,7 kg.

#### 4.1.8 OPC3-1: Mechanisms

In the GSST satellite, either for OPC3-1 and OPC3-2 options, there are three elements that must be deployed in orbit: The communication antennas, the magnetometer sensors, and the solar panels. The dimensions and mass properties of the SAG, and magnetometer booms and their sensors are the same for both options. Dimensions and mass of the X-band and Ka-band antennas are different, but they are not big enough to justify a dedicated solution for each type of antenna so, for the purposes

of the present study, the same mechanical solution for their deployment was adopted. Hence, the mechanisms adopted for OPC3-1, described in the following paragraphs, were also adopted for OPC3-2.

The mechanical configuration proposed for the X-band antennas in OPC3-1 is composed of the following components:

- Hold and release mechanism: Its function is to keep the antenna properly folded during launch, and ready for deployment after being commanded;
- Deployment and holding: Its function is to allow the correct antenna deployment and properly held in the open position;
- Dynamic pointing: Its function is to allow the proper pointing of the antenna towards the ground station during the satellite's orbital movement.

The X-band antenna is mounted in a substructure which the main objective is to allow the antenna to be positioned sufficiently far from the satellite's body when deployed, such that it can be properly pointed to the ground station. At launching, the communication antennas are folded and positioned close to the satellite's body. In Figure 28 it can be seen the position of the communication antennas when folded and deployed.

Commercial options of mechanisms, that perform the functions needed for the X-band antennas, are available, and one of them was chosen as a reference for the estimation of dimensional and mass characteristics of such kind of devices, as can be seen in Table 20.

*Table 20 - Nominal dimensional, mass and functional characteristics of X-band antennas mechanisms.*

Component	Characteristics
Hold and release mechanism	Mass: 0.6 kg; Dimensional envelope: 60x60x60 mm; Operational temperature: -40°C to +80 °C; Power: Not applicable; Movement amplitude: 90°.
Deployment and holding mechanism	Mass: 1.3 kg; Dimensional envelope: 100x80x80 mm; Operational temperature: -40°C to +80 °C; Power: Not applicable; Movement amplitude: 90°.
Pointing mechanism	Two-axis gimbal (360° azimuth, 90° elevation); Mass: 10.5 kg; Dimensional envelope: 300x150x150 mm; Operational temperature: -40°C to +80 °C; Power: 6.5 W.

The same mechanisms used for “hold and release”, and “deployment and holding” of the X-band antennas were chosen to perform these same functions for the magnetometers sensors. In Figure 28 the magnetometers booms and sensors are shown in the deployed and folded positions.

For the SAG, the mechanisms should guarantee that: i) it is firmly held to the satellite body in launch configuration; ii) allow its full deployment to a 90° angle in relation to the satellite's side where it is fixed and; iii) be hold at this position after deployment. Note that the SAG of the GSST satellite has not a rotational movement. After deployment, it is kept in the same relative position to the satellite's body. The SAG's “hold and release” mechanism uses the same principle of the one used in the antennas and magnetometers booms, but due to specific requirements associated with the solar arrays, a different “deployment and holding” mechanism is used for it, which main characteristics are: Mass: 0.7 kg; dimensional envelope: 120x60x60 mm; operational temperature -40°C to +80 °C and; amplitude of movement: 90°. It is a passive device.

#### 4.1.9 OPC3-1: Layout and structure concept

In Figure 29 the conceived layout for the GSST satellite, OPC3-1 GEO option, is shown. It is composed of two modules: Service (SM) and Payload (PM). The service module is composed of two compartments SM1 and SM2, which are in turn made of 22 Aluminium sandwich panels. The payload module is composed of 19 Aluminium sandwich panels. A carbon fiber composite material cylinder of 1194 mm in diameter connects the service and payload modules. Its base is in the interface plane between the satellite and launcher, and its top flush to the PM top panel.

The SAG is composed of two solar panels, with a total area of 6 m<sup>2</sup>, disposed of in fixed wings. They are made of carbon fiber composite material.

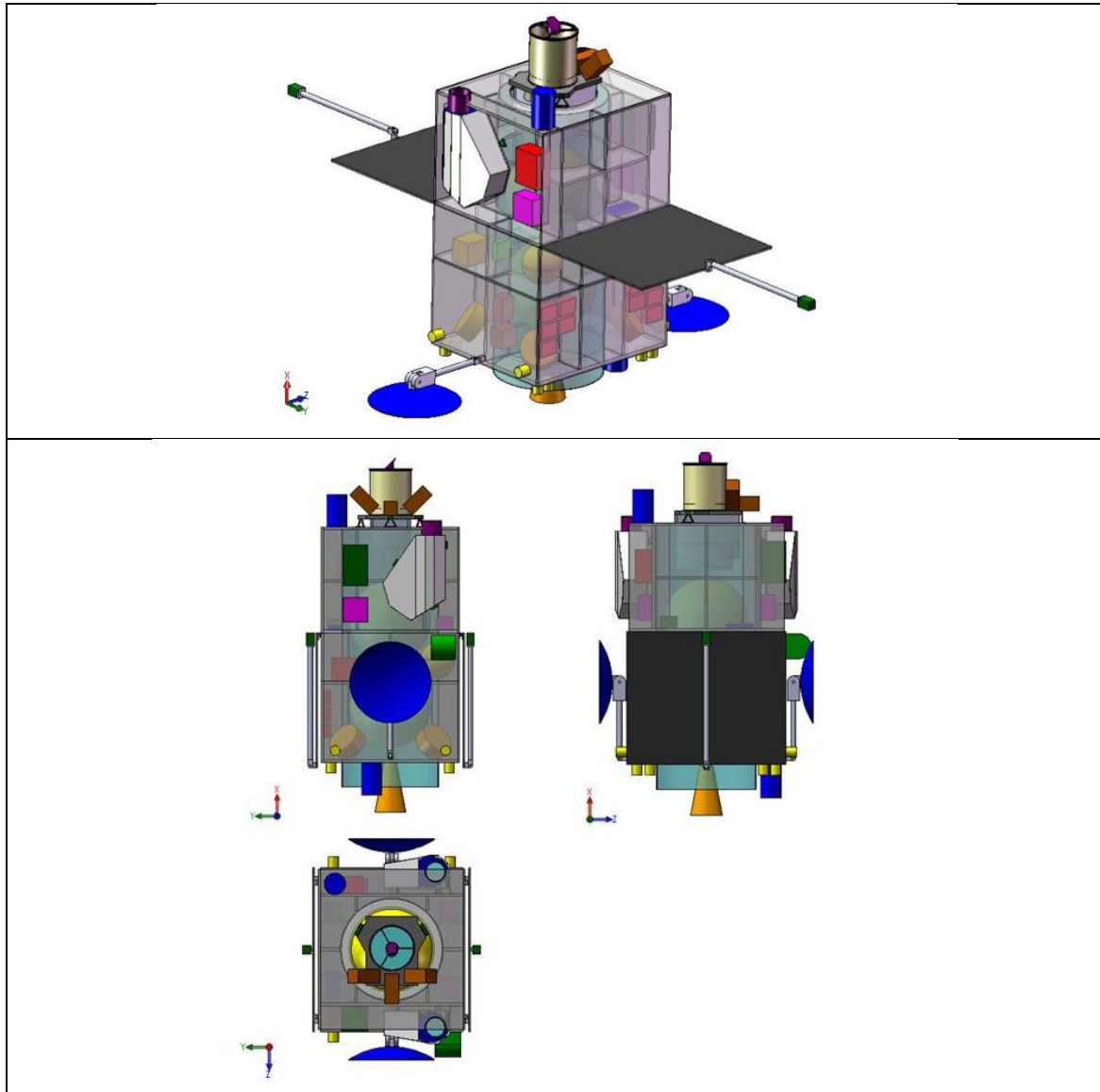


Figure 29 - OPC3-1 satellite external layout. Views for orbit (X-band antennas, SAG and magnetometers booms deployed) and launch configurations.

In Figure 30 the external dimensions of the GSST satellite, OPC3-1 option, is shown. The dimensions of its structural envelope are shown in Figure 31.



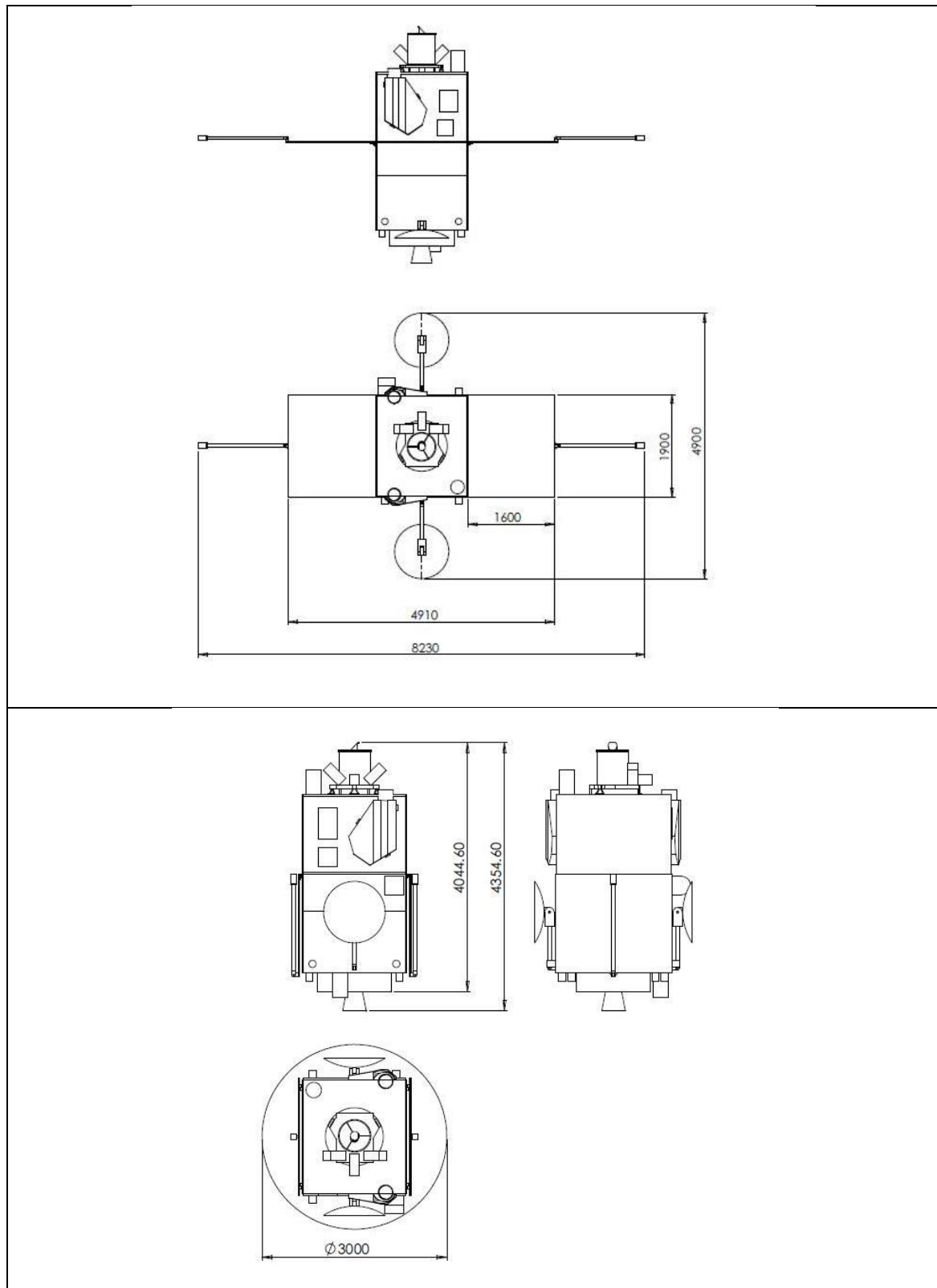


Figure 30 - OPC3-1 external dimensions, for orbit and launch configurations (dimensions in mm).

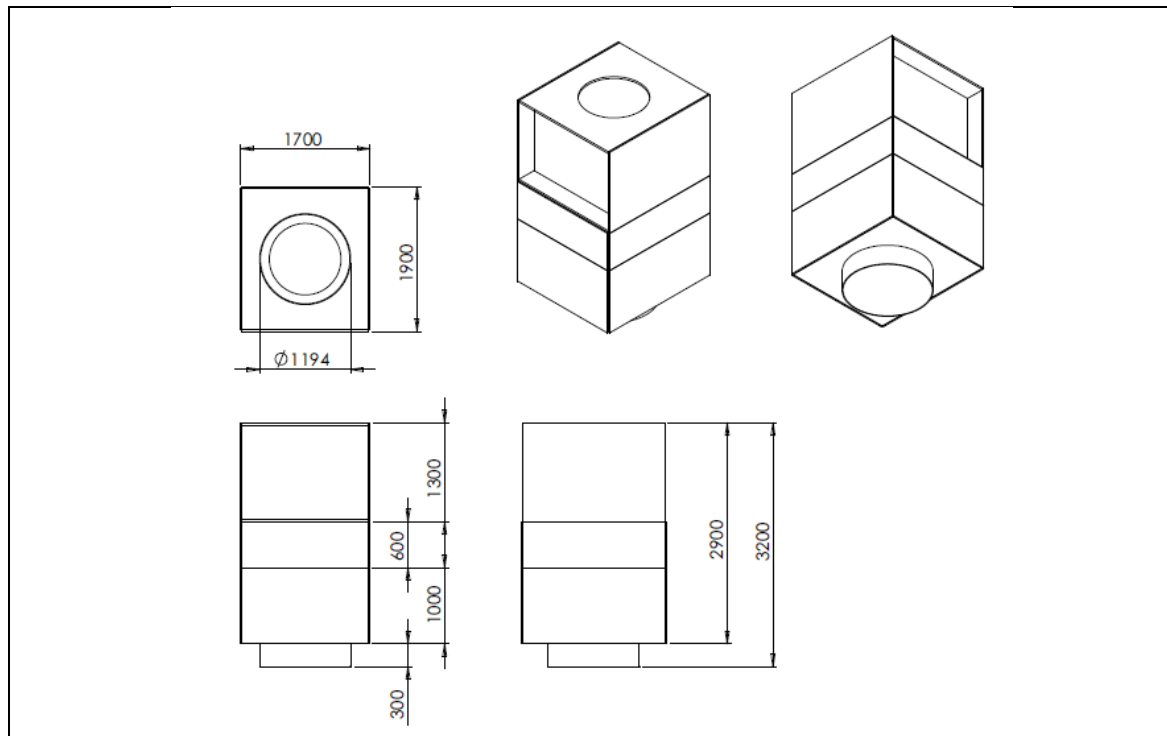


Figure 31 - Dimensions of GSST satellite structure for OPC3-1 (dimensions in mm).

The equipment positioning over the satellite panels is presented in Table 21. From Figure 32 to Figure 38 this positioning is shown through views of the satellite.

Table 21 - Equipment positioning at satellite panels, for OPC3-1.

Panel	Equipament	Units
SM1 Lower Panel	Reaction wheel	4
	S-Band antenna	1
	Thruster	8
SM1 Lateral Y+	Batery pack	10
SM1 Lateral Z+	Thruster	2
	X-band antenna	1
SM1 Lateral Z-	Thruster	2
	X-band antenna	1
SM1 Shear 6	Gyroscope (sensor)	1
	Gyroscope (electronics)	1
SM1 Top Panel	ACDH computer	1
	PCDU	1
	Pressurizer tank	2
SM2 Lateral Z+	HEP detector	1
SM2 Lateral Y+	Solar panel	1
	Magnetometer (sensor)	1
SM2 Lateral Y-	Solar panel	1
	Magnetometer (sensor)	1
SM2 Shear 3	Gimble electronics	1
SM2 Shear 6	Gimble electronics	1
PM Lower Panel	DDR	1
	Magnetometer (electronics)	1
	S-band transponder	2
PM Vertical Z+	Broadband radiometer	1
	X-band transmitter	1
	FD camera	1
PM Vertical Z-	Optics central unit	1
	X-band transmitter	1
	FD camera	1
PM Top Panel	S-Band antenna	1
Cylinder	Apogee motor	1
	Propellent tank	2
	HR camera	1
	Star sensor	3

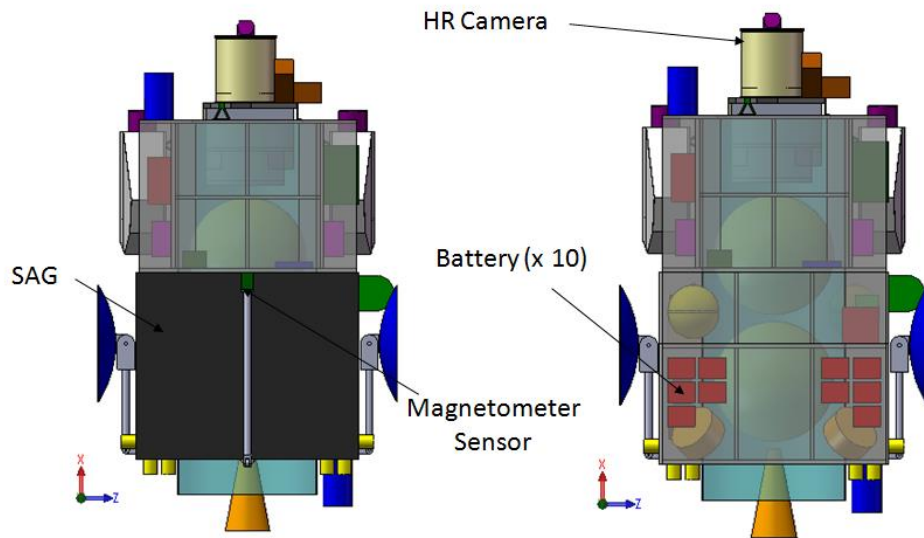


Figure 32 - Y+ side view of GSST satellite, showing equipment layout for OPC3-1.

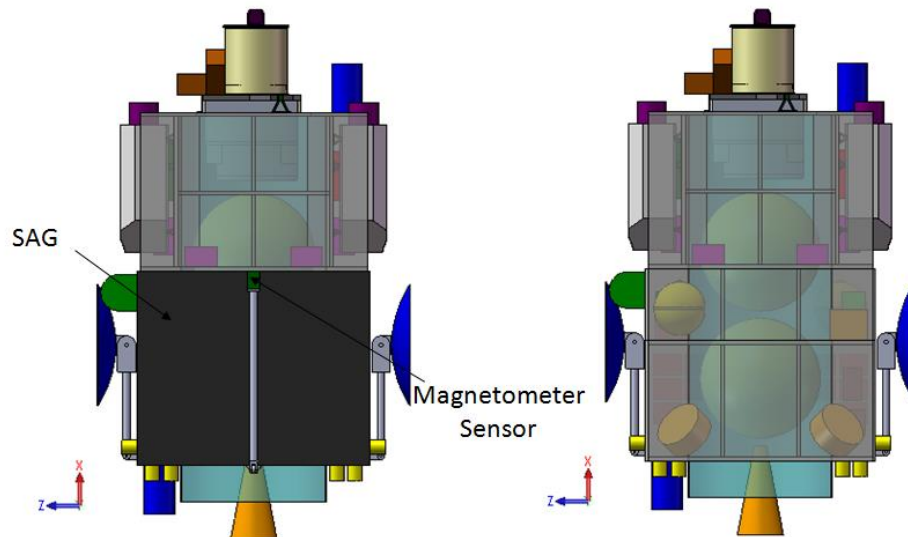


Figure 33 - Y- side view of GSST satellite, showing equipment layout for OPC3-1.

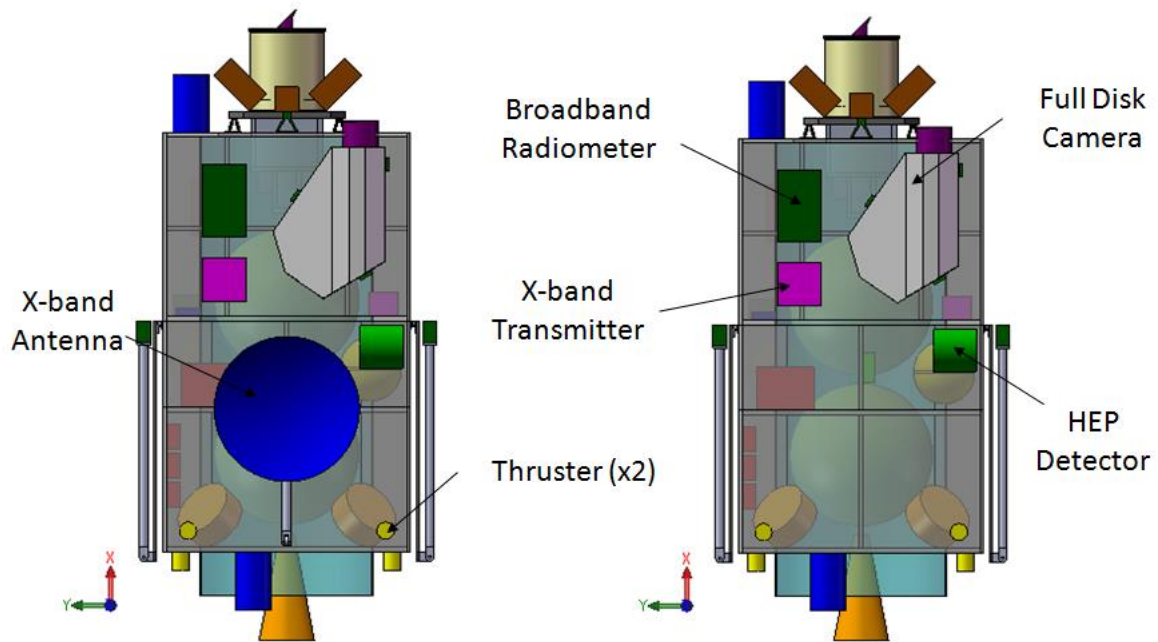


Figure 34 - Z+ side view of GSST satellite, showing equipment layout for OPC3-1.

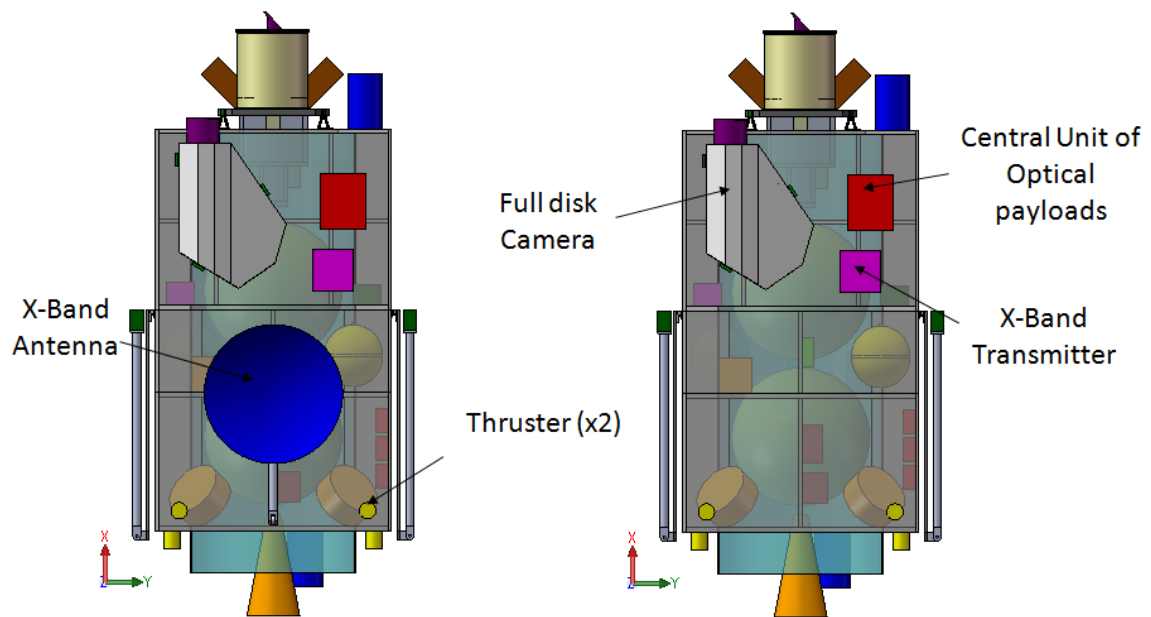


Figure 35-Z- side view of GSST satellite, showing equipment layout for OPC3-1.

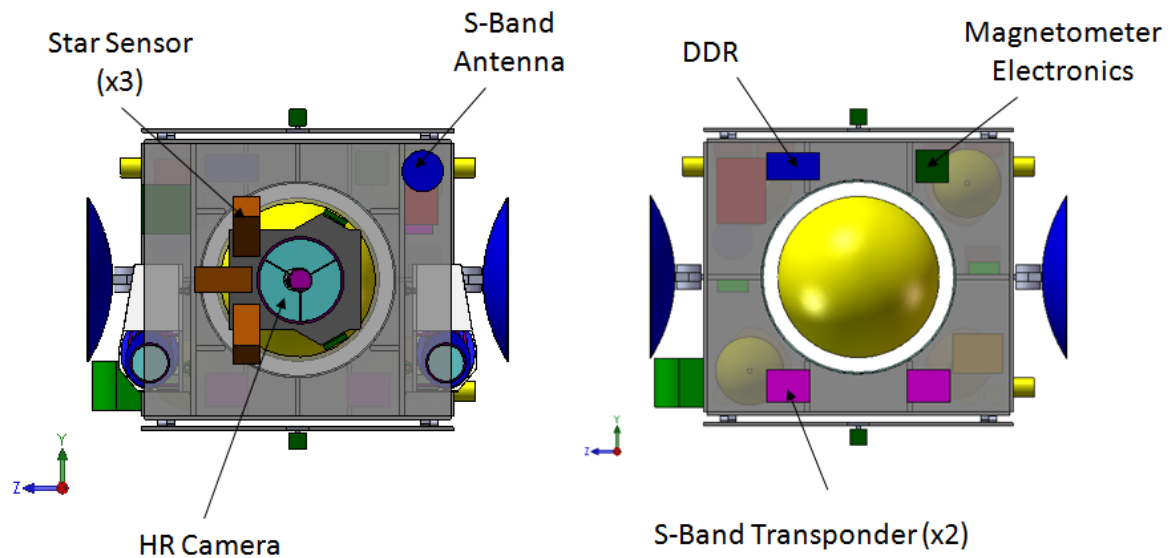


Figure 36 - PM Top Panel & PM Lower Panel side views of GSST satellite, showing equipment layout for OPC3-1.

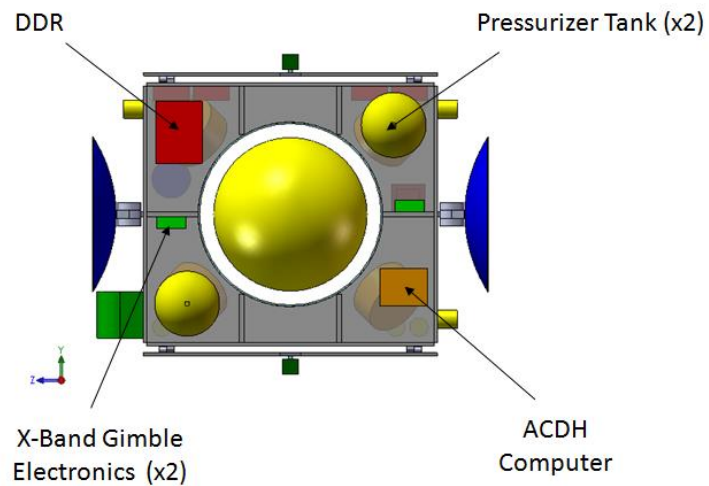


Figure 37 - SM1 Top Panel side view of GSST satellite, showing equipment layout for OPC3-1.

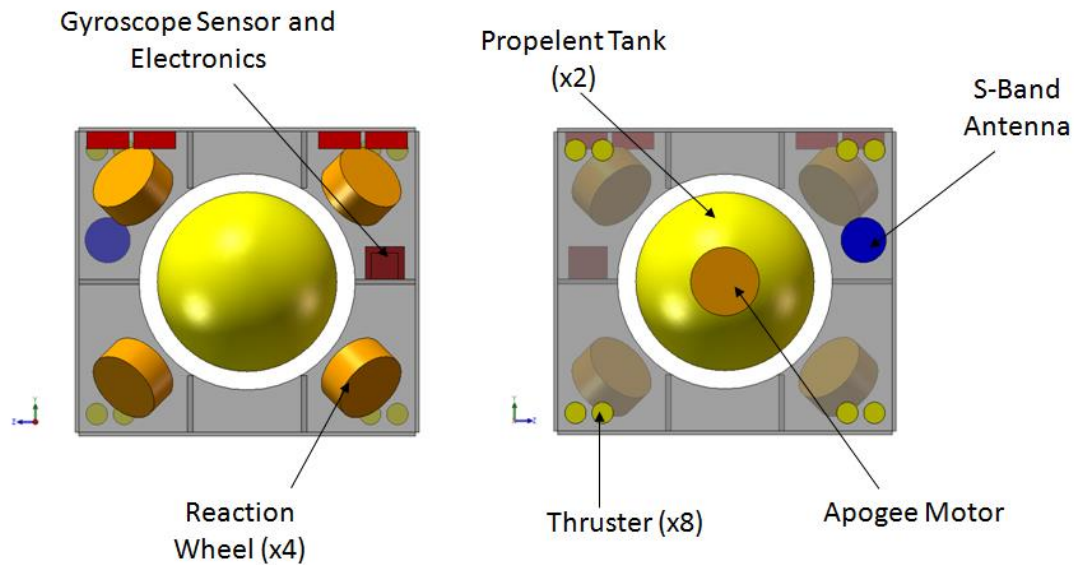


Figure 38 - SM1 Lower Panel side view of GSST satellite, showing equipment layout for OPC3-1.

In Figure 39 the satellite's mass properties are presented for the launch and orbit configurations.

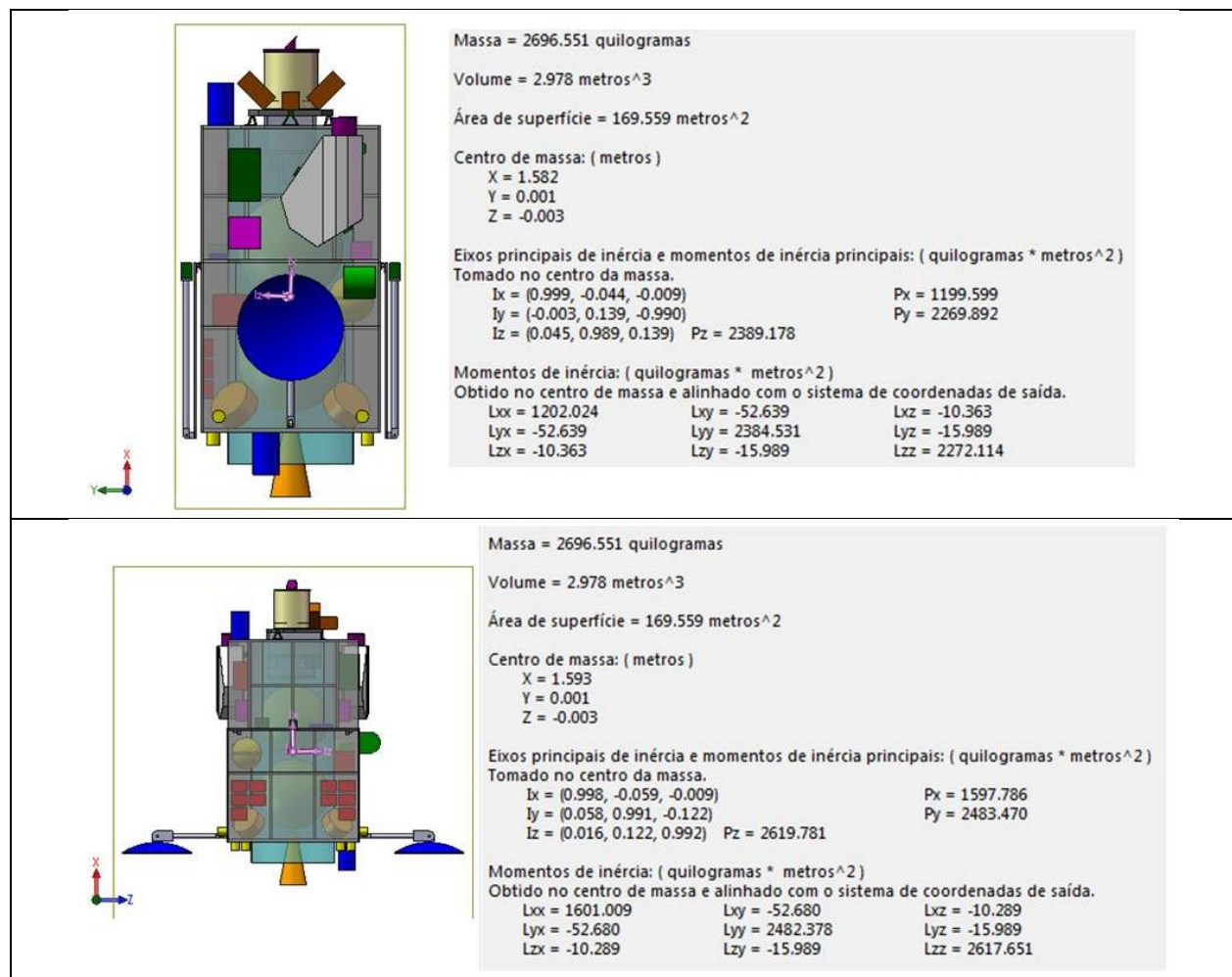


Figure 39 - GSST satellite mass properties for OPC3-1, in launch and orbit configurations.



In Table 22 the dimensions and mass properties of the GSST satellite panels for OPC3-1 are shown. The total structure mass, including a margin of 20 %, summed up to 468,2 kg.

Table 22 - Structure panels breakdown for OPC3-1. Mass in kg.

	Panel	Length (m)	Width (m)	Height (m)	Area (m <sup>2</sup> )	Mass without margin (kg)	Mass with margin (kg)
1	SM1 Lower Panel	1.860	1.660	0.040	3.088	24.701	29.641
2	SM1 Lateral Z+	1.660	1.000	0.020	1.660	4.980	5.976
3	SM1 Lateral Z-	1.660	1.000	0.020	1.660	4.980	5.976
4	SM1 Lateral Y+	1.860	1.000	0.020	1.860	9.300	11.160
5	SM1 Lateral Y-	1.860	1.000	0.020	1.860	9.300	11.160
6	SM1 Shear 1	0.314	0.930	0.030	0.292	2.043	2.452
7	SM1 Shear 2	0.314	0.930	0.030	0.292	2.043	2.452
8	SM1 Shear 3	0.333	0.930	0.030	0.310	2.168	2.601
9	SM1 Shear 4	0.314	0.930	0.030	0.292	2.043	2.452
10	SM1 Shear 5	0.314	0.930	0.030	0.292	2.043	2.452
11	SM1 Shear 6	0.333	0.930	0.030	0.310	2.168	2.601
12	SM1 Top Panel	1.860	1.660	0.030	3.088	24.701	29.641
13	SM2 Lateral Z+	1.660	0.600	0.020	0.996	2.988	3.586
14	SM2 Lateral Z-	1.660	0.600	0.020	0.996	2.988	3.586
15	SM2 Lateral Y+	1.860	0.600	0.020	1.116	3.348	4.018
16	SM2 Lateral Y-	1.860	0.600	0.020	1.116	3.348	4.018
17	SM2 Shear 1	0.314	0.600	0.030	0.188	1.318	1.582
18	SM2 Shear 2	0.314	0.600	0.030	0.188	1.318	1.582
19	SM2 Shear 3	0.333	0.600	0.030	0.200	1.399	1.678
20	SM2 Shear 4	0.314	0.600	0.030	0.188	1.318	1.582
21	SM2 Shear 5	0.314	0.600	0.030	0.188	1.318	1.582
22	SM2 Shear 6	0.333	0.600	0.030	0.200	1.399	1.678
23	PM Lower Panel	1.860	1.660	0.030	3.088	24.701	29.641
24	PM Vertical Z+	1.660	1.240	0.030	2.058	14.409	17.291
25	PM Vertical Z-	1.660	1.240	0.030	2.058	14.409	17.291
26	PM Lateral Y+	1.860	1.300	0.020	2.418	7.254	8.705
27	PM Lateral Y-	1.860	1.300	0.020	2.418	7.254	8.705
28	PM Shear 1	0.177	0.590	0.030	0.104	0.730	0.876
29	PM Shear 2	0.177	0.590	0.030	0.104	0.730	0.876
30	PM Shear 3	0.177	0.590	0.030	0.104	0.730	0.876
31	PM Shear 4	0.177	0.590	0.030	0.104	0.730	0.876
32	PM Shear 5	0.233	0.590	0.030	0.137	0.962	1.155
33	PM Shear 6	0.233	0.590	0.030	0.137	0.962	1.155
34	PM Central Panel	1.240	1.660	0.030	2.058	14.409	17.291
35	PM Shear 7	0.177	0.620	0.030	0.110	0.767	0.921
36	PM Shear 8	0.177	0.620	0.030	0.110	0.767	0.921
37	PM Shear 9	0.177	0.620	0.030	0.110	0.767	0.921
38	PM Shear 10	0.177	0.620	0.030	0.110	0.767	0.921
39	PM Shear 11	0.233	0.620	0.030	0.144	1.011	1.213
40	PM Shear 12	0.233	0.620	0.030	0.144	1.011	1.213
41	PM Top Panel	1.860	1.660	0.030	3.088	21.613	25.936
42	Cilindro					85.000	102.000
43	Angle Bars & Fasteners					40.000	48.000
44	Suportes					40.000	48.000
					TOTAL	390.198	468.238

#### 4.1.10 OPC3-1: Launcher options

The selection of candidate options for launching the GSST satellite, OPC3-1 GEO option, was based taking into account parameters such as of orbit, satellite mass and its external dimensional envelope during launch (Figure 30). These parameters are summarized below.

- Orbit type – GTO with perigee at 2,500 km and apogee at 42,164 km;
- Orbit inclination – 5.2° or 28.5°;
- Satellite mass – 2.697Kg;
- CG height in relation to the separation plane – 1.58 m;
- Satellite static envelope – 3.00 m (diameter) x 4.355 m (height).

In Table 23 a set of candidate commercial launchers, which performance characteristics are adequate for an OPC3-1 launch is shown.

*Table 23 - Candidate launchers for the GSST satellite in configuration OPC3-1.*

Launcher	Maximum mass capacity [kg]	Orbit inclination [deg]	Estimated launch cost US\$	Launch base
LM-3C	5100	28.5	50 to 70 million	Xichang
Ariane 5	6700	5.2	125 to 155 million	Kourou
H-IIA 202	4100	28.5	70 to 80 million	Tanegashima
Proton K	4930	28.5 ou 5.2	Negotiable	Baikonur
Delta IV	3934	28.5	80 to 100 million	Cabo Canaveral
Zenit 3S	6066	28.5	Negotiable	Baikonur Sea Launch Odyssey

#### 4.1.11 OPC3-1: Ground system concept

The ground segment for the OPC3-1 option considers the utilization of the existing INPE's infrastructure, with minimum adaptation, which means that the X-band and S-band antennas located at Cuiabá/MT would be used for receiving scientific and transmitting/receiving service data, respectively. The satellite will be operated by INPE's satellite control center (CCS), which would also house a science mission center. The EMBRACE would be responsible to distribute the science and associated satellite service data do the mission's users. In Figure 39 a sketch of the conceived OPC3-1 ground segment is depicted.

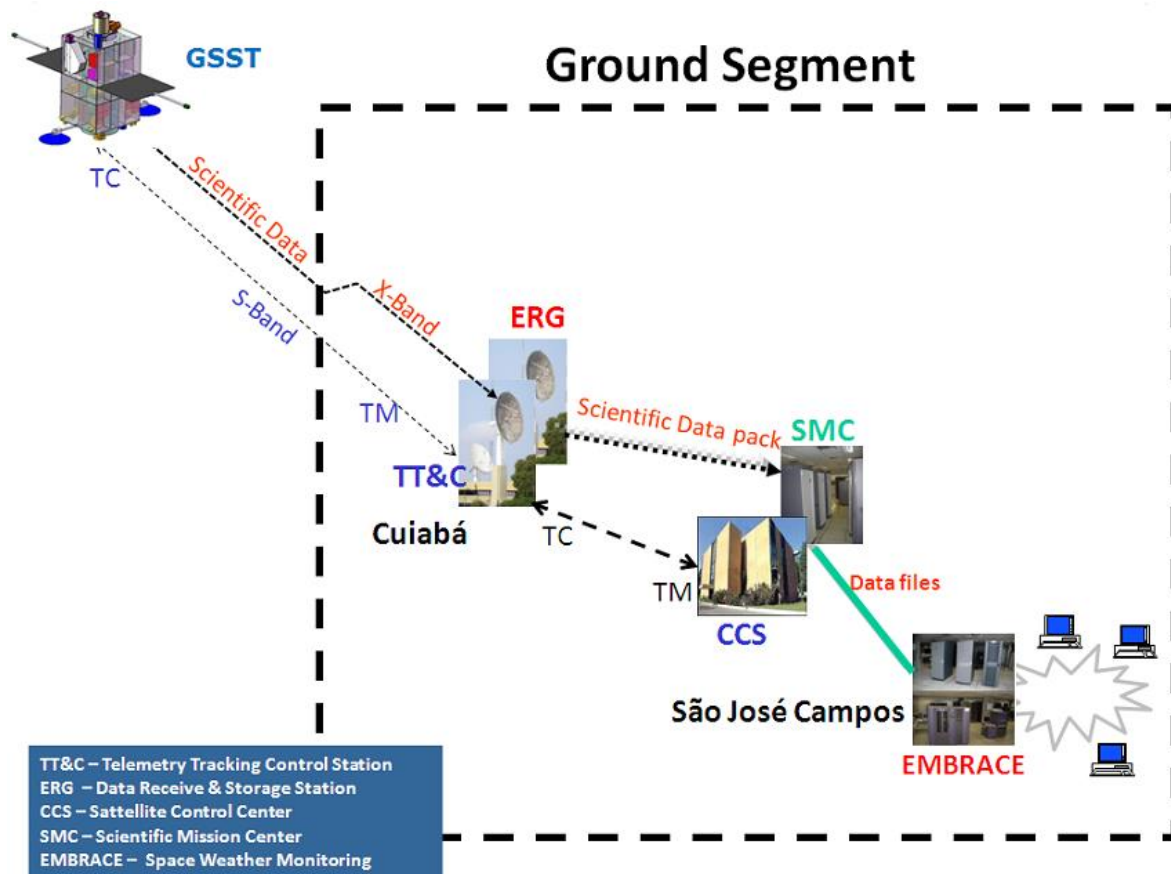


Figure 40 - Ground segment concept for OPC3-1.

#### 4.1.12 OPC3-1: Satellite disposal analysis

The Inter-Agency Space Debris Coordination Committee (IADC) guidelines (IADC, 2007) define two protected regions of space: low Earth Orbit (LEO) and geosynchronous Earth orbit (GEO). The GEO protected region is defined as  $35,786 \pm 200$  km, with a latitude of  $0 \pm 15$  deg. Any mission that passes through that protected region must be maneuvered as the end of the mission to remain clear. Disposal from GEO is performed by increasing the orbital radius sufficiently to remain well in excess of 200 km above the GEO altitude for a minimum of 100 years. The disposal process is carried out to avoid an accumulation of debris and to prevent potential signal interference. In addition to increasing the orbital radius, the final orbit should be circularized to an eccentricity of no more than 0.003, and the satellite needs to be passivated.

Due to the effects of solar radiation pressure, as well as lunar-solar and geopotential perturbations, the recommended minimum increase,  $\Delta H$ , above GEO (in km) is defined as (Wertz and Larson, 2011)

$$\Delta H = 200 + 35 + \left( 1000 C_R \frac{A}{m} \right),$$

where the constant 35 is incorporated due to effects from lunar-solar and geopotential perturbations;  $C_R$  is the solar radiation pressure coefficient (usually assumed as 2); and  $A/m$  is the satellite cross-sectional area to dry mass ratio (given in  $\text{m}^2/\text{kg}$ ).

Since the satellite from Opc3-1 presents an area to dry mass ratio of 0.007, the equation above provides a minimum increase of 249 km above GEO. Then a total velocity change of approximately 10 m/s is required to perform the transfer and circularization maneuvers. The transfer time, based on the Hohmann transfer approach, to achieve the disposal orbital is approximately 12 hours.

#### **4.1.13 OPC3-1: Satellite mass and power budget**

In Table 24 the mass and power budgets for OPC3-1 is shown.

Table 24 - Mass and power budget for OPC3-1.

Subsystem	Component	Units	Unit Dimensions (LxWxH) mm	Mass per Unit unidade (kg)		Total Mass (kg)				Power consumption per unit (W)					
				Best Estimate (kg)	Margin (%)	Total Units (kg)	Subsystem (kg)	Subsystem Mass / Total Mass (%)	Total Mass (kg)	Nominal operation	Margin (%)	Operation with margin	Nominal stand-by	Margin (%)	Standby with margin
Thermal Control	Heaters	1	NA				53.640	2.0		155.0	20.0	186.0	155.0	20.0	186.0
	MLJs	1	NA	20.8	20	24.960				NA			NA		
	Radiators (OSR)	1	NA	2	20	2.400				NA			NA		
	Internal Painting	1	NA	6.9	20	8.280				NA			NA		
	Miscellaneous	1	NA	15.000	20	18.000				NA			NA		
Power	PCDU	1	400x300x300	15.000	5.0	15.750	102.900	3.9		100.0	5.0	105.0	50.0	5.0	52.5
	Battery	10	230x170x95	4.300	5.0	45.150				6.0	5.0	6.3	6.0	5.0	6.3
	Solar Panel	2	3m2	20.000	5.0	42.000				NA			NA		
Propulsion	Propellant	1	967.371	1050.930	5.0	1103.477	1553.108	58.8		0.0	5.0	0.0	0.0	5.0	0.0
	Propellant tank	2	991 x 991 x 991	17.100	5.0	35.910				0.0	5.0	0.0	0.0	5.0	0.0
	Pressurizer tank	2	442.2 x 420.1 x 420.1	8.400	5.0	17.640				0.0	5.0	0.0	0.0	5.0	0.0
	Thruster	12	127 x 59 x 46	0.350	5.0	4.410				30.0	5.0	31.5	30.0	5.0	31.5
	Apogee Motor	1	737 x 381 x 381	4.310	5.0	4.526				46.0	5.0	48.3	46.0	5.0	48.3
	Other	1	NA	368.710	5.0	387.146				0.0	5.0	0.0	0.0	5.0	0.0
OBDH	Computer	1	307x242x263	13.600	5.0	14.280	14.280	0.5		35.0	5.0	36.8	35.0	5.0	36.8
Communications	X-band transmitter	2	300x300x170	6.000	5.0	12.600	37.800	1.4		100.0	5.0	105.0	50.0	5.0	52.5
	X-band antenna	2	1000D	6.000	5.0	12.600				0.0	5.0	0.0	0.0	5.0	0.0
	S-band transponder	2	260x200x170	5.000	5.0	10.500				46.0	5.0	48.3	23.0	5.0	24.2
	S-band antenna	2	250Dx400A	1.000	5.0	2.100				0.0	5.0	0.0	0.0	5.0	0.0
Attitude and Orbit Control	Reaction wheel	4	412 x 412 x 178	12.000	5.0	50.400	69.048	2.6		22.0	5.0	23.1	22.0	5.0	23.1
	Star Sensor	3	160 x 170 x 350	3.700	5.0	11.655				10.0	5.0	10.5	10.0	5.0	10.5
	Solar Sensor	8	28 x 28 x 3	0.020	5.0	0.168				0.0	5.0	0.0	0.0	5.0	0.0
	Gyroscope	1	215 x 215 x 180	2.000	5.0	2.100				0.0	5.0	0.0	0.0	5.0	0.0
	Gyroscope electronics	1	270 x 150 x 145	4.500	5.0	4.725				24.0	5.0	25.2	24.0	5.0	25.2
Mechanisms	X-band antenna gimbal (2 axis)	2	300x150x150	10.500	5.0	22.050	46.620	1.8		6.5	5.0	6.8	1.0	5.0	1.1
	Gimbal electronics	2	212x190x75	3.500	5.0	7.350				12.0	5.0	12.6	2.5	5.0	2.6
	Hinges of X-band antenna (2x) and magnetometer booms (2x)	4	100x80x80	1.300	5.0	5.460				Not Applicable			Not Applicable		
	Hold down & Release of X-band antennas (6x) and magnetometer booms (4x)	10	60x60x60	0.600	5.0	6.300				Not Applicable			Not Applicable		
	SAG hinge	4	120x60x60	0.700	5.0	2.940				Not Applicable			Not Applicable		
	SAG Hold down & Release	4	60x60x60	0.600	5.0	2.520				Not Applicable			Not Applicable		
Structure	Satellite structure	1		390.198	20.0	468.238	468.238	17.7		Not Applicable					
Payloads	High resolution telescope and proximity electronics	1	See Figure 10	88.600	10.0	97.460	285.918	10.8		55.0	20.0	66.0			0.0
	Wide field telescope 1 and proximity electronics	1	See Figure 12	47.670	20.0	57.204				25.0	20.0	30.0			0.0
	Wide field telescope 2 and proximity electronics	1	See Figure 12	47.670	20.0	57.204				25.0	20.0	30.0			0.0
	Digital data recorder	1	320x170x55	1.000	5.0	1.050				15.0	5.0	15.8	3.5	5.0	3.7
	Optical Payload Central Unit	1	Dimensões no CAD	25.000	20.0	30.000				150.0	20.0	180.0	15.0	20.0	18.0
	Broadband radiometer	1	500x300x300	3.500	20.0	4.200				10.0	20.0	12.0	8.3	20.0	9.9
	High energy particle telescope	1	300x300x300	10.000	20.0	12.000				10.0	20.0	12.0	1.0	20.0	1.2
	Magnetometer (electronics)	1	200x200x150	3.000	20.0	3.600				3.0	20.0	3.6	1.0	20.0	1.2
	Magnetometer (sensor)	2	150x100x100	1.000	10.0	2.200				1.0	10.0	1.1	1.0	10.0	1.1
	Magnetometer (Booms) (without wiring or instruments)	2	3m	10.000	5.0	21.000				0.0	10.0	0.0	0.0	10.0	0.0
Harness	Satellite harness	1		65.000		65.000	65.000	2.459		Not Applicable					
						TOTAL =	2642.911	100.000							

## 4.2 OPC3-2

### 4.2.1 OPC3-2: Orbit Analysis

The OPC3-2 is a Low Earth Orbit mission. Among all possible orbits, the most suitable one is a Sun-synchronous orbit with RAAN positioned at 6:00 AM. Ideally, the orbit should be a polar one (inclination equal to  $90^\circ$ ) with the aforementioned RAAN. In this case, no eclipse will be experienced by the satellite during its lifetime. However, the gravitational perturbations will eventually drive the orbit plane to another position and the correction maneuvers will require a high amount of fuel. This can be mitigated by selecting a Sun-synchronous orbit so that the gravitational perturbations will be used to maintain the geometrical configuration of the orbit plane with respect to the Sun. In this case, only minor orbit corrections are necessary to keep the orbit parameters as closest as possible to the nominal ones. This will highly decrease the fuel requirement, but eclipses will exist in some periods of the mission.

The altitude of the selected Sun-synchronous orbit is 601.599 km, which leads to a ground repetition period of 23 days. This means that all the analysis that are related to elements in the ground shall be performed at least by 23 days. The altitude was selected so that no maneuver will be necessary to de-orbit the satellite, which, in this case, decreases the amount of fuel required by the mission. The orbit parameters summary for OPC3-2 can be seen in Table 25.

*Table 25 - Orbit parameters summary for OPC3-2.*

Parameter	Value
<b>Semi-major axis</b>	6979.736 km
<b>Altitude</b>	601.599 km above the Equator
<b>Revolutions per Day</b>	14 20/23
<b>Revs. Before Repeating</b>	342
<b>Orbit period</b>	5810.526 s (96.84 min)
<b>Eccentricity</b>	$\approx 0.0$ (can be chosen to yield a frozen orbit)
<b>Inclination</b>	$97.749^\circ$
<b>RAAN</b>	6:00 AM ( $190.933^\circ$ at January 1 <sup>st</sup> , 2025, 0:00 GMT)
<b>True anomaly</b>	Any

#### 4.2.1.1 Eclipse Time

The eclipse time for OPC3-2 can be seen in Figure 41. The analysis was performed for 1 year starting on January 1<sup>st</sup>, 2025. Notice that, in the worst day, the eclipse time is equivalent to 21% of the orbit, which is approximately 21 min, and eclipses only occur in the Summer (South hemisphere). Notice that in some days the satellite will not acquire images from the Sun during 90% of the time, but this requirement is indeed fulfilled by the selected orbit considering the entire mission lifetime.

## Eclipse time

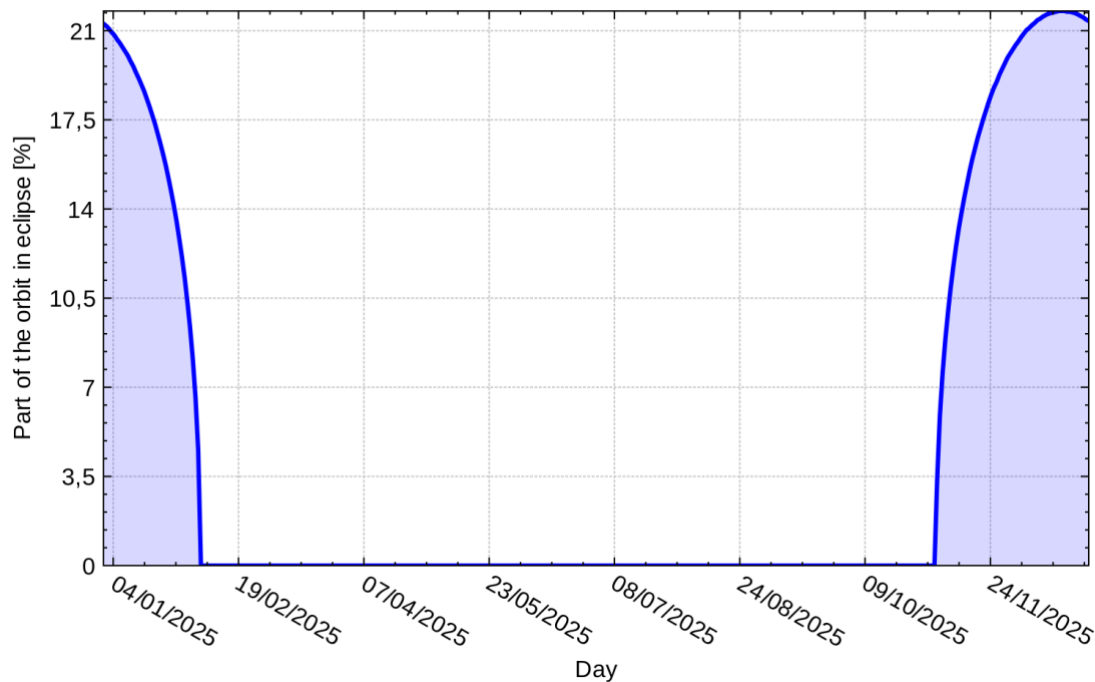


Figure 41 - Eclipse time for OPC3-2.

### 4.2.1.2 $\Delta V$ budget

The  $\Delta V$  budget was computed using the parameters in Table 26. The mission will need 64 m/s to acquire the nominal orbit after injection and to maintain its orbit during the predicted lifetime. Notice that it is not necessary to consider a maneuver to disposal the satellite because it will re-enter within 25 years after the end of the mission in the designed nominal orbit as shown in Section 4.2.12.

The time between maneuvers to maintain the orbit will depend on the Solar Flux and the maximum allowed drift of the ground track. At the solar maximum ( $F_{10.7} = 225$ ,  $AP = 20$ ), one can expect a time between maneuvers of approximately 20 days if the ground track is allowed to drift 20 km. Furthermore, since the designated mission lifetime is five (5) years, then it is possible to provide an initial inclination offset such that a correction maneuver for this parameter will not be necessary during the mission lifetime. Notice that the acquisition of scientific data is suspended when an orbit maneuver is performed.

Table 26 -Parameters to compute the  $\Delta V$  for OPC3-2.

Parameter	Value
Mass	964.079 kg
Cross-sectional area in the direction of velocity vector	5.0 m <sup>2</sup>
Drag coefficient (Cd)	2.2
Mission lifetime	5 years
Solar flux to compute the mean atmospheric density	$F_{10.7} = 225$ , $AP = 20$ for 1 year; $F_{10.7} = 175$ , $AP = 16$ for 3 years; and $F_{10.7} = 125$ , $AP = 12$ for 1 year.
Launcher errors	20 km in semi-major axis. 0.05° in inclination.
De-orbit perigee	The same as the nominal orbit, since the satellite reenters within 25 years without changing its perigee.



Parameter	Value
Margin	10%

#### 4.2.2 OPC3-2: Orbit and attitude control subsystem analysis

##### 4.2.2.1 Actuators design

The actuators design of the attitude and orbit control subsystem (AOCS) depends on the system requirements (see Section 1.2) and the disturbances that will be applied to the satellite. The worst-case scenario perturbations were computed employing the input parameters in Table 27. The results are presented in Table 28.

Table 27 - Input parameters used to compute the disturbance torques for OPC3-2.

Parameter	Value
Orbit radius	6979,736 km
Orbital period	5803.23 s
Sunlight period	5803.23 s
Spacecraft orbital velocity	7.560 km/s
Spacecraft inertia matrix	$\begin{bmatrix} 904.9 & -12.7 & -11.6 \\ -12.7 & 920.2 & 0.4 \\ -11.6 & 0.4 & 1226.3 \end{bmatrix} \text{ kg.m}^2$
Sunlit surface area	8.4 m <sup>2</sup>
Distance between the center of solar radiation pressure and the center of mass	0.01 m
Unitless reflectance factor	0.6
Spacecraft residual dipole moment	0.1
Ram area, which is the cross section in the ram direction that points towards the satellite motion <sup>4</sup>	5 m <sup>2</sup>
Drag coefficient	2.2
Distance between the center of aerodynamic pressure and the center of mass in the plane orthogonal to the velocity vector	0.1 m

Table 28 - Disturbance torques computed for OPC3-2.

Disturbance	Value (10 <sup>-5</sup> Nm)
Solar radiation pressure	0.0613
Atmospheric drag	0.3143
Magnetic field	0.2952
Gravity gradient <sup>5</sup>	9.8140
<b>Total disturbance torque</b>	<b>10.4849</b>

It is also necessary to define how the satellite will incorporate the tip-off angular velocity after separation from the launcher to acquire the initial Sun pointing. Considering a worst-case scenario in

<sup>4</sup>Since the satellite is inertially pointed, the velocity vector performs a full rotation per orbit as seen by the satellite body. Hence, the ram area was computed considering a mean value.

<sup>5</sup>Since the satellite is inertially pointed, the gravity gradient vector will ideally yield a periodic vector with possibly small secular component. However, the gravity gradient disturbance torque was computed as it was pointed to the Earth to obtain a worst-case scenario, because this geometry will indeed occur during the orbit correction maneuver. In this case, it was considered a misalignment between the body reference frame and the principal axes of 5° in pitch and roll.

which the launcher left the satellite with 2°/s in each one of its axes, it can be seen that the angular velocity after the release of the solar panels will be

$$\omega_b = \begin{bmatrix} 1.0 \\ 1.7 \\ 1.2 \end{bmatrix} ^\circ/s. \quad (1)$$

To simplify the AOCS design, it was decided that the thrusters will not be used for attitude control. Hence, this velocity must be removed from the satellite body within one orbit using reaction wheels and magneto-torquers. The amount of velocity to be incorporated in reaction wheels and to be removed with the magneto-torquers at the initial orbit can be seen in Table 29.

Table 29 - Angular velocity that each actuator set must remove from the satellite body.

Axis	Velocity incorporated by reaction wheels (°/s)	Velocity removed by the magneto-torquers (°/s)
X	0,11	0,89
Y	0,77	0,93
Z	0,55	0,65

Thus, it was possible to design the reaction wheels and the magneto-torquers. Notice that, since the design must be redundant, it was chosen a solution with 3 magneto-torquers with redundant coils and a set of 4 reaction wheels in a pyramid configuration. The later was computed with a 100% of margin so that if a reaction wheel fails, the others can replace it with no impact for the system. The design parameters for the actuators can be seen in Table 30.

Table 30 - Design parameters of the AOCS actuators.

Design parameter	Value
<b>Reaction Wheels</b>	
Maximum torque	0.14021 Nm
Momentum storage capacity	38.2480 Nms
<b>Magneto-torquers</b>	
Maximum dipole	250 Am <sup>2</sup>

Finally, the set of the actuators selected for OPC3-2 are:

- **4 reaction wheels placed in a pyramid configuration responsible to control the satellite attitude.**
  - **Maximum torque capacity:** 0.2 Nm.
  - **Momentum storage capacity:** 50 Nms.
  - **Mass:** 8.5 kg.
  - **Peak power:** 195 W.
  - **Mean power during nominal operation:** 22 W.
- **3 magneto-torquers with redundant coils responsible to remove angular momentum from the reaction wheel set.**
  - **Maximum dipole:** 250 Am<sup>2</sup>.
  - **Mass:** 5.5 kg.
  - **Power:** 4.8 W.

Notice that this set of reaction wheels is capable to maneuver the satellite  $180^\circ$  in 480 s when one of them is failed.

#### 4.2.2.2 Sensors design

A set of 8 coarse solar sensors was selected to provide a rough Sun position estimate during the initial Sun point acquisition and in the emergency mode. Those sensors must be positioned on the corners of the satellite, similar to the solution chosen for the satellite Amazonia-1.

A set of two magnetometers must also be present to measure the magnetic field to command the magneto-torquers to desaturate the reaction wheels.

A redundant GPS receiver shall provide the orbit determination. The accuracy in position determination is 10m, and the accuracy in velocity measurement is 0.25 m/s.

The mission requires a very stringent pointing knowledge. The absolute accuracy must be better than 10 arcsec ( $3\sigma$ ). A set of two star-trackers can provide this accuracy. However, since the system must be redundant, a third one must be used, because with only one star-tracker the attitude estimation accuracy about the optical axis is degraded.

The pointing stability requirement ( $< 0.833$  arcsec/s) calls for a navigation-grade gyro. It was selected a gyro with four channels, for redundancy purposes, with bias stability of  $0.01^\circ/\text{h}$  ( $3\sigma$ ) and angular random walk of  $0.0016^\circ/\sqrt{\text{h}}$  ( $1\sigma$ ).

This set of sensors will not provide the pointing accuracy to a selected feature in the Sun that is required for the mission. Hence, the AOCS needs to receive data from the tracking camera, which can measure the position of a point in the Sun with respect to a reference with a precision better than 0.25 arcsec ( $3\sigma$ ). Notice that the pointing knowledge is not absolute, but relative to a reference point selected in the Sun. Thus, we can define two operation modes. The first one uses the star tracker to provide an initial pointing of the satellite to the desired direction in the Sun. The second one discards the star trackers measurements and uses only the tracking camera data to keep the pointing error relative to a selected point in the Sun within the required interval.

Finally, the set of sensors selected for this mission is:

- **8 coarse solar sensors responsible to provide a rough Sun position estimation for initial pointing acquisition and in emergency mode.**
  - **Mass:** 0.02 kg.
  - **Power:** 0.01 W.
- **2 magnetometers responsible to measure the magnetic field so that the magneto-torquers can be commanded to remove angular momentum from the reaction wheels.**
  - **Mass:** 0.19 kg.
  - **Power:** 0.3 W.
- **A redundant GPS receiver with two antennas to determine the satellite orbit.**
  - **Mass:** 0.95 kg.
  - **Power:** 5.5 W.
  - **Antenna mass:** 0.05 Kg.
- **3 star trackers positioned on the edges of a cube to provide the absolute attitude determination.**
  - **Mass:** 3.7 kg.
  - **Power:** 10 W.

- **Thermo-elastic error:** 0.055 arcsec/°C ( $1\sigma$ ).
- **FOV spatial error:** 0.7 arcsec ( $3\sigma$ ).
- **Pixel spatial error:** 3.4 arcsec ( $3\sigma$ ).
- **Noise equivalent angle:** 0.8 arcsec/√s ( $3\sigma$ ).
- **1 inertial rotating unit with four sensing channels responsible to measure the satellite body velocity.**
  - **Mass of sensing head:** 2 kg.
  - **Mass of electronics:** 4.5 kg.
  - **Power:** 24 W.
  - **Bias stability:** 0.01°/h ( $3\sigma$ ).
  - **Angular random walk:** 0.0016 °/√h ( $1\sigma$ ).
- **1 tracking camera for fine attitude measurement with respect to a selected point in the Sun.**
  - For more information, see Section 2.

#### 4.2.2.3 AOCS design validation

Since this mission requires a very stringent pointing accuracy, it was decided to simulate the AOCS so that the design can be validated. The simulation was programmed using all the available information: actuators and sensors parameters, satellite perturbations, actuators saturation, DA/AD conversion resolution, etc. Notice, however, that many other parameters are not available in this mission phase, such as, for example, the reaction wheels unbalancing. This fact limits the fidelity of the results presented here that should be seen as a lower bound for the AOCS performance.

It is possible to see in Figure 42 the simulation results when the spacecraft is operating using the star trackers and the control subsystem was commanded to point the satellite to a fix location. This is the result of a Monte Carlo simulation with 100 realizations in which the initial pointing errors were sampled from a Gaussian distribution. On the left, it is possible to see the absolute pointing error statistics whereas, on the right, it is possible to see the angular velocity statistics. The black line is the mean value, the orange range encompasses all the results within  $1\sigma$  from the mean, and the blue range contains all the results within  $3\sigma$  from the mean. It is possible to verify that the selected gyro is capable of providing the angular stability required due to the camera design ( $< 0.833$  arcsec/s). However, the absolute pointing error considering only the star trackers is much larger than the requirement to observe a specific feature on the Sun. Thus, the measurements from the tracking camera are paramount to comply with the requirements.

It is possible to see in Figure 43 the simulation results when the spacecraft is operating using the tracking camera. In this case, the pointing error is not absolute, but relative to a point on the Sun that was chosen as reference. It is possible to see that all the requirements are met with margins. This is important because all non-modeled effects will increase the error as seen in those results, but the margin appears to be larger enough to encompass those error sources.

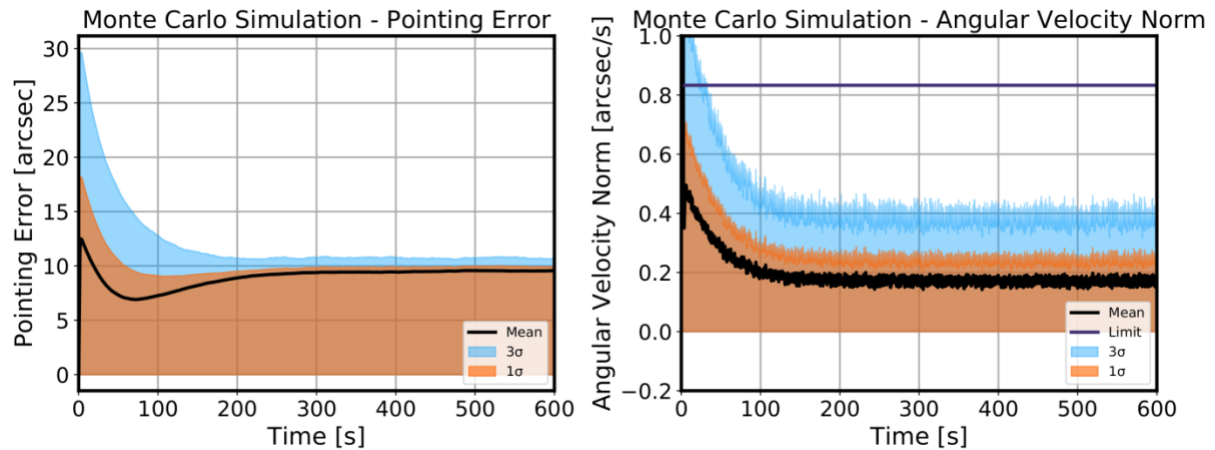


Figure 42 - Absolute pointing error (left) and angular velocity norm (right) for OPC3-2 (LEO) obtained from a simplified simulation using the star trackers.

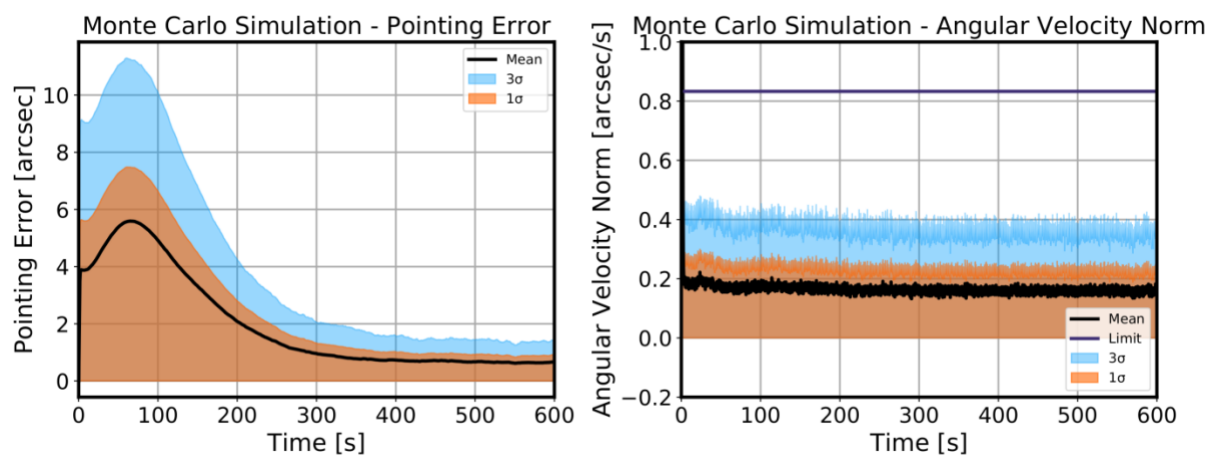


Figure 43 - Relative pointing error (left) and angular velocity norm (right) for OPC3-2 (LEO) obtained from a simplified simulation using the tracking camera.

#### 4.2.2.4 Antenna gimbals pointing

The AOCS will be responsible for pointing the antenna gimbals to the ground stations so that the communication link for the scientific data can be acquired. Since this solution uses a GPS receiver, then the satellite position is known with an error of few meters. Furthermore, since the star trackers continuously measure the satellite attitude concerning a known inertial frame, then the gimbals can be commanded with enough accuracy.

#### 4.2.2.5 General considerations

It is important to mention the following consideration about the AOCS design for this mission:

- The fine pointing mode highly depends on the tracking camera. However, very little information was found about the operation and errors of this instrument. Furthermore, it is not a commercial product. Hence, it is not guaranteed that it will be available for purchase. This is the major risk of the AOCS design.
- The navigation-grade gyro necessary for the mission can be challenging to acquire.
- The attitude control software requires a more sophisticated approach than usual missions. The simulation results have shown that different PD gains must be used to maneuver the satellite in short times and to keep the attitude and angular velocity errors small during

imaging mode. Hence, perhaps non-linear control techniques should be used, such as gain scheduling, for example.

#### 4.2.3 OPC3-2: Propulsion analysis

In this option of design, the propulsion subsystem should be able to keep the orbital parameters within acceptable limits, during the lifetime mission, and to execute the disposal process. The input data for the propulsion subsystem designed here is presented in Table 31.

*Table 31 - Input data for the design of the propulsion subsystem for Opc3-2.*

Parameter	Value	Unit
Dry mass	898	kg
Total $\Delta V$	64	m/s

Figure 44 shows results of the total mass and the required electrical power for the following types of propulsion subsystems: cold-gas, monopropellant, bipropellant, and electrical system. The cold gas propulsion system presented the highest value of mass, whereas the electrical system requires the highest electrical power to activate the thruster. The minimum value of mass is achieved with the bipropellant system. However, the **monopropellant system** has been selected as the baseline design for the Opc3-2 solution, due to its lesser complexity in assembly, lower cost of manufacturing, and to be just 6 kg heavier, approximately, than bipropellant systems.

In a monopropellant system, there is one propellant which decomposes exothermically as it passes through a catalytic bed. This results in heated, high-pressure gases which are expanded through a converging-diverging nozzle to produce thrust. One advantage of this kind of system is that it avoids the mixing step of a two-propellant system which could lead to combustion roughness or even instabilities. A typical monopropellant system consists of a pressurization system, a propellant tank, a propellant valve, a catalyst bed (including a heater for the catalyst material) and a converging-diverging nozzle. In general, monopropellant systems have an impulse specific range from 165 to 244 sec, and they are used for  $\Delta V$  requirements below 1,000 m/s (Wertz and Larson, 2011; Brown, 2002). Figure 43 shows the schematic example of a monopropellant propulsion subsystem.

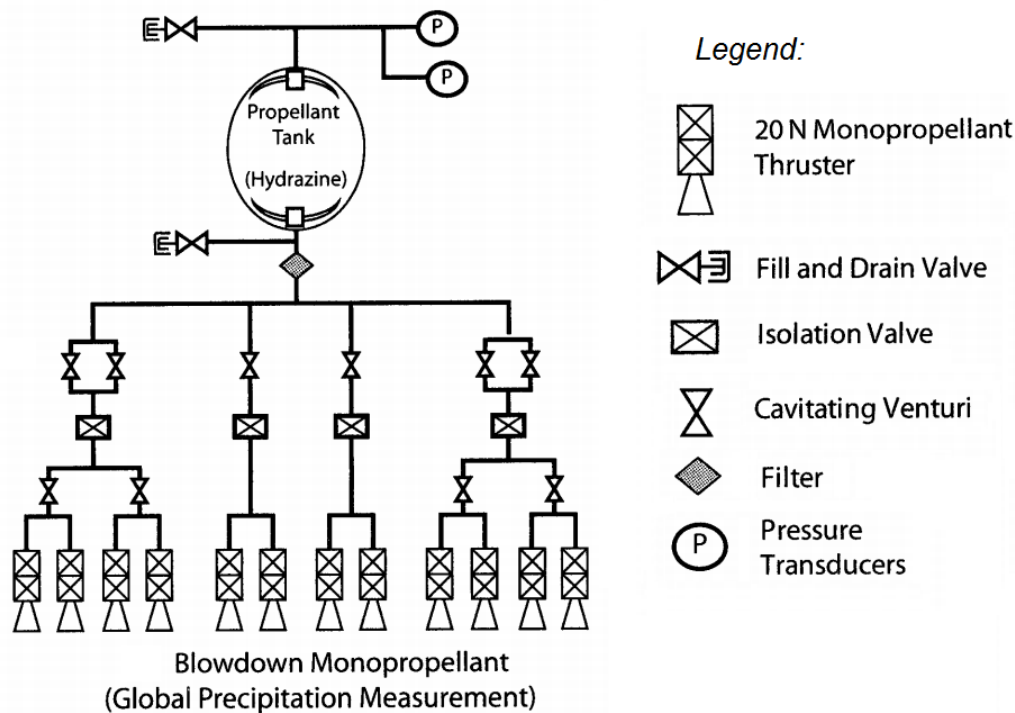


Figure 44 - Monopropellant propulsion subsystem (Wertz, 2011).

The mass budget of the propulsion subsystem for the Opc3-2 solution is presented in Table 32.

Table 32 - Mass budget of the monopropellant subsystem for Opc3-2 solution.

Component	Unit mass, kg	Quantity	Total mass, kg
Propellant	34.13	-	34.13
Tank of fuel	3.5	1	3.5
Thrusters	0.32	4	1.30
Feed system <sup>§</sup>	12.97	-	12.97
<b>Total mass</b>			<b>51.90</b>

<sup>§</sup> Valves, filters, lines and fittings, temperature and pressure transducers, heaters, etc.

In the design process, it was assumed the blowdown pressurization technique with a blowdown ratio of 4. For the tank design, the working pressure input was considered to be of 27.60 bar. Each thruster requires a power of 10W to operate. Based on a commercial database, it was selected models of tank and thruster that best meet the requirements of volume capacity and thrust levels, respectively. Some technical data, such as dimension and capacity, are described in Table 33.

Table 33 - Specification of monopropellant subsystem's components.

Component	Dimension (L x W x H), mm	Capacity
Tank of fuel	484 x 484 x 484	58.6 l
Thruster	162 x 61 x 53	5 N

The propulsion subsystem design considers hydrazine as the fuel, and nitrogen as the pressurant gas. The mass propellant inventory is shown in Table 34. Concerning the pressurization system, a value of 0.321 kg of nitrogen pressurant mass is required to pressurize the fuel tank. The required pressurant volume is approximately 11 liters.

*Table 34 - Inventory mass of hydrazine propellant.*

Propellant use	Mass, kg
Usable propellant	29.79
Trapped propellant, 3%	0.89
Loading error, 0.5%	0.15
Propellant reserve, 10%	2.98
<b>Loaded propellant</b>	<b>33.81</b>

Since the propulsion subsystem is used, in this case, just for orbital maneuvers purposes, then, the four thrusters should be placed on the -X axis panel. Also, it was not realized thruster plume analysis due to the direction of the gases be located far away from the equipment.

#### 4.2.4 OPC3-2: Communications analysis

The main characteristics of the communications science data subsystem conceived for OPC3-1 are presented below.

**Transmitter:** Carrier at 27 GHz, 16 PSK modulation, 2000 Mbps rate, RHCP and LHCP polarizations.

Consumption (2 x 10 W RF): 185 W

Dimensions: 300mm x 170mm x 300mm (W x H x D)

Mass: 10 Kg

**Antennas:** Two parabolic, 25 W transmit power, RHCP and LHCP polarizations.

Dimensions (each): 0.5 m in diameter

Mass (each): 6 kg (including mechanisms, auxiliary structures.)

**RF Subsystem:**

Redundancy: Cold for data transmission.

Dimensions: 2 boxes of 300 mm x 170 mm x 300 mm (W x H x D)

Consumption: 185 W

Mass: 20 kg

**Internal Storage:** Minimum capacity of 2 Tbits

Writing rate: 300 Mbps minimum

Read rate: minimum 3 Gbps

Consumption: 25 W

Dimensions: 200mm x 250mm x 250mm (W x H x D)

Mass: 10 Kg

In Figure 45 a summary of the science data link chain is presented.



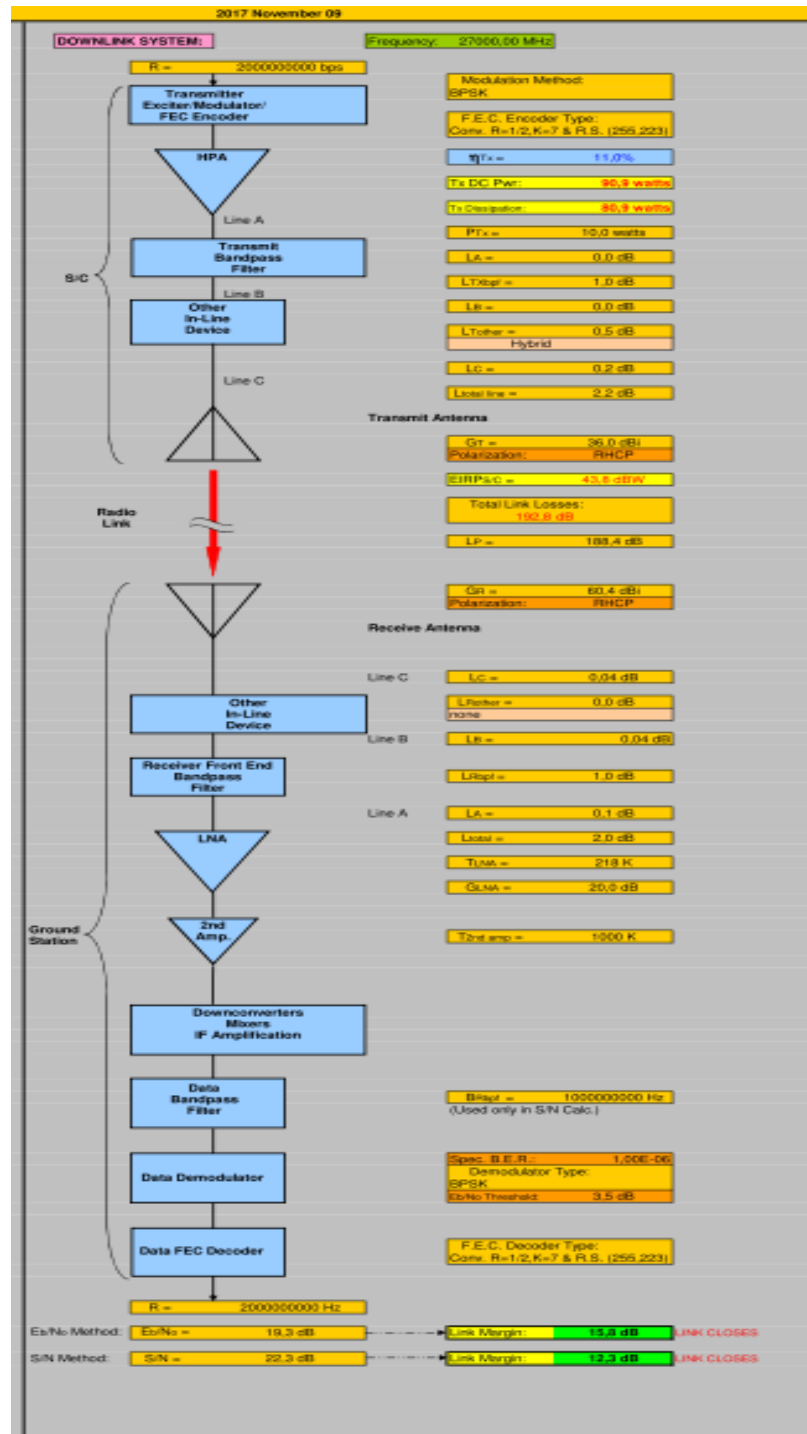


Figure 45 - Science data Ka-band communication link chain for OPC3-2.

For the service communication (telemetry and telecommand) of OPC3-2, was conceived a redundant subsystem with the following characteristics:

**Command Receiver (TC):** Carrier in 2208 MHz, BPSK modulation, rate of 9.6 Kbps.

**Telemetry Transmitter (TM):** Carrier in 2033.2 MHz, BPSK modulation, rate of 512 Kbps.

#### Transponder:

TC Receiver Consumption: 6 W

TM Transmitter TM Consumption (5 W RF): 24 W

Total Consumption: 30 W

Dimensions: 260 mm x 170 mm x 200 mm (W x H x D)

Mass: 4 kg

**TT&C subsystem:**

Redundancy:

- Cold for telemetry transmission.
- Warm up for remote commander reception.

**Transponders:**

Mass: 8 kg

Dimensions: 2 boxes of 260 mm x 170 mm x 200 mm (W x H x D)

**Antennas:** Helicoidal (two Helix Quadrifilar antennas @ 4 dBi, for almost omnidirectional coverage).

Transmit Power: 5 W

Dimensions: 250mm x 400mm (W x D)

Mass: 2 kg (including auxiliary structures).

Total Consumption (1TX + 2RX): 36 W

Total mass: 10 kg (including auxiliary structures).

In Figure 46, the satellite from-to ground station service communication link is summarized, for OPC3-2.

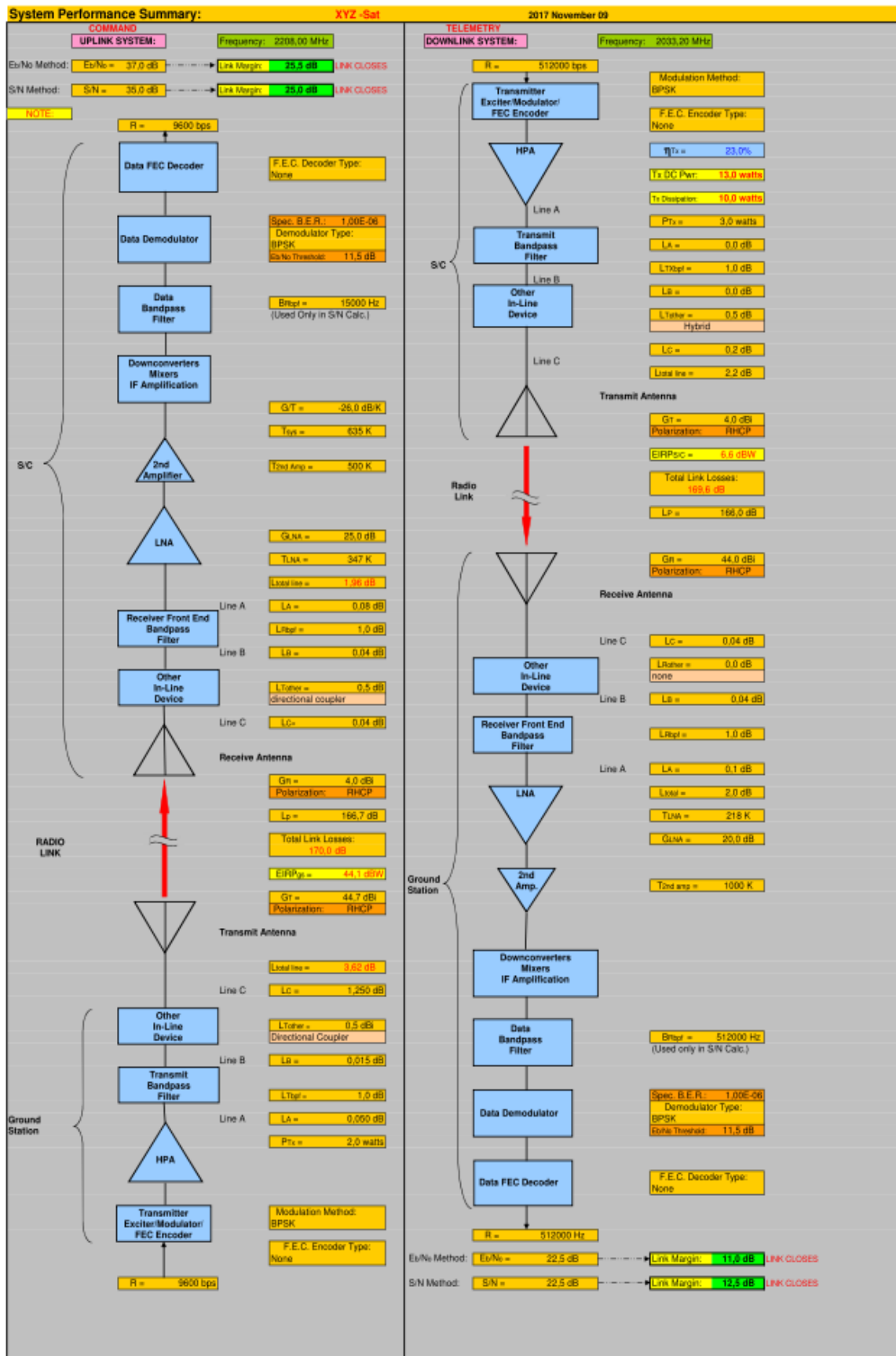


Figure 46 - Service data S-band communication link chain for OPC3-2.

#### 4.2.5 OPC3-2: On-board computer analysis

The computer envisioned for the LEO option has the same functions as the one envisioned for the GEO, and for the present study, as a reference, it was chosen to be used in OPC3-2 the same computer selected for OPC3-1.

#### 4.2.6 OPC3-2: Power analysis

The same non-regulated architecture used in the concept of the power subsystem for OPC3-1, shown in Figure 27, was chosen to be used in OPC3-2. Hence, the kind of equipment used in OPC3-2 is the same as the ones used for OPC3-1, as described in Table 15. However, due to the shorter time the satellite in LEO needs to get to its nominal orbital attitude, than the time needed for the GEO mission, the former option needs less energy stored in this phase than the later, what translates to fewer batteries. While in the GEO option 10 battery packs are used, in the LEO only four are needed.

The conceived power subsystem for OPC3-2 generates 1400 W and allows a satellite power consumption of approximately 1210 W.

#### 4.2.7 OPC3-2: Thermal analysis

The same strategy used to design the thermal concept of OPC3-1 was employed for OPC3-2. However, as the latter is in LEO orbit, while the former is GEO, the thermal environment parameters are different. Moreover, the layout and most of the equipment used in OPC3-2 is different from OPC3-1, what means that the satellite is subject also to different internal thermal loads.

In Table 35 are shown temperature intervals allowable for each satellite panel, and the heat dissipation, from the OPC3-2 equipment, applied over them. The heat dissipations presented are average values, over one orbit.

*Table 35 - Structure panels allowed temperature intervals, and average minimum and maximum equipment thermal loads applied over them in one orbit, for OPC3-2.*

Element	Temperature (°C)		Heat dissipation (W)	
	Min.	Max.	Min.	Máx.
SM Lower Panel	0	40	124.7	150.5
SM Lower Panel (Batteries)	0	5	22.8	25.2
SM Lateral Z+	0	30	0.8	12.0
SM Lateral Z-	-15	25	0	0
SM Lateral Y+	0	30	84.7	105
SM Lateral Y-	0	30	121.1	231.0
SM Shear 1	0	40	0	0
SM Shear 2	0	30	4.6	5.0
SM Shear 3	0	30	39.4	75.6
SM Shear 4	0	40	0	0
SM Shear 5	0	30	0.3	0.3
SM Shear 6	0	30	30.9	56.2
PM Lower Panel	0	40	0	0
PM Vertical Z+	0	30	17.9	39.5
PM Vertical Z-	0	30	120.0	180.0
PM Lateral Y+	0	40	0	0
PM Lateral Y-	0	40	0	0
PM Shear 1	0	40	0	0

Element	Temperature (°C)		Heat dissipation (W)	
	Min.	Max.	Min.	Máx.
PM Shear 2	0	40	0	0
PM Shear 3	0	40	0	0
PM Shear 4	0	40	0	0
PM Shear 5	0	40	0	0
PM Shear 6	0	40	0	0
PM Central Panel	0	40	0	0
PM Shear 7	0	40	0	0
PM Shear 8	0	40	0	0
PM Shear 9	0	40	0	0
PM Shear 10	0	40	0	0
PM Shear 11	0	40	0	0
PM Shear 12	0	40	0	0
PM Top Panel	0	30	0	0
Tank	15	35	0	0

In Table 36 are presented the thermal coatings, and their properties at BOL and EOL, devised to be used in OPC3-2. Most of the satellite external thermal surfaces are covered with MLI blankets, with an estimated effective emissivity of 0.02. The EOL values considered a mission lifetime of five years.

*Table 36 - OPC3-2 thermal optical coatings properties.*

Coating	Absorptivity		Emissivity	
	BOL	EOL	BOL	EOL
Aluminum tape	0.15	0.15	0.05	0.05
*Kapton Al. 3 mil.	0.41	0.76	0.8	0,8
White paint	0.20	0.50	0.94	0.88
Black paint	0.95	0.95	0.88	0.88

\*External layer of MLI blankets

In Table 37 are presented the external minimum and maximum heat loads values and Beta angles used for OPC3-2 satellite's thermal control concept design, for cold and hot cases, respectively. In Figure 47 the estimated variation on the Beta angle in one-year period is presented.

*Table 37 - Environment thermal parameters for OPC3-2.*

Parameter	Case	
	Hot	Cold
Solar radiation	1418 W/m <sup>2</sup>	1326 W/m <sup>2</sup>
Earth radiation	236 W/m <sup>2</sup>	233 W/m <sup>2</sup>
Albedo	0.42	0.34
Beta angle	-90	-58

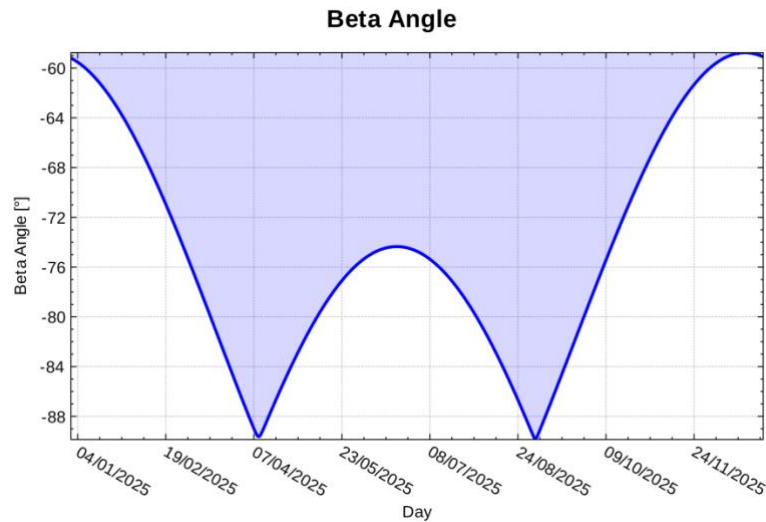


Figure 47 - Beta angle variation in one year.

As for OPC3-1, in OPC3-2 the satellite has its X-axis always pointing towards the Sun. Though the RAAN chosen for the orbit would prevent the satellite from being the Earth's through most of the year, due to the variation in the Beta angle it may be subject to eclipse on some orbits during the year, and this condition was considered as the "cold case" for the satellite concept thermal design, as shown in Figure 48.

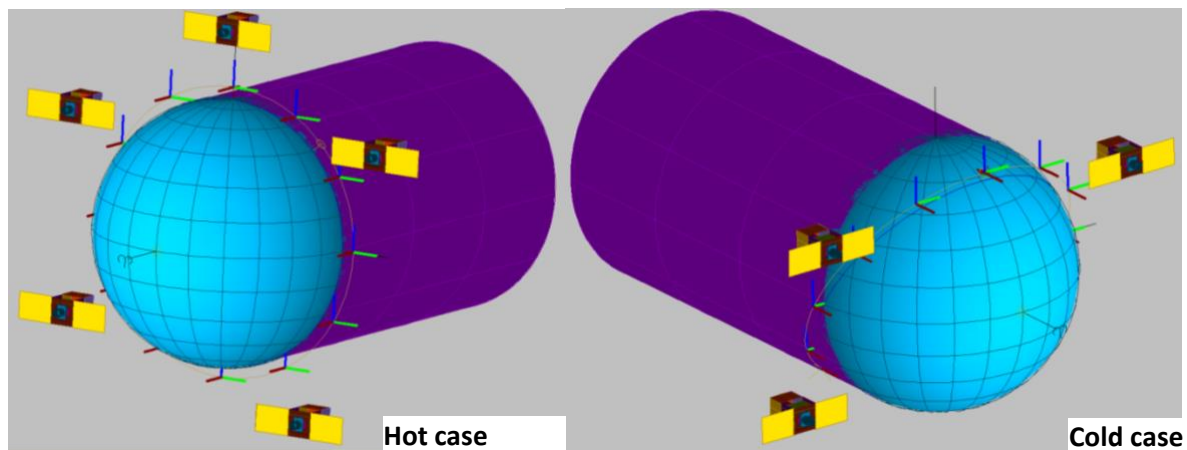


Figure 48 - Satellite orbit and attitude for the cold and hot cases, for OPC3-2.

In Table 38 are shown the estimated radiator areas and average heater power dissipation, for each satellite panel, necessary to keep the satellite's elements within their required orbit temperature ranges.

Table 38 - Estimated Radiator area and heater power at satellite structural panels, for OPC3-2.

Element	Radiator area (m <sup>2</sup> )	Heater power (W)
SM Lower Panel	0.67	0
SM Lower Panel (Batteries)	0.18	0
SM Lateral Z+	0.94	66.0
SM Lateral Z-	0.60	0
SM Lateral Y+	0.82	0
SM Lateral Y-	1.06	0

Element	Radiator area (m <sup>2</sup> )	Heater power (W)
SM Shear 1	0	0
SM Shear 2	0	18.0
SM Shear 3	0	0
SM Shear 4	0	0
SM Shear 5	0	0
SM Shear 6	0	0
PM Lower Panel	0	0
PM Vertical Z+	0	0
PM Vertical Z-	0	0
PM Lateral Y+	0.52	0
PM Lateral Y-	0	0
PM Shear 1	0	0
PM Shear 2	0	0
PM Shear 3	0	0
PM Shear 4	0	0
PM Shear 5	0	0
PM Shear 6	0	0
PM Central Panel	0	0
PM Shear 7	0	0
PM Shear 8	0	0
PM Shear 9	0	0
PM Shear 10	0	0
PM Shear 11	0	0
PM Shear 12	0	0
PM Top Panel	0	10.0
Tank	0	1
<b>Total</b>	<b>4.78</b>	<b>95.0</b>

From Table 38 it can be seen that a total of 95 W (114 W considering a margin of 20 %) must be available from the power to the thermal control subsystem.

In Table 39 the mass breakdown for the elements estimated to be used in the thermal control of the GSST satellite, OPC3-2 option, is shown. The “other” elements refer to devices such as doublers, interfiller, heaters, thermistors and propulsion lines MLIs.

*Table 39 - Nominal mass estimate for the components of the thermal control subsystem of OPC3-2.*

Component	Area(m <sup>2</sup> )	Density(kg/m <sup>2</sup> )	Mass(kg)
MLI blankets	19.3	0.50	9.7
Radiators (white paint)	4.8	0.27	1.3
Internal side of structural panels (white paint)	34.0	0.13	4.4
Other	-	-	12.0
<b>Total</b>			<b>27.4</b>

#### 4.2.8 OPC3-2: Mechanisms

As mentioned previously in the text, the mechanisms in OPC3-1 and 2 have the same function, and the structures they deploy are the same, except the communication antennas. The devices chosen to be used in option OPC3-1 are also applicable to OPC3-2. Hence, for the present study, was decided to use the same mechanisms, which are described in Section 4.1.8, for both options.

#### 4.2.9 OPC3-2: Layout and structures analysis

Figure 49 shows the conceived layout for the GSST, option OPC3-2 (LEO). It follows the same architecture devised for OPC3-1 (GEO): It is composed of two modules, Service (SM) and Payload (PM), but its mass and overall dimensions are much lesser than the ones of the GEO satellite, due to the fact that the LEO option doesn't have the apogee motor necessary to take OPC3-1 from GTO to GEO. Hence, its service module is much smaller than the SM in OPC3-1, while the PM is the same in both cases.

In OPC3-2 the SM and PM are composed of 11 and 19 Al sandwich panels, respectively. A carbon fiber composite cylinder with a diameter of 937 mm connects the SM and PM. Its base is in the interface plane between the satellite and launcher, and its top is flush to the PM top panel.

As for OPC3-1, the OPC3-2 SAG is composed of two solar panels, with a total area of 6 m<sup>2</sup>, disposed of in fixed wings. They are made of carbon fiber composite material.

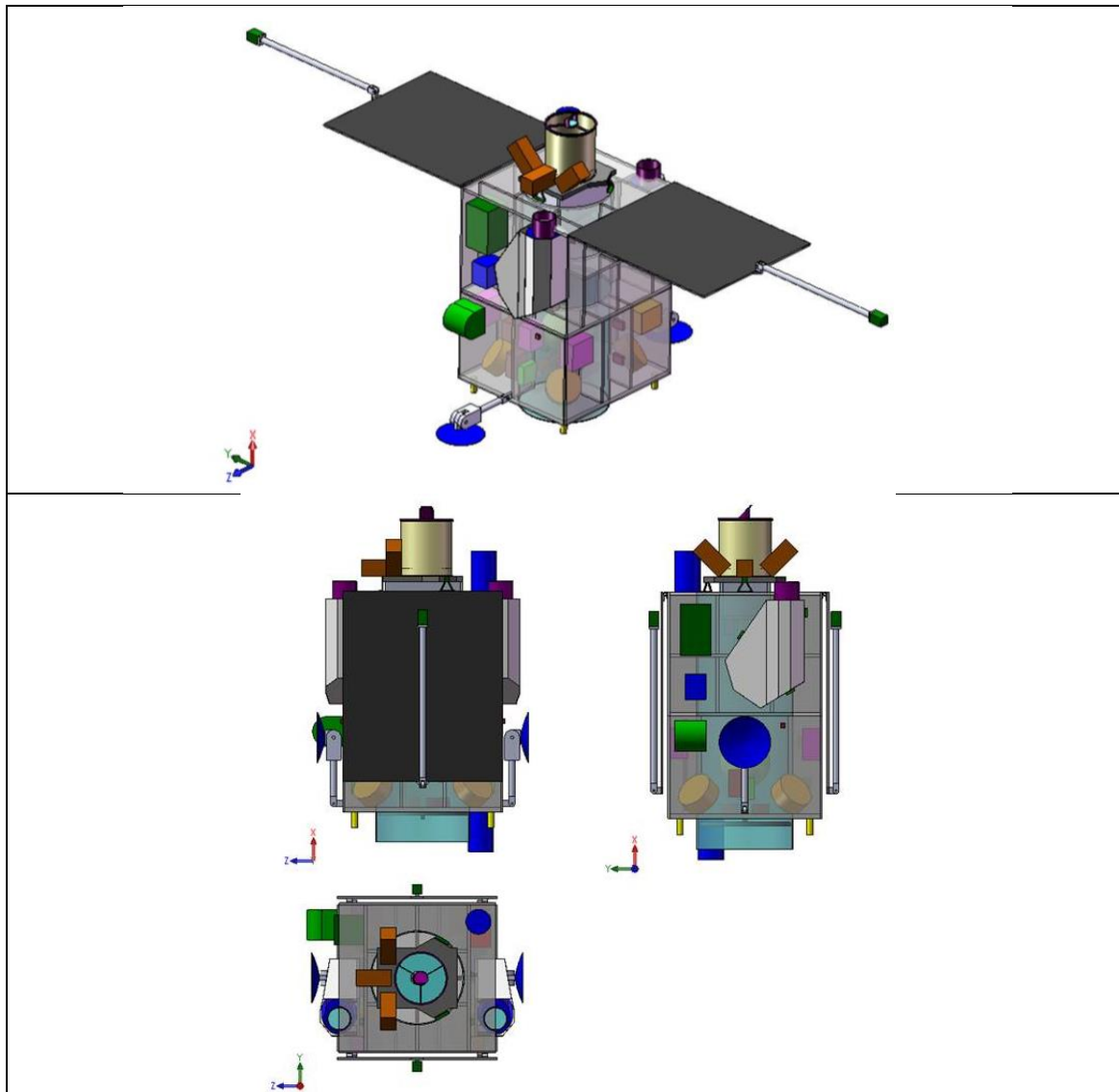


Figure 49 - OPC3-2 satellite external layout. Views for orbit and launch configurations.



Figure 50 presents the external dimensions of the GSST satellite (OPC3-2 option). The dimensions of its structural envelope are shown in Figure 51.

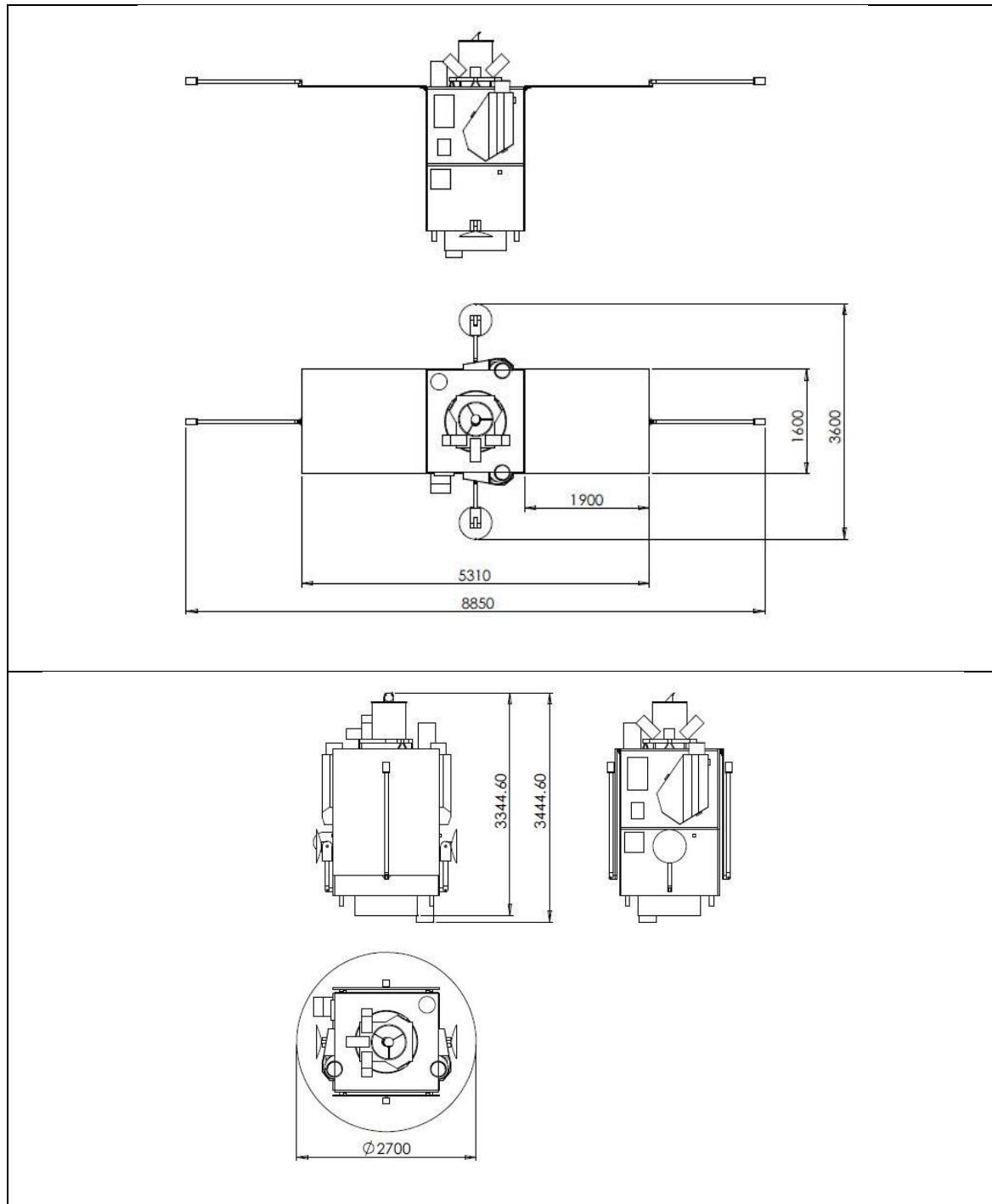


Figure 50 - OPC3-2 external dimensions, for orbit and launch configurations.

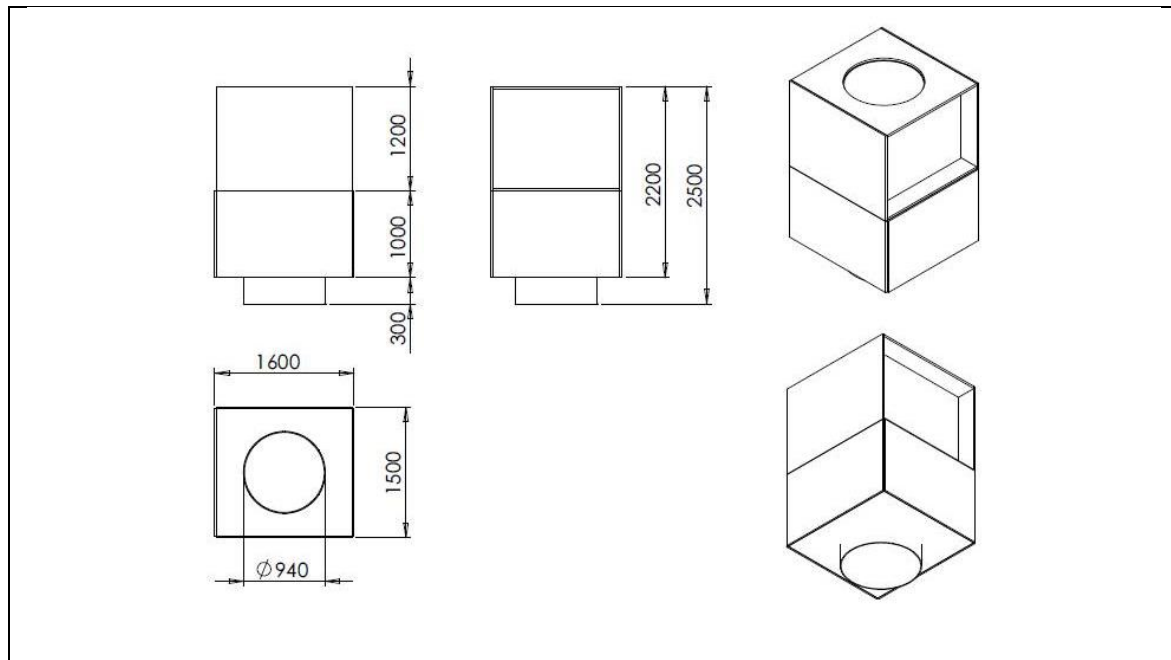


Figure 51 - Dimensions of GSST satellite structure for OPC3-2.

The equipment positioning over the OPC3-2 satellite panels is presented in Table 40. From Figure 52 to Figure 59 this positioning is shown through views of the satellite.

Table 40 - Equipment positioning at satellite panels, for OPC3-2.

Panel	Equipament	Units
SM Lower Panel	Reaction wheel	4
	S-band antenna	1
	Thruster	4
SM Lateral Z+	Ka-band antenna	1
	GPS antenna	1
	HEP detector	1
SM Lateral Z-	Ka-band antenna	1
	GPS antenna	1
SM Lateral Y+	Ka-band transmitter	1
	PCDU	1
SM Lateral Y-	Ka-band transmitter	1
	ACDH computer	1
SM Shear 2	Magnetotorque	1
SM Shear 3	Gyroscope (sensor)	1
	Gyroscope (electronics)	1
	S-band transponder	1
	Gimble electronics	1
SM Shear 5	Magnetometer	2
SM Shear 6	GPS electronics	1
	S-band transponder	1
	Gimble electronics	1
PM Vertical Z+	Broadband radiometer	1
	DDR	1
	FD camera	1
PM Vertical Z-	Optics central unit	1
	Magnetometer electronics	1
	FD camera	1
PM Lateral Y+	Solar panel	1
	Magnetometer sensor	1
PM Lateral Y-	Solar panel	1
	Magnetometer sensor	1
PM Top Panel	S-band antenna	1
Cylinder	propellent tank	1
	HR camera	1
	Star sensor	3
	Battery pack	4
	Magnetotorquer	2

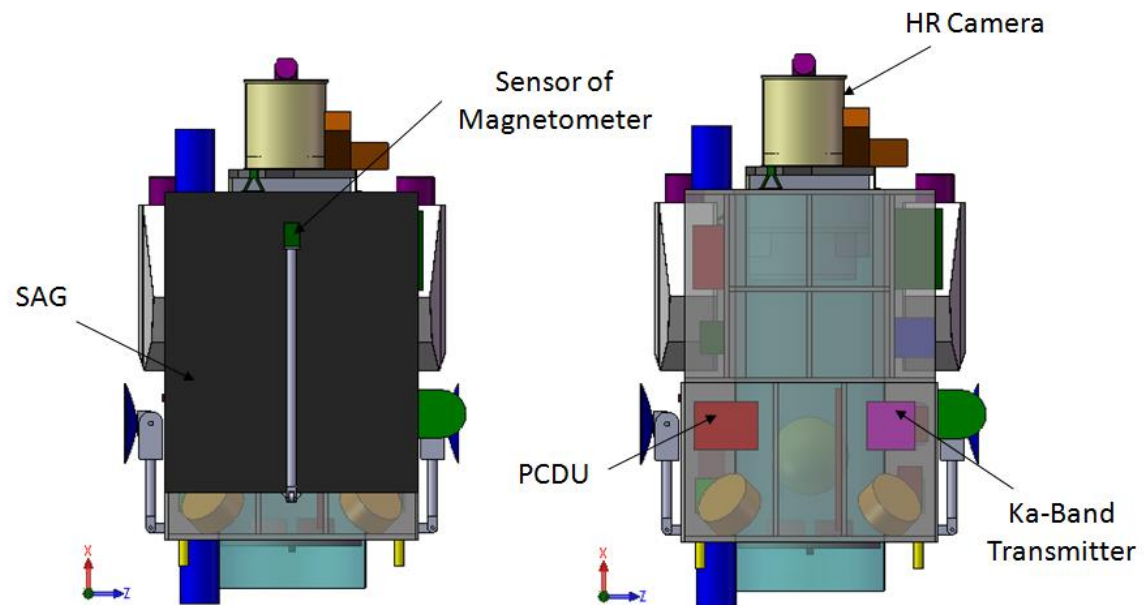


Figure 52 - Y+ side view of GSST satellite, showing equipment layout for OPC3-2.

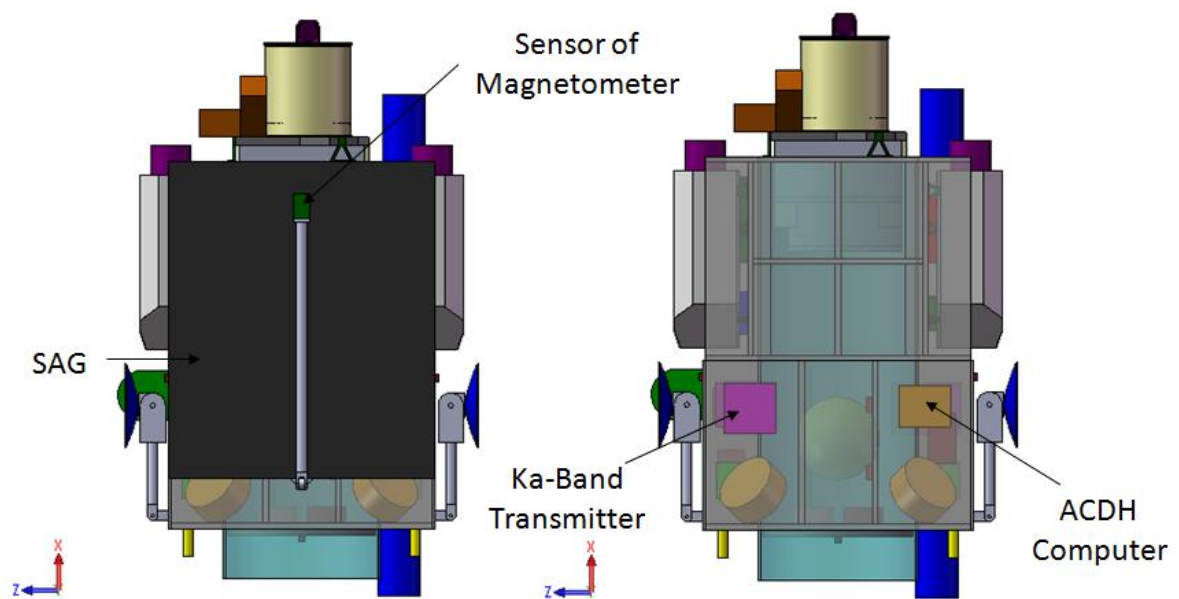


Figure 53 - Y- side view of GSST satellite, showing equipment layout for OPC3-2.

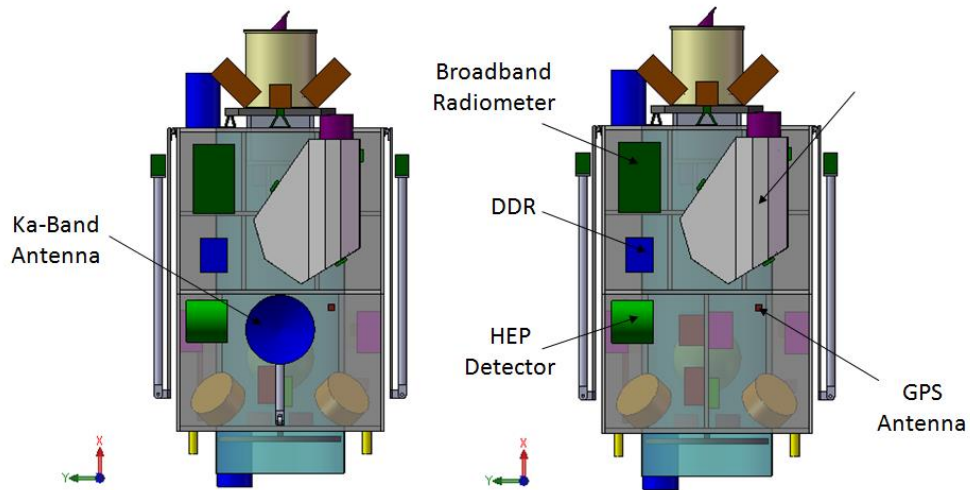


Figure 54 - Z+ side view of GSST satellite, showing equipment layout for OPC3-2.

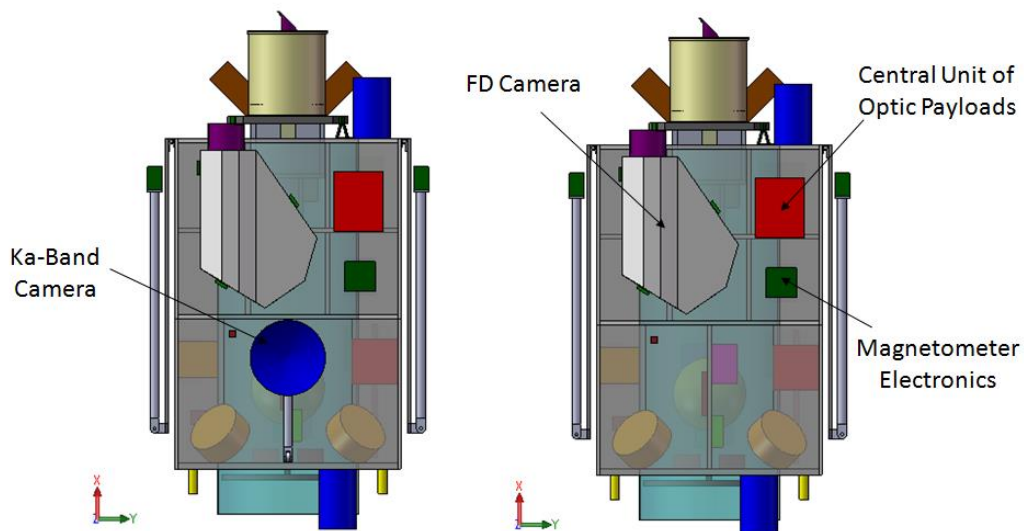


Figure 55 - Z- side view of GSST satellite, showing equipment layout for OPC3-2.

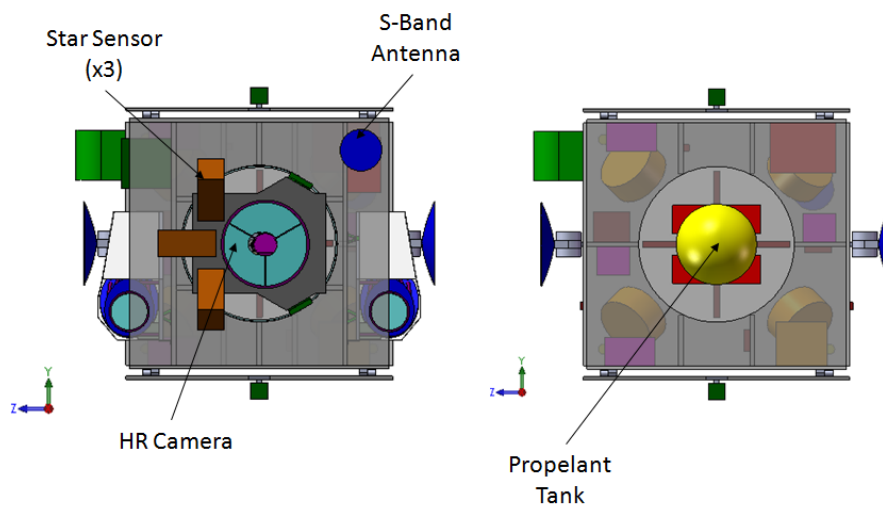


Figure 56 - PM Top Panel & PM Lower Panel side views of GSST satellite, showing equipment layout for OPC3-2.

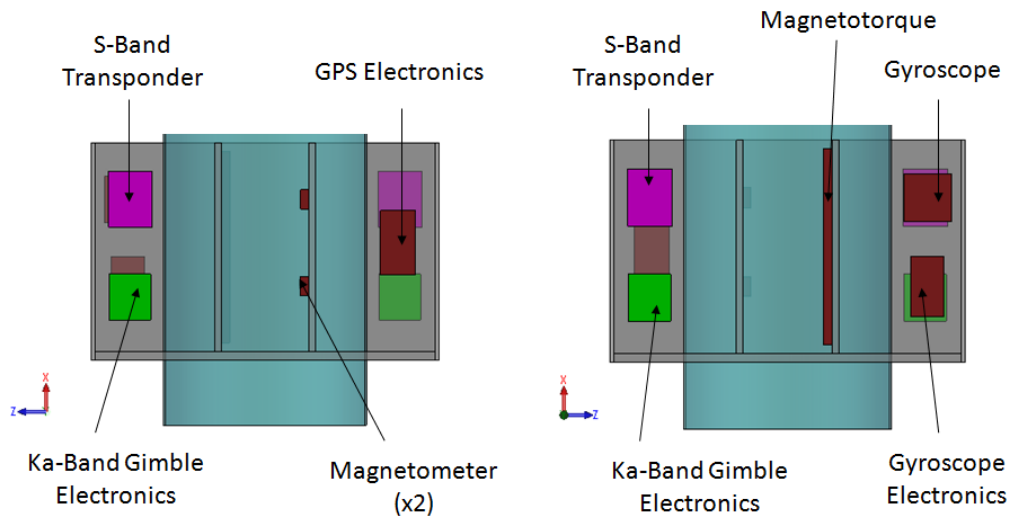


Figure 57 - SM Shear Panels side views of GSST satellite, showing equipment layout for OPC3-2.

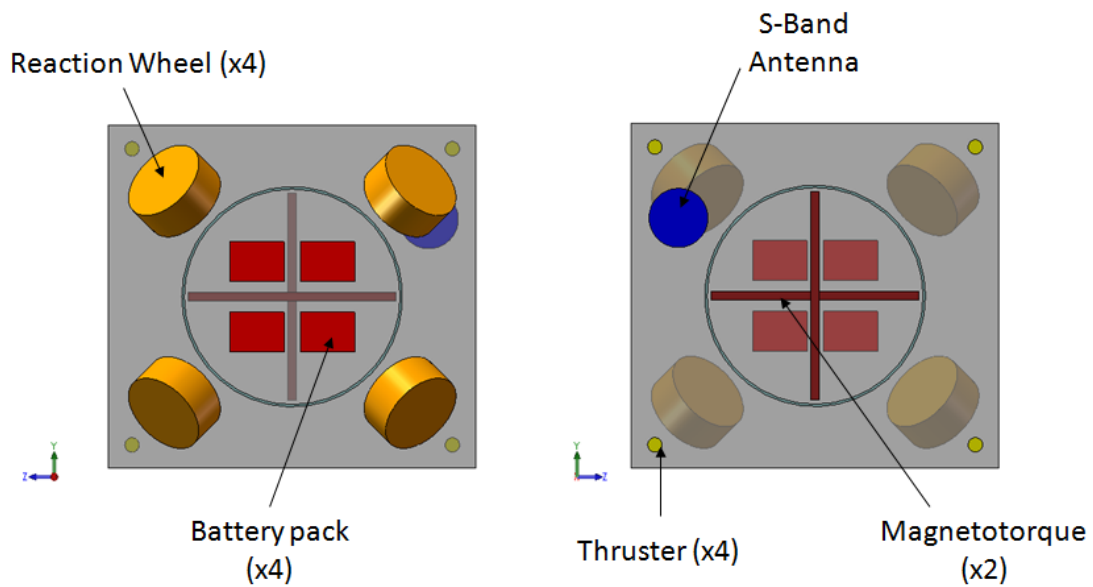


Figure 58 - SM Lower Panel side view of GSST satellite, showing equipment layout for OPC3-2.

In Figure 59 the satellite's mass properties are presented for OPC3-2 launch and orbit configurations.

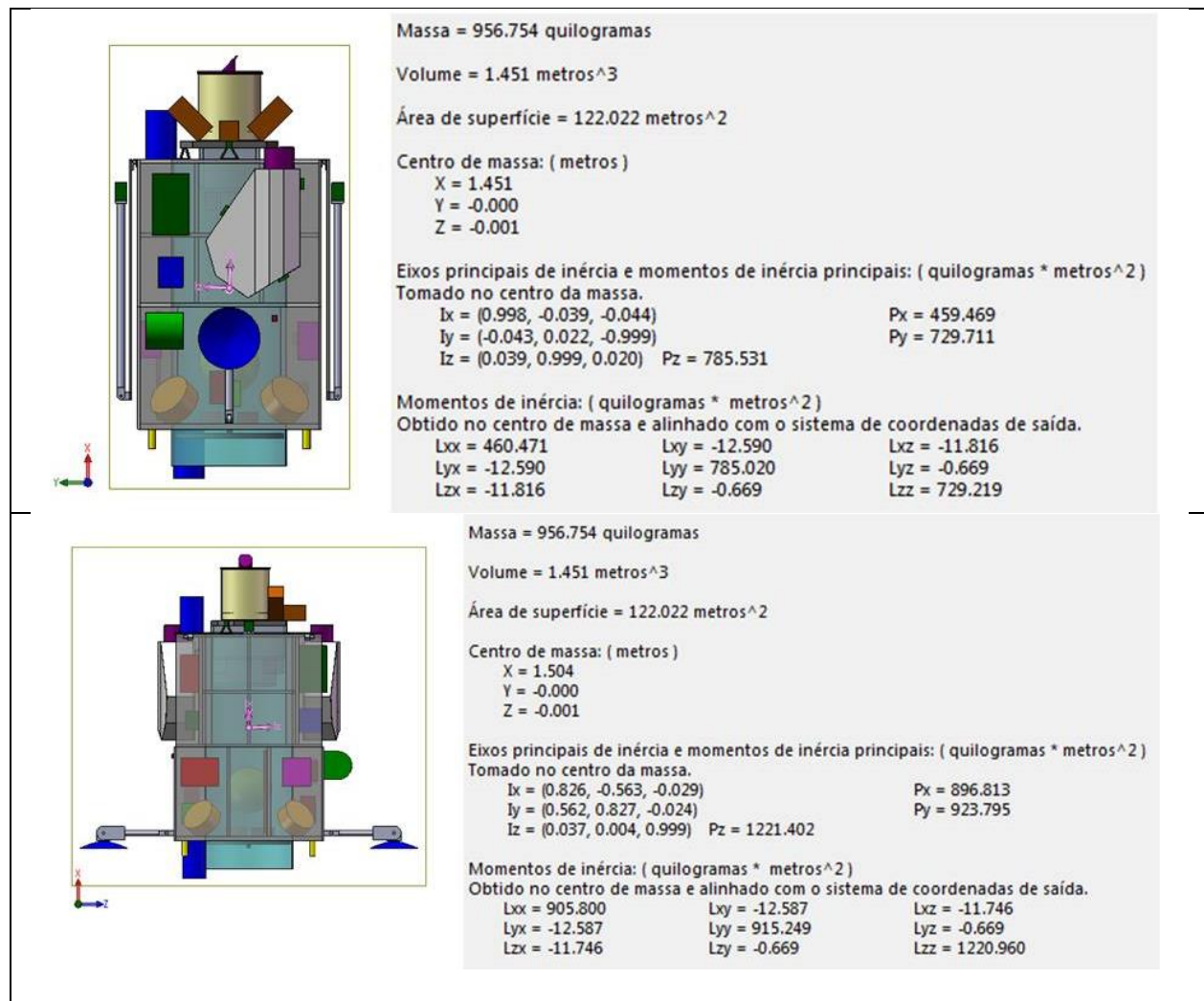


Figure 59 - GSST satellite mass properties for OPC3-2, in launch and orbit configurations.



In Table 41 the dimensions and mass properties of the GSST satellite panels for OPC3-1 are shown. The total structure mass, including a margin of 20 %, summed up to 267,85 kg.

Table 41 - Structure mass breakdown for OPC3-2.

	Panel	Length (m)	Width (m)	Height (m)	Area (m <sup>2</sup> )	Mass without margin (kg)	Mass with margin (kg)
1	SM Lower Panel	1.560	1.460	0.040	2.278	18.2	21.86
2	SM Lateral Z+	1.460	1.000	0.020	1.460	4.4	5.26
3	SM Lateral Z-	1.460	1.000	0.020	1.460	4.4	5.26
4	SM Lateral Y-	1.560	1.000	0.020	1.560	7.8	9.36
5	SM Lateral Y+	1.560	1.000	0.020	1.560	7.8	9.36
6	SM Shear 1	0.306	0.960	0.030	0.294	2.1	2.47
7	SM Shear 2	0.306	0.960	0.030	0.294	2.1	2.47
8	SM Shear 3	0.312	0.960	0.030	0.299	2.1	2.51
9	SM Shear 4	0.306	0.960	0.030	0.294	2.1	2.47
10	SM Shear 5	0.306	0.960	0.030	0.294	2.1	2.47
11	SM Shear 6	0.312	0.960	0.030	0.299	2.1	2.51
12	PM Lower Panel	1.560	1.460	0.030	2.278	18.2	21.86
13	PM Vertical Z+	1.460	1.140	0.030	1.664	11.7	13.98
14	PM Vertical Z-	1.460	1.140	0.030	1.664	11.7	13.98
15	PM Lateral Y-	1.560	1.200	0.020	1.872	5.6	6.74
16	PM Lateral Y+	1.560	1.200	0.020	1.872	5.6	6.74
17	PM Shear 1	0.104	0.540	0.030	0.056	0.4	0.47
18	PM Shear 2	0.104	0.540	0.030	0.056	0.4	0.47
19	PM Shear 3	0.104	0.540	0.030	0.056	0.4	0.47
20	PM Shear 4	0.104	0.540	0.030	0.056	0.4	0.47
21	PM Shear 5	0.262	0.540	0.030	0.141	1.0	1.19
22	PM Shear 6	0.262	0.540	0.030	0.141	1.0	1.19
23	PM Central Panel	1.000	1.460	0.030	1.460	10.2	12.26
24	PM Shear 7	0.104	0.570	0.030	0.059	0.4	0.50
25	PM Shear 8	0.104	0.570	0.030	0.059	0.4	0.50
26	PM Shear 9	0.104	0.570	0.030	0.059	0.4	0.50
27	PM Shear 10	0.104	0.570	0.030	0.059	0.4	0.50
28	PM Shear 11	0.262	0.570	0.030	0.149	1.0	1.25
29	PM Shear 12	0.262	0.570	0.030	0.149	1.0	1.25
30	PM Top Panel	1.560	1.460	0.030	2.278	15.9	19.13
31	Cilindro					52	62.40
32	Angle Bars & Fasteners					30	36.00
						223.208	267.85

#### 4.2.10 OPC3-2: Launcher options

The selection of candidate options for launching the GSST satellite, OPC3-1 GEO option, was based taking into account parameters such as of orbit, satellite mass and its external dimensional envelope during launch (Figure 50). These parameters are summarized below.

- Orbit type – LEO (SSO) with altitude of 601 km;
- Orbit inclination – 97.749°;
- Satellite mass – 965 kg;



- CG height in relation to the separation plane – 1.45 m;
- Satellite static envelope –2.70 m (diameter)x 3.45 m (height).

In Table 42 a set of candidate commercial launchers, which performance characteristics are adequate for an OPC3-1 launch is shown.

*Table 42 - Candidate launchers for the GSST satellite in configuration OPC3-2.*

Launcher	Maximum mass capacity [kg]	Estimated launch cost US\$	Launch base
Minotaur V	1730	50 to 70 million	Vandenberg
Soyuz (Molniya)	1500	30 to 50 million	Plesetsk
H-IIA 202	4100	70 million	Tanegashima
PSLV	1350	20 to 30 million	Satish Dhawanr
Vega	1395	20 to 40 million	Kourou
Delta II	1650	100 million	Vandenberg
LM 3C	1320	50 to 70 million	Xichang
Angara 1.2	2500	68 million	Plesetsk

#### 4.2.11 OPC3-2: Ground systems concept

Due to the band used (Ka) and the necessity of a polar ground station for accomplishing its scientific data transmission requirement, the concept of the OPC3-2 ground segment considered the renting of the service of a polar station (for example, Svalbard) and the acquisition of a Ka band antenna to be installed at one of INPE's Centers, for receiving scientific data transmitted from the satellite. The infrastructure for transmitting and receiving service data, the satellite control and mission centers, and data distribution for the mission's users would be the same as the ones considered for OPC3-1. In Figure 60, the ground segment concept for the OPC3-2 is depicted.

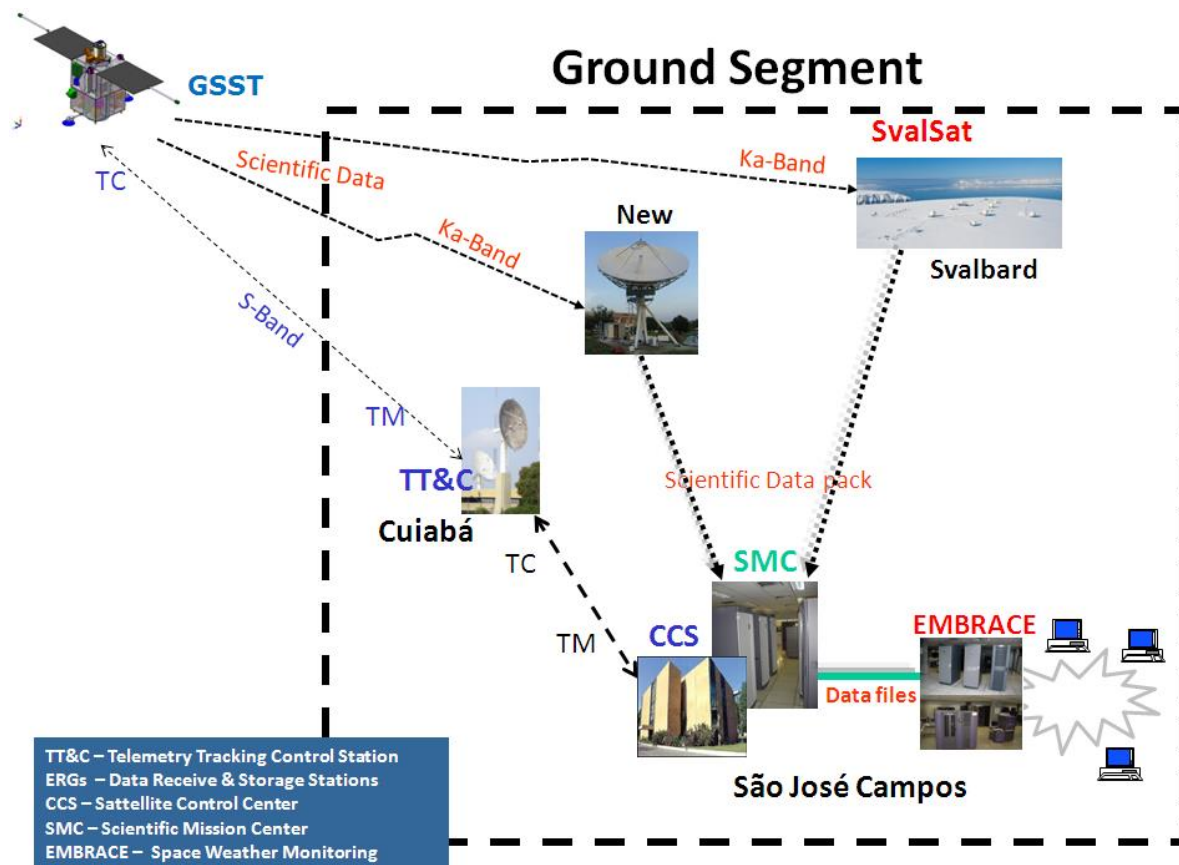


Figure 60 - Ground segment concept for OPC3-2.

#### 4.2.12 OPC3-2: Satellite disposal analysis

Responsible disposal of LEO satellites is one of the most important steps to limit the growth of debris in that region. According to the IADC guidelines, the satellite's reentry by atmospheric drag must be predicted to occur within 25 years after the end of the mission. An IADC study have concluded that this orbit duration is a reasonable compromise between unlimited orbital lifetime and immediate de-orbit at the end of the mission.

The decay of an orbiting object due to atmospheric drag is mainly a function of its mass, projected area on the direction of the velocity vector, drag coefficient and the characteristics of the atmosphere. In Table 43 the value of the parameters used for the analysis of the decay of OPC3-2 solution are presented.

Table 43 - Input parameters for the disposal analysis.

Parameter	Value	Unit
Satellite altitude	600	km
Minimal area-to-mass ratio	0.006	m <sup>2</sup> /kg
Start year	2025	year

NASA's DAS<sup>®</sup>v2.0.1 software was used to estimate the satellite decay through the atmosphere. The result is shown in Figure 61. Note that the satellite will decay within the deadline of 25 years.

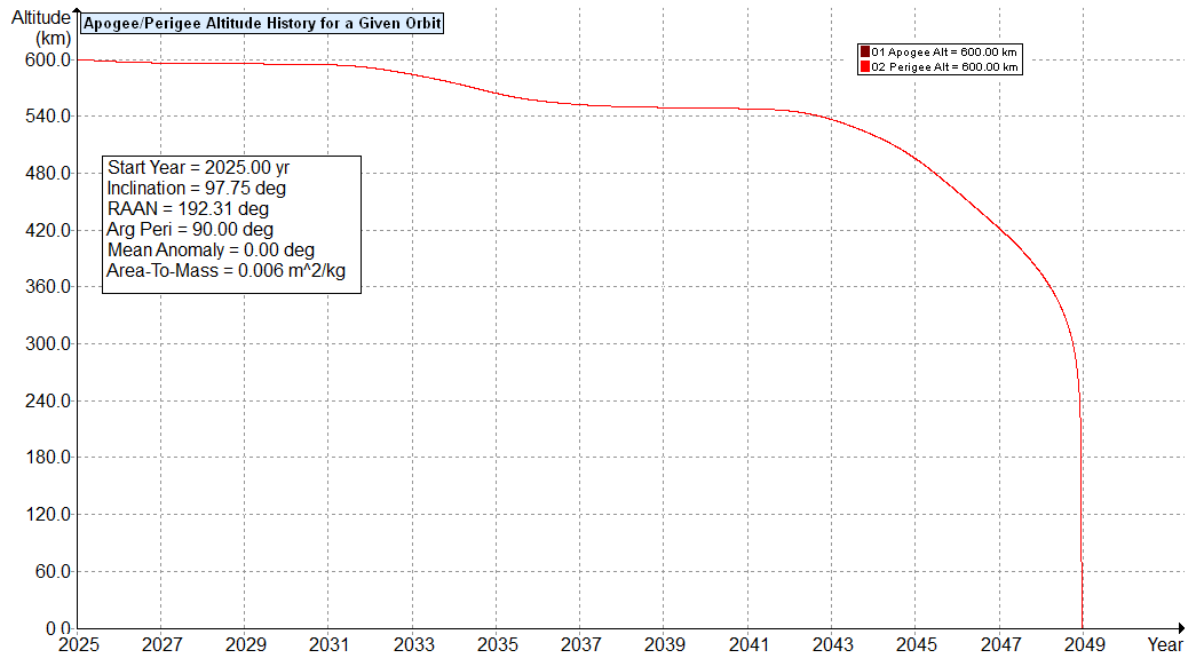


Figure 61 - GSST satellite decay results for OPC3-2.

## 4.2.13 OPC3-2: Satellite mass and power budget

Table 44 - Mass and power budget for OPC3-2.

Subsystem	Component	Units	Unit Dimensions (LxWxH) mm	Mass per Unit unidade (kg)		Total Mass (kg)				Power consumption per unit (W)					
				Best Estimate (kg)	Margin (%)	Total Units (kg)	Subsystem (kg)	Subsystem Mass / Total Mass (%)	Total Mass (kg)	Nominal operation	Margin (%)	Operation with margin	Nominal stand-by	Margin (%)	Standby with margin
Thermal Control	Heaters	1	NA							95	20		95	20	
	MLIs	1	NA	9.700	20.0	11.640									
	Radiators (white paint)	1	NA	1.300	20.0	1.560	32.880	3.6							
	Internal Painting	1	NA	4.400	20.0	5.280									
	Miscellaneous	1	NA	12.000	20.0	14.400									
Power	PCDU	1	400x300x300	15.000	5.0	15.750	75.810	8.3		100.0	5.0	105.0	50.0	5.0	52.5
	Battery	4	230x170x95	4.300	5.0	18.060				6.0	5.0	6.3	6.0	5.0	6.3
	Solar Panel	2	3,0 m2	20.000	5.0	42.000				NA			NA		
Propulsion	Propellent	1	45.922 L	35.117	5.000	36.873	56.072	6.1		NA			NA		
	Propellent tank	1	484 x 484 x 484	3.500	5.0	3.675				NA			NA		
	Thruster	4	163 x 61 x 54	0.324	20.0	1.555				10.0	20.0	12.0	10.0	20.0	12.0
	Other	1	-	13.304	5.0	13.969									
OBDH	Computer	1	307x242x263	13.600	5.0	14.280	14.280	1.6		35.0	5.0	36.8	35.0	5.0	36.8
Communications	Ka-band Transmitter	2	300x300x170	10.000	5.0	21.000	37.800	4.1		185.0	5.0	194.3	92.5	5.0	97.1
	Ka-band antenna	2	500D	2.000	5.0	4.200				0.0	5.0	0.0	0.0	5.0	0.0
	S-band transponder	2	260x200x170	4.000	5.0	8.400				30.0	5.0	31.5	15.0	5.0	15.8
	S-band antenna	2	250Dx400A	2.000	5.0	4.200				0.0	5.0	0.0	0.0	5.0	0.0
Orbit and attitude control	Reaction wheel	4	366 x 366 x 159	8.500	5.0	35.700	73.175	8.0		22.0	5.0	23.1	22.0	5.0	23.1
	Magnetotorquers	3	37 x 37 x 883	5.500	5.0	17.325				4.8	5.0	5.0	4.8	5.0	5.0
	Star sensor	3	160 x 170 x 350	3.700	5.0	11.655				10.0	5.0	10.5	10.0	5.0	10.5
	solar sensor	8	28 x 28 x 3	0.020	5.0	0.168				0.0	5.0	0.0	0.0	5.0	0.0
	Magnetometer	2	36 x 90 x 130	0.190	5.0	0.399				0.3	5.0	0.3	0.3	5.0	0.3
	GPS	1	295 x 160 x 35	0.950	5.0	0.998				5.5	5.0	5.8	5.5	5.0	5.8
	GPS antenna	2	45 x 45 x 20	0.050	5.0	0.105				0.0	5.0	0.0	0.0	5.0	0.0
	Gyroscope	1	215 x 215 x 180	2.000	5.0	2.100				0.0	5.0	0.0	0.0	5.0	0.0
	Gyroscope electronics	1	270 x 150 x 145	4.500	5.0	4.725				24.0	5.0	25.2	24.0	5.0	25.2
	Ka-band antenna gimbal	2	300x150x150	10.500	5.0	22.050				6.5	5.0	6.8	1.0	5.0	1.1
Mechanisms	Gimbal electronics	2	212x190x75	3.500	5.0	7.350	46.620	5.1		12.0	5.0	12.6	2.5	5.0	2.6
	Hinges of Ka-band antenna (2x) and of the magnetometer booms (2x)	4	100x80x80	1.300	5.0	5.460				Not Applicable			Not Applicable		
	Hold down and Release of the Ka-band antennas (6x) and of the magnetometer booms (4x)	10	60x60x60	0.600	5.0	6.300				Not Applicable			Not Applicable		
	SAG hinge	4	120x60x60	0.700	5.0	2.940				Not Applicable			Not Applicable		
	SAG hold down and release	4	60x60x60	0.600	5.0	2.520				Not Applicable			Not Applicable		
Structure	Satellite structure	1		223.208	20.0	267.850	267.850	29.3		Not Applicable					
Payloads	High resolution telescope and proximity electronics	1	See Figure 10	88.600	10.0	97.460	295.868	32.3		55.0	20.0	66.0			0.0
	Wide field telescope 1 and proximity electronics	1	See Figure 12	47.670	20.0	57.204				25.0	20.0	30.0			0.0
	Wide field telescope 2 and proximity electronics	1	See Figure 12	47.670	20.0	57.204				25.0	20.0	30.0			0.0
	Digital data recorder	1	200x250x250	10.000	10.0	11.000				25.0	10.0	27.5	12.5	10.0	13.8
	Optical Payload Central Unit	1	Dimensões no CAD	25.000	20.0	30.000				150.0	20.0	180.0	15.0	20.0	18.0
	Broadband radiometer	1	500x300x300	3.500	20.0	4.200				10.0	20.0	12.0	8.3	20.0	9.9
	High energy particle telescope	1	300x300x300	10.000	20.0	12.000				10.0	20.0	12.0	1.0	20.0	1.2
	Magnetometer (electronics)	1	200x200x150	3.000	20.0	3.600				3.0	20.0	3.6	1.0	20.0	1.2
	Magnetometer (sensor)	2	150x100x100	1.000	10.0	2.200				1.0	10.0	1.1	1.0	10.0	1.1
	Magnetometer (Booms) (without wiring or instruments)	2	3m	10.000	5.0	21.000				0.0	10.0	0.0	0.0	10.0	0.0
Harness	Satellite harness	1		48.000		48.000	48.000	5.2		Not Applicable					
						TOTAL	915.474	100.0							

## 5 Programmatics, mission risk and cost analysis

---

In the present study, two different system technical solutions for the GSST mission were conceived. Each of them has associated risks and costs, which are also dependent on the way the mission is implemented.

Due to the novelty of this kind of mission to INPE, associated mainly to the high technological challenges posed by the optical payload design and in the eventual development of a GEO solution (in case OPC3-1 is chosen), estimates of system developing schedule, risk and cost are difficult to assess, resulting in a high margin of uncertainty associated to their figures. Hence, the analysis reported in this document should be taken as a rough preliminary assessment on those subjects.

Cost estimates for implementing OPC3-1 or 2 were performed using parametric cost models, but the results of this analysis are not reported in the present document. They are reported in a separate technical note delivered to the customer of the study.

In the following paragraphs of this Section, firstly are estimated the developing schedules for the space segments of options OPC3-1 and 2. It is assumed that the implementation time of the ground and application segments are encompassed by the time necessary to develop the satellites and that those activities can be done simultaneously. Then, follow a risk assessment for both system options, focusing on the main issues that would compromise the mission.

### 5.1 Programmatics Analysis

For the estimation of the developing schedule of options OPC3-1 and OPC3-2 the following aspects were considered:

- INPE has no experience in developing space missions for solar observation;
- INPE has already development equipment for measuring total solar irradiance, but for Earth-based measurements;
- INPE has experience in developing instruments for *in situ* measurements of the Earth's magnetosphere, but with no flight validation;
- INPE has experience in developing optical cameras for space applications, but not with high resolution;
- The solution conceived for the SM of the LEO option (OPC3-2), has many similarities with the SM of the CBERS satellites family, and of the PMM. Hence, it is reasonable to suppose that if the OPC3-2 is chosen, the development of its SM module would not pose a significant technical challenge for INPE and the Brazilian industry.
- No GEO satellite has been developed in Brazil. The experience of INPE, or the Brazilian industry, on this kind of system is few;
- It is desirable the maximization of the participation of the Brazilian industry in the system development;
- Considering INPE and the Brazilian industry few heritage on the kind of payloads to be flown in the GSST satellite, it was assumed that they will be developed following a traditional approach, with the construction of Engineering, Qualification and Flight models of the instruments (camera sensors and associated electronics). However, for the cameras telescopes, it was decided that a protoflight approach for their development would be more appropriate, so that development costs associated with a device of high optic/mechanic complexity, would be mitigated.

- For both system solutions (GEO and LEO) it is assumed that the satellite SM is developed following a protoflight approach, and two batches for the SM's equipment are acquired (1 FM and 1 spare). For the satellite structure, thermal control elements and propulsion subsystem, only one protoflight unit is built. Note that the main difference between the SM for the GEO option compared to the one for the LEO option, is the presence of an apogee motor in the former one, what would imply in higher cost and development time for it.
- The payloads are the same either for the GEO or LEO orbit options. Except for the cameras telescopes, all instrumentation, including the magnetometer, particle detectors, and radiometer, were considered to be developed following a traditional approach, with 1 EM, 1 QM and 2 FMs (1 spare).

In Figure 62 and Figure 63 schedule estimates for the GSST mission, for OPC3-1 (GEO) and OPC3-2 (LEO), respectively, are shown. For either option is estimated a total of roughly ten years to develop the system, from conceptual phase to satellite launching. This is due to the developing time be dominated primarily by the payloads, specifically the optical cameras. Hence, even if developing the SM for the GEO option would require more time than for the LEO option, the total development time for both options does not differ significantly, since the development times for their PMs are the same. Note that in either orbit case is estimated a much more significant time to develop the PM than the SM.

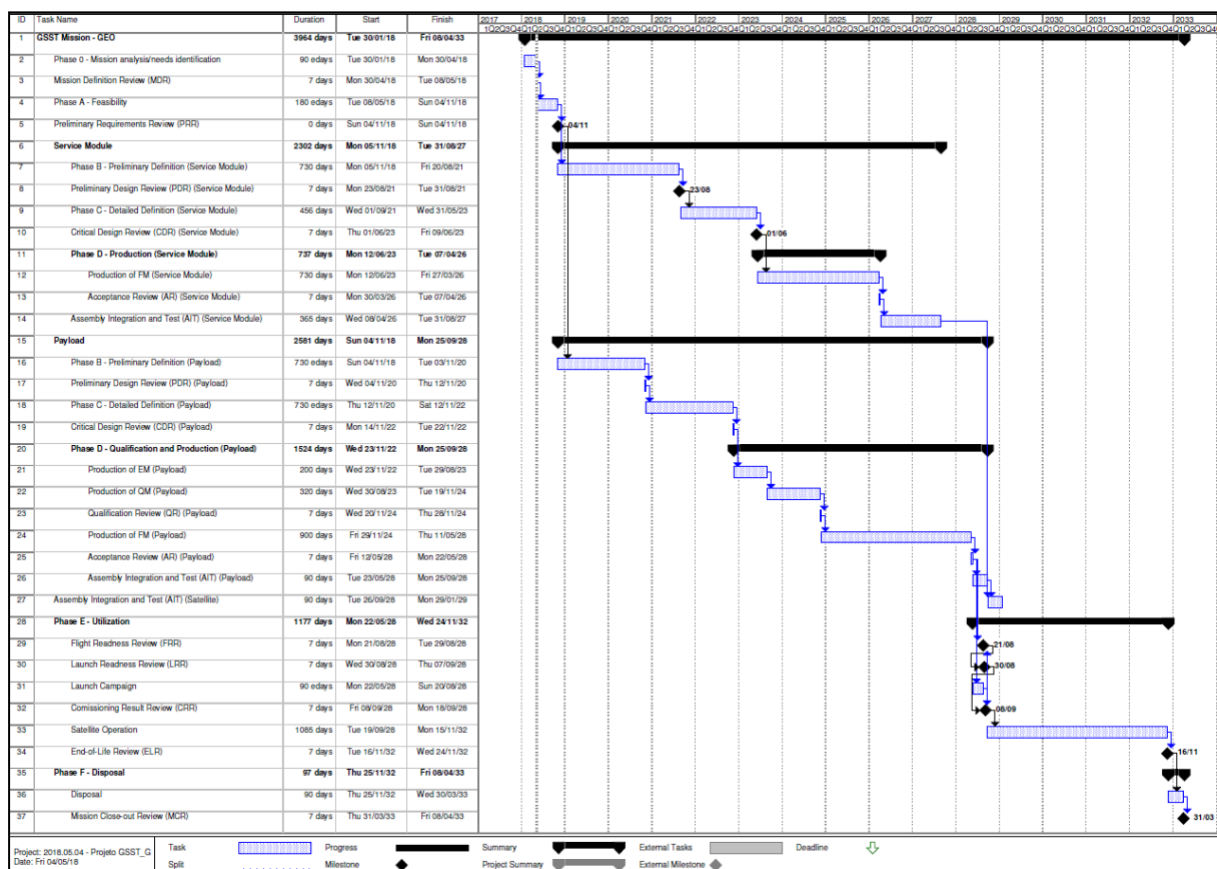


Figure 62 - Estimated development schedule for the GSST mission, option OPC3-1 (GEO).

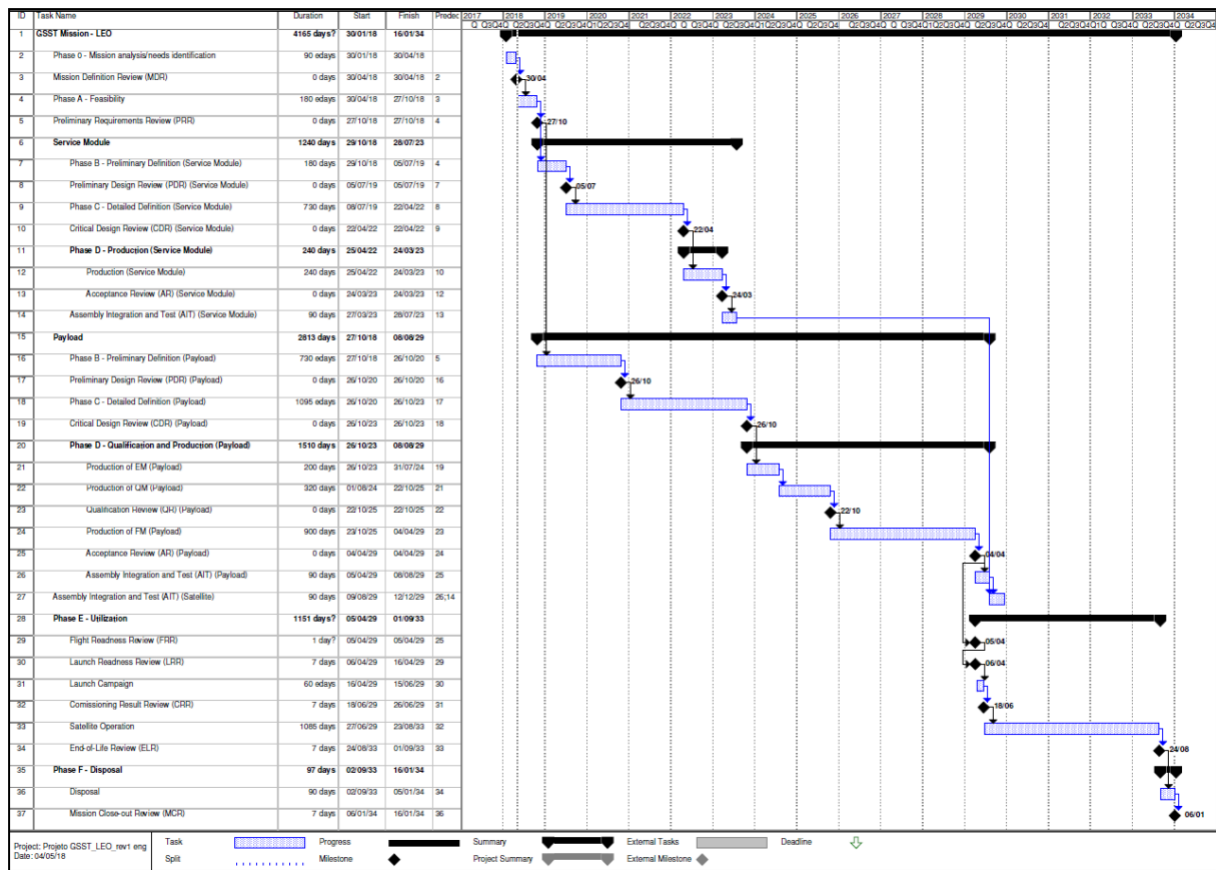


Figure 63 - Estimated development schedule for the GSST mission, option OPC3-2 (LEO).

## 5.2 Risk Analysis

A preliminary risk assessment was performed using the traditional 5x5 risk matrix with qualitative evaluation. The main technical and operational risks associated with developing the GSST mission are summarized below:

### 1) Technological:

- The cameras pose a significant technological challenge regarding optical, thermal designs, and pointing accuracy. For this last issue, it is necessary an auxiliary device (tracking camera) provide information to the satellite's AOCS and the HR camera stabilizer mechanism, which increases the system complexity. It is noteworthy that neither INPE nor the Brazilian industry has experience in developing optical equipment with such complexity level. It is highly recommended that a comprehensive study of the technical and programmatic aspects related to the development of the cameras in Brazil be made, before the beginning of the mission development.
- The use of mobile antennas for transmitting scientific data from the satellite to the ground stations could induce vibration on the PM and compromise the pointing accuracy required for the HR camera.
- Transmission in Ka-band frequency is more subject to atmospheric interference than in X-band. The use of such frequency for OPC3-2 may increase the possibility of loss of data when atmospheric conditions are degraded.
- If the OPC3-1 is chosen as the system solution for the GSST mission, the use of an apogee motor will represent a technological challenge for the Brazilian industry, due to its inexperience on this kind of propulsion system.



## 2) Operational:

- The continuous transmission of scientific data through the orbit requires a functional link handover between the mobile antennas since only one of them will have a field of view to the ground station during segments of the orbit. This handover poses a risk to the continuity of data reception along the orbit.
- OPC3-1 considers the use of the X-band receiving antenna located at Cuiaba. This antenna is used today to receive data from other satellites, and there is a risk of conflict between the time necessary to download the scientific data from the GSST satellite and other missions. A more in-depth operation analysis shall be performed to assess this potential conflict in the future.
- It is necessary to verify the risk of no availability of a slot in the GEO belt that would be occupied by the GSST satellite if option OPC3-1 is chosen.
- In OPC3-2 it is mandatory the use of a polar station for receiving the scientific data. An additional communication link between this polar station and the mission center in Brazil is introduced to the communication architecture, hence increasing the risk of loss of data.

## 6 Final Remarks

---

From the analysis of the requirements posed by the GSST mission, it was conceived two candidate solutions for a space system which could meet the mission objectives.

The requirement of imaging the Sun almost continuously, associated with the desired resolution for the cameras, resulted in a very high payload data acquisition ratio, which led to the consideration of a GEO solution, since in this case the data acquired would be downloaded almost in real time to the ground, requiring almost no storage of payload data onboard the satellite. In this case, INPE's X-band ground antenna at Cuiaba could be, in principle, used to receive the scientific data downloaded from the satellite. On the other hand, a GEO solution implies a more massive, costlier satellite. The mission objectives can be met by an LEO satellite, but in this case, the use of a polar station for receiving the scientific data from the satellite will be mandatory. In fact, it is in principle possible to avoid the use of a polar station in the LEO option, if a GEO relay satellite is available for transmitting the payload data to the ground station. In the present study, this option was not further investigated, due to the high uncertainties related to the availability of the relay satellite.

Finally, it should be highlighted that the optical payloads pose a high technical challenge for the mission and are the primary drivers of the development mission time, estimated roughly in ten years, from conceptual phase to satellite launching.



## References

---

Brown, C. D. Elements of Spacecraft Engineering. AIAA Education Series. 2002IADC. Space Debris Mitigation Guidelines. 10 p. 2007

CGCEA. “Encaminhamento de Solicitação de Avaliação de Missão Solar”. Documento 00340.013491/2016, 06/Dez/2016.

Jr. Anderson, J. D. Fundamentals of Aerodynamics. McGraw-Hill International Editors, New York, 1985.

De Sousa, F. L., and Muraoka, I. Analysis of the thermal impact of the thruster plume impingement on PMM Satellite. Technical Report A822300-TRP-005-01, Instituto Nacional de Pesquisas Espaciais, São José dos Campos, 2006.

Leyva, I.A. Spacecraft Subsystems I – Propulsion. In Wertz, J.R., Everett, D.F., and Puschell, J.J. (Editors). Space Mission Engineering: The New SMAD. Microcosm Press, 2011.

Wertz, J.R., Everett, D.F., and Puschell, J.J. (Editors). Space Mission Engineering: The New SMAD. Microcosm Press, 2011.